J. Phys. Condensed Matter: TOPICAL REVIEW

Electrowetting: from Basics to Applications

Frieder Mugele[1,*] and Jean-Christophe Baret[1,2]

1: University of Twente; Faculty of Science and Technology; Physics of Complex Fluids; P.O. Box 217; 7500 AE Enschede (The Netherlands)

2: Philips Research Laboratories Eindhoven; Health Care Devices and Instrumentation; WAG01; Prof. Holstlaan 4; 5656 AA Eindhoven (The Netherlands)

***: corresponding author**

phone: ++31 / 53 489 3094; fax: ++31 / 53 489 1096; email: f.mugele@utwente.nl

Abstract. Electrowetting has become one of the most widely used tools to manipulate tiny amount of liquids on surfaces. Applications range from lab-on-a-chip devices to adjustable lenses or new types of electronic displays. In the present article, we review the recent progress in this rapidly growing field including both fundamental and applied aspects. We compare the various approaches used to derive the basic electrowetting equation, which has been shown to be very reliable as long as the applied voltage is not too high. We discuss in detail the origin of the electrostatic forces that induce both the contact angle reduction as well as the motion of entire droplets. We examine the limitations of the electrowetting equation and present a variety of recent extensions to the theory that account for distortions of the liquid surface due to local electric fields, for the finite penetration depth of electric fields into the liquid, as well as for finite conductivity effects in the presence of AC voltage. The most prominent failure of the electrowetting equation, namely the saturation of the contact angle at high voltage, is discussed in a separate section. Recent work in this direction indicates that a variety of distinct physical effects - rather than a unique one – is responsible for the saturation phenomenon, depending on experimental details. In the presence of suitable electrode patterns or topographic structures on the substrate surface, variations of the contact angle can not only give rise to continuous changes of the droplet shape, but also to discontinuous morphological transitions between distinct liquid morphologies. The dynamics of electrowetting are discussed briefly. Finally, we give an overview of recent work aimed at commercial applications, in particular in the fields of adjustable lenses, display technology, fiber optics, and biotechnology-related microfluidic devices.

1. Introduction

Miniaturization has been a technological trend for several decades. What started out initially in the microelectronics industry has long reached the area of mechanical engineering, including fluid mechanics. Reducing size has been shown to allow for integration and automation of many processes on a single device giving rise to a tremendous performance increase, e.g. in terms of precision, throughput, and functionality. One prominent example from the area of fluid mechanics are Lab-on-a-Chip systems for applications such as DNA- or protein analysis, and biomedical diagnostics [1-3]. Most of the devices developed so far are based on continuous flow through closed channels that are either etched into hard solids such as silicon or glass, or replicated from a hard master into a soft polymeric matrix. Recently, devices based on the manipulation of individual droplets with volumes in the range of nanoliters or less have attracted increasing attention [4-10].

From a fundamental perspective the most important consequence of miniaturization is a tremendous increase in the surface-to-volume ratio, which makes the control of surfaces and surface energies one of the most important challenges both in microtechnology in general as well as in microfluidcs. For liquid droplets of submillimeter dimensions, capillary forces dominate [11, 12]. The control of interfacial energies has therefore become an important strategy to manipulate droplets at surfaces [13-17]. Both liquid-vapor and solid-liquid interfaces have been influenced in order to control droplets, as recently reviewed by Darhuber and Troian [15]. Temperature gradients as well as gradients in the concentration of surfactants across droplets give rise to gradients in interfacial energies, mainly at the liquid-vapor interface, and thus produce forces that can propel droplets making use of the thermocapillary and Marangoni effects.

Chemical and topographical structuring of surfaces has received even more attention. Compared to local heating, both of these two approaches offer much finer control of the equilibrium morphology. The local wettability and the substrate topography together provide boundary conditions within which the droplets adjust their morphology to reach the most energetically favorable configuration. For complex surface patterns, however, this is not always possible as several metastable morphologies may exist. This

can lead to rather abrupt changes in the droplet shape, so-called morphological transitions, when the liquid is forced to switch from one family of morphologies to another by varying a control parameter, such as the wettability or the liquid volume [13, 16, 18-20].

The main disadvantage of chemical and topographical patterns is their static nature, which prevents active control of the liquids. Considerable work has been devoted to the development of surfaces with controllable wettability – typically coated by self-assembled monolayers. Notwithstanding some progress, the degree of switchability, the switching speed, the long-term reliability, and the compatibility with variable environments that have been achieved so far are not suitable for most practical applications. In contrast, electrowetting (EW) has proven very successful in all these respects: contact angle variations of several tens of degrees are routinely achieved. Switching speeds are limited (typically to several milliseconds) by the hydrodynamic response of the droplet rather than the actual switching of the equilibrium value of the contact angle. Hundreds of thousands of switching cycles were performed in long term stability tests without noticeable degradation [21, 22]. Nowadays, droplets can be moved along freely programmable paths on surfaces, they can be split, merged and mixed with a high degree of flexibility. Most of these results were achieved within the past five years by a steadily growing community of researchers in the field [23].

Electrocapillarity, the basis of modern electrowetting, was first described in detail in 1875 by Gabriel Lippmann [24]. This ingenious physicist, who won the Noble prize in 1908 for the discovery of the first color photography method, found that the capillary depression of mercury in contact with electrolyte solutions could be varied by applying a voltage between the mercury and electrolyte. He formulated not only a theory of the electrocapillary effect but developed several applications, including a very sensitive electrometer and a motor based on his observations. In order to make his fascinating work, which has only been available in French up to now, available to a broader readership, we included a translation of his work in the Appendix of this review. The work of Lippmann and of those who followed him in the following more than hundred years was devoted to aqueous electrolytes in direct contact with mercury surfaces or mercury droplets in contact with insulators. A major obstacle to broader applications was

electrolytic decomposition of water upon applying voltages beyond a few hundred millivolts. The recent developments were initiated by Berge [25] in the early 1990s, who introduced the idea of using a thin insulating layer to separate the conductive liquid from the metallic electrode in order to eliminate the problem of electrolysis. This is the concept that has also become known as electrowetting on dielectric (EWOD).

In the present review, we are going to give an overview of the recent developments in electrowetting, touching only briefly on some of the early activities that were already described in a short review by Quilliet and Berge [26]. The article is organized as follows: in section 2 we discuss the theoretical background of electrowetting, comparing different fundamental approaches, and present some extensions of the classical models. Section 3 is devoted to materials issues. In section 4, we discuss the phenomenon of contact angle saturation, which has probably been the most fundamental challenge in electrowetting for some time. Section 5 is devoted to the fundamental principles of electrowetting on complex surfaces, which is the basis for most applications. Section 6 deals with some aspects of dynamic electrowetting, and finally, before concluding, a variety of current applications ranging from lab-on-a-chip to lens systems and display technology are presented in section 7.

2. Theoretical Background

Electrowetting has been studied by researchers from various fields, such as applied physics, physical chemistry, electrochemistry, and electrical engineering. Given the various backgrounds, different approaches were used to describe the electrowetting phenomenon, i.e. to determine the dependence of the contact angle on the applied voltage. In this chapter, we will – after a few introductory remarks about wetting in section 2.1 – discuss the main approaches of electrowetting theory (sec. 2.2): the classical thermodynamic approach (2.2.1), the energy minimization approach (2.2.2), and the electromechanical approach (2.2.3). In section 2.3, we will describe some extensions of the basic theories that give more insight into the microscopic surface profile near the three phase contact line (2.3.1), the distribution of charge carriers near the interface (2.3.2), and the behavior at finite frequencies (2.3.3).

2.1. Basic Aspects of Wetting

In electrowetting, one is generically dealing with droplets of partially wetting liquids on planar solid substrates (see Figure 1). In most applications of interest, the droplets are aqueous salt solutions with a typical size on the order of 1mm or less. The ambient medium can be either air or another immiscible liquid, frequently an oil. Under these conditions, the Bond number $Bo = \sqrt{g\Delta\rho R^2/\sigma_{lv}}$, which measures the strength of gravity with respect to surface tension, is smaller than unit. Therefore we neglect gravity throughout the rest of this paper. In the absence of external electric fields, the behavior of the droplets is then determined by surface tension alone. The free energy F of a droplet is a functional of the droplet shape. Its value is given by the sum of the areas A_i interfaces between three phases, the solid substrate (s), the liquid droplet (l), and the ambient phase, which we will denote as vapor (v) for simplicity [27], weighted by the respective interfacial energies σ_i, i.e. σ_{sv} (solid-vapor), σ_{sl} (solid-liquid), and σ_{lv} (liquid-vapor).

$$F = F_{if} = \sum_i A_i \sigma_i - \lambda V \qquad (1)$$

Here, λ is a Lagrangian variable to enforce the constant volume constraint. λ is equal to the pressure drop Δp across the liquid-vapor interface. Variational minimization of eq. (1) leads to the two well-known necessary conditions that any equilibrium liquid morphology has to fulfill [11, 12]: the first one is the Laplace equation, stating that Δp is a constant, independent of the position on the interface:

$$\Delta p = \sigma_{lv}\left(\frac{1}{r_1} + \frac{1}{r_2}\right) = \sigma_{lv} \cdot \kappa \,. \qquad (2)$$

Here, r_1 and r_2 are the two – in general position-dependent – principal radii of curvature of the surface, and κ is the constant mean curvature. For homogeneous substrates, this means that droplets adopt a spherical cap shape in mechanical equilibrium. The second condition is given by Young's equation

$$\cos\theta_Y = \frac{\sigma_{sv} - \sigma_{sl}}{\sigma_{lv}}, \qquad (3)$$

which relates Young's equilibrium contact angle θ_Y to the interfacial energies [28]. Alternatively to this energetic derivation, the interfacial energies σ_i can also be

interpreted as interfacial tensions, i.e. as forces pulling on the three phase contact line. Within this picture, eq. (3) is obtained by balancing the horizontal component of the forces acting on the three phase contact line (TCL), see Figure 2 [29].

Note that both derivations are approximations intended for mesoscopic scales. On the molecular scale, equilibrium surface profiles deviate from the wedge shape in the vicinity of the TCL [30, 31]. Within the range of molecular forces, i.e. typically a few nanometers from the surface, the equilibrium surface profiles are determined by the local force balance (at the surface) between the Laplace pressure and the disjoining pressure, in which the molecular forces are subsumed. Despite the complexity of the profiles that arise, these details are not relevant if one is only interested in the apparent contact angle at the mesoscopic scale. On that latter scale, the contact line can be considered as a one-dimensional object on which the interfacial tensions are pulling. As we will see below, a comparable situation arises in electrowetting.

2.2. Electrowetting Theory for Homogeneous Substrates

2.2.1. The Thermodynamic and Electrochemical Approach

Lippmann's classical derivation of the electrowetting or electrocapillarity equation is based on general Gibbsian interfacial thermodynamics [32]. Unlike the recent applications of electrowetting where the liquid is separated from the electrode by an insulating layer, Lippmann's original experiments dealt with direct metal- (in particular mercury) electrolyte interfaces (see Appendix and [24]). For mercury, several tenths of a volt can be applied between the metal and the electrolyte without any current flowing. Upon applying a voltage dU, an electric double layer builds up spontaneously at the solid-liquid interface consisting of charges on the metal surface on the one hand and of a cloud of oppositely charged counter ions on the liquid side of the interface. Since the accumulation is a spontaneous process, such as for instance the adsorption of surfactant molecules at an air-water interface, it leads to a reduction of the (effective) interfacial tension σ_{sl}^{eff}

$$d\sigma_{sl}^{eff} = -\rho_{sl} dU \qquad (4)$$

($\rho_{sl} = \rho_{sl}(U)$ is the surface charge density of the counter ions [33].) (Our reasons for denoting the voltage-dependent tension as "effective" will become clear below.) The voltage-dependence of σ_{sl}^{eff} is calculated by integrating eq. (4). In general, this integral requires additional knowledge about the voltage-dependent distribution of counter ions near the interface. Section 2.3.2 describes such a calculation based on the Poisson-Boltzmann distribution. For now, we make the simplifying assumption that the counter ions are all located at a fixed distance d_H (on the order of a few nanometers) from the surface (Helmholtz model). In this case, the double layer has a fixed capacitance per unit area, $c_H = \varepsilon_0 \varepsilon_l / d_H$, where ε_l is the dielectric constant of the liquid. We obtain [34, 35]

$$\sigma_{sl}^{eff}(U) = \sigma_{sl} - \int_{U_{pzc}}^{U} \rho_{sl} d\tilde{U} = \sigma_{sl} - \int_{U_{pzc}}^{U} c_H \tilde{U} d\tilde{U} = \sigma_{sl} - \frac{\varepsilon_0 \varepsilon_l}{2 d_H} (U - U_{pzc})^2 \qquad (5)$$

Here, U_{pzc} is the potential (difference) of zero charge. (Note that mercury surfaces – like most other materials – acquire a spontaneous charge when immersed into electrolyte solutions at zero voltage. The voltage required to compensate for this spontaneous charging is U_{PZC}; see also Figure 4 in the Appendix) The chemical contribution σ_{sl} to the interfacial energy, which appeared previously in Young's equation (eq. (3)) is assumed to be independent of the applied voltage. To obtain the response of the contact angle, eq. (5) is inserted into Young's equation (eq. (3)). For an electrolyte droplet placed directly on an electrode surface we find

$$\cos\theta = \cos\theta_Y + \frac{\varepsilon_0 \varepsilon_l}{2 d_H \sigma_{lv}} (U - U_{pzc})^2, \qquad (6)$$

For typical values of d_H (2nm), ε_l (81), and σ_{lv} (0.072 mJ/m^2) we find that the ratio on the r.h.s. of eq. (6) is on the order of 1V^{-2}. The contact angle thus decreases rapidly upon the application of a voltage. It should be noted, however, that eq. (6) is only applicable within a voltage range below the onset of electrolytic processes, i.e. typically up to a few hundred millivolts. As mentioned already in the introduction, modern applications of electrowetting usually circumvent this problem by introducing a thin dielectric film, which insulates the droplet from the electrode, see (1). In this EWOD configuration, the electric double layer builds up at the insulator-droplet interface. Since the insulator thickness d is usually much larger than d_H, the total capacitance of the

system is reduced tremendously. The system may be described as two capacitors in series [34, 35], namely the double at the solid-insulator interface (capacitance c_H) and the dielectric layer with $c_d = \varepsilon_0 \varepsilon_d / d$ (ε_d is the dielectric constant of the insulator). Since $c_d << c_H$, the total capacitance per unit area $c \approx c_d$. With this approximation, we neglect the finite penetration of the electric field into the liquid, i.e. we treat the latter as a perfect conductor. As a result, we find that the voltage drop occurs within the dielectric layer, and eq. (5) is replaced by

$$\sigma_{sl}^{eff}(U) = \sigma_{sl} - \frac{\varepsilon_0 \varepsilon_d}{2d} U^2 \qquad (7)$$

(Here and in the following, we assume that the surface of the insulating layer does not give rise to spontaneous adsorption of charge in the absence of an applied voltage, i.e. we set U_{pzc}=0.) In this equation the entire dielectric layer is considered part of one effective solid-liquid interface [35] with a thickness on the order of d, i.e. in practice typically O(1μm). In that sense, the interfacial energy in eq. (7) is clearly an "effective" quantity. Combining eq. (7) with eq. (3), we obtain the basic equation for EWOD:

$$\cos\theta = \cos\theta_Y + \frac{\varepsilon_0 \varepsilon_d}{2d\sigma_{lv}} U^2 = \cos\theta_Y + \eta \qquad (8)$$

Here, we have introduced the dimensionless electrowetting number $\eta = \varepsilon_0 \varepsilon_r U^2 / (2d\sigma_{lv})$, which measures the strength of the electrostatic energy compared to surface tension. The ratio in the middle part of eq. (8) is typically four to six orders of magnitude smaller than in eq. (6), depending on the properties of the insulating layer. Consequently, the voltage required to achieve a substantial contact angle decrease in EWOD is much higher.

Figure 3 shows a typical experimental example. As in many other experiments, eq. (8) is found to hold as long as the voltage is not too high. Beyond a certain system-dependent threshold voltage, however, the contact angle has always been found to become independent of the applied voltage [36-42]. This so-called contact angle saturation phenomenon will be discussed in detail in section 4.

2.2.2. *Energy Minimization Method*

For EWOD, eq. (8) was first derived by Berge [25]. His derivation, however, was based on energy minimization rather than interfacial thermodynamics: the free energy F of a droplet in an EWOD configuration (Fig. 1) is composed of two contributions - in addition to the interfacial energy contribution F_{if} that appeared already in eq. (1), there is an electrostatic contribution F_{el}:

$$F_{el} = \frac{1}{2}\int \vec{E}(\vec{r}) \cdot \vec{D}(\vec{r})\, dV \qquad (9)$$

$\vec{E}(\vec{r})$ and $\vec{D}(\vec{r}) = \varepsilon_0 \varepsilon(\vec{r}) \vec{E}(\vec{r})$ denote the electric field and the electric displacement at $\vec{r}$. $\varepsilon(\vec{r})$ is the dielectric constant of the medium at the location $\vec{r}$. The volume integral extends over the entire system. As in the previous section, the liquid is considered a perfect conductor, hence surface charges screen the electric fields completely from the interior of the liquid and the integral vanishes inside the droplet.

Before performing the minimization of the free energy, we have to identify the correct thermodynamic potential for electrowetting. In electrical problems, there are two limiting constraints: constant charge and constant voltage. The corresponding thermodynamic potentials are related by a Legendre transformation [43]. In electrowetting, the voltage is controlled. The thermodynamic potential corresponding to this situation is given by

$$F = F_{if} - F_{el} = \sum_i A_i \sigma_i - \Delta p V - \frac{1}{2}\int \vec{E}(\vec{r}) \cdot \vec{D}(\vec{r})\, dV \qquad (10)$$

Before computing the contact angle decrease, one usually introduces another simplification: the electrostatic energy may be split into two parts. The first part arises from the parallel plate capacitor formed by the droplet and the electrode, with $C = c_d A_{sl}$. The second part is due to the stray capacitance along the edge of the droplet. The fringe fields are mainly localized within a small range around the contact line. Therefore, their contribution to the total energy is negligible for sufficiently large droplets. (In section 2.3.1, we will consider the effect of fringe fields in more detail.) Hence, we find $F_{el} \approx CU^2/2 = \varepsilon_0 \varepsilon_d U^2 A_{sl} / (2d)$.

Apart from this formal explanation, the negative sign in eq. (10) can also be understood intuitively by considering the entire system consisting of both the droplet and

the power supply (the "battery") required to apply the voltage. Upon connecting the initially uncharged droplet to the battery, the charge δQ flows from the battery ($\delta Q_b = -\delta Q$) to the droplet (and to the electrode). The work done on the droplet-electrode capacitor is given by $\delta W = U(Q)\delta Q = Q/C\ \delta Q$, with $U(Q)$ being the charge-dependent voltage on the capacitor. The electrostatic energy stored in the droplet in the final state is $E_{drop} = \int \delta W = Q^2/(2C) = CU_b^2/2$. The work done on the battery is $\delta W_b = U_b \delta Q_b = -U_b \delta Q$. In contrast to $U(Q)$, the battery voltage U_b is constant, such that we obtain a release of electrostatic energy of $\Delta E_{batt} = \int \delta W_b = \int U_b \delta Q_b = -\int U_b \delta Q = -CU_b^2$. Hence the net electrostatic contribution to the free energy is $-CU_b^2/2$. Electrowetting is thus driven by the energy gain upon redistributing charge from the battery to the droplet. The contact angle decreases because this increases C and thus allows for the redistribution of even more charge.

For homogeneous electrodes, the free energy thus reads

$$F = A_{lv}\sigma_{lv} + A_{sv}\sigma_{sv} + A_{sl}\left(\sigma_{sl} - \frac{\varepsilon_0 \varepsilon_d U^2}{2d}\right) - \Delta pV \,. \qquad (11)$$

Eq. (11) has the same structure as the free energy in the absence of electric fields (eq. (1)). By comparing the coefficients, the electrowetting equation (8) is rediscovered. As in the previous section, this derivation is based on the assumptions that (i) the σ_i s are voltage-independent, (ii) the liquid is perfectly conductive, and (iii) contributions from the region around the contact line (due to fringe fields) can be neglected. An important additional insight from this derivation is the fact that the energy gain in electrowetting is actually taking place in the battery, i.e. quite remotely from the droplet itself. This illustrates again effective character of the definition in (eq. (7)).

2.2.3. Electromechanical Approach

Both methods discussed so far predict the same contact angle reduction. However, they do not provide a physical picture of how the contact angle reduction is achieved in mechanical terms. Such a picture can be obtained by considering the forces exerted on the liquid by the electric field. These forces contain contributions due to the response of the free electric charge density ρ_f and the polarization density in the presence of electric

field gradients. This approach was introduced to the field of electrowetting by Jones et al. [39, 44] and recently reviewed by Zeng and Korsmeyer [4]. In the case of simple liquids, one of the most frequently used formulations is the Korteweg-Helmholtz body force density [43]

$$\vec{f}_k = \rho_f \vec{E} - \frac{\varepsilon_0}{2} E^2 \nabla\varepsilon + \nabla\left[\frac{\varepsilon_0}{2} E^2 \frac{\partial\varepsilon}{\partial\rho}\rho\right] \qquad (12)$$

where ρ and ε are the mass density and the dielectric constant of the liquid, respectively. The last term in eq. (12) describes electrostriction and can be neglected in the present context. The net force acting on a volume element dV of the fluid is obtained by a volume integral over eq. (12). As a fundamental consequence of momentum conservation, the same force can also be obtained by an integral along the surface of dV over the momentum flux density of the electric fields, i.e. the Maxwell stress tensor. It seems particularly appropriate because in the perfect conductor limit of electrowetting the entire "body" force actually acts at the surface: ρ_f is zero within the bulk, and free surface charges screen the electric field from the interior. The second term on the r.h.s. of eq. (12), the so-called ponderomotive force density, $\propto\nabla\varepsilon$ vanishes everywhere except at the surface. Neglecting electrostriction, the Maxwell stress tensor consistent with eq. (12) is [43]

$$T_{ik} = \varepsilon_0\varepsilon(E_i E_k - \frac{1}{2}\delta_{ik}E^2) \qquad (13)$$

Here, δ_{ik} is the Kronecker delta function, and $i, k = x, y, z$.

Let us now consider a volume element dV at the liquid-air interface of a perfectly conductive liquid droplet (see Figure (4)). The tangential component of the electric field at the surface vanishes and the normal component is related to the local surface charge density by $\rho_s = \varepsilon_0 \vec{E}\cdot\vec{n}$, where $\vec{n}$ is the (outward) unit normal vector. Furthermore, $\vec{E}$ vanishes within the liquid. To obtain the net force acting on the liquid volume element, we calculate

$$F_i = \oint_\Sigma T_{ik} n_k dA \qquad (14)$$

using the Einstein summation convention. We find that the only non-vanishing contribution is a force per unit surface area dA directed along the outward surface normal $\vec{n}$

$$\vec{F}/dA = P_{el}\,\vec{n} = \frac{\varepsilon_0}{2}E^2\vec{n} = \frac{\rho_s}{2}\vec{E} \qquad (15)$$

where we have introduced the electrostatic pressure $P_{el} = \varepsilon_0 E^2/2$ acting on the liquid surface. P_{el} is thus a negative contribution to the total pressure within the liquid.

How does this local pressure at the surface affect the contact angle of a sessile droplet? The solution of the problem requires a calculation of the field (and charge) distribution along the surface of the droplet. Far away from the contact line, the charge density at the solid-liquid interface is $\rho_{sl} = \varepsilon_0\varepsilon_d U/d$ and the liquid-vapor surface charge density vanishes. As the three-phase contact line is approached, both charge densities increase due to sharp edge effects, as first pointed out in [36]. The force arising from the charges at the solid-liquid interface leads to a normal stress on the insulator surface, which is balanced by the elastic stress. The forces at the liquid-vapor interface, however, contain both a vertical and a horizontal component pulling on the liquid. Kang [45] assumed that the droplet remains wedge shaped and calculated the net horizontal force acting on the liquid by integrating the horizontal component of eq. (15) along the liquid-vapor interface [46]. The field and charge distribution are found by solving the Laplace equation for an electrostatic potential ϕ with appropriate boundary conditions. For the wedge geometry, an analytic solution can be obtained using conformal mapping as first described by Vallet et al. [36] in the context of electrowetting. Both the field and charge distribution are found to diverge algebraically upon approaching the contact line. The resulting Maxwell stress is thus maximal at the contact line and decays to a practically negligible value at a distance of a few d from the TCL [45]. Integrating the horizontal component of the Maxwell stress, we obtain the net force acting on the droplet. For the horizontal component, the result reads

$$F_x = \frac{\varepsilon_0\varepsilon_d}{2d}U^2 = \sigma_{lv}\eta\,. \qquad (16)$$

Given the rapid decay of the Maxwell stress, this force can be considered as localized at the contact line, in a coarse grained sense – on a length scale much larger than d.

Expression (16) can thus be used in the force balance at the contact line in the spirit of Young. As a result, we rediscover eq. (8) for the third time. All three methods are thus equivalent.

It is worth pointing out that the result in eq. (16) can be obtained much more easily if we presuppose that the force *is* localized close to the contact line, as we did implicitly in the previous section when we neglected the contribution of fringe fields. Adapting the ideas of Jones et al. [39, 40, 44, 47], we can calculate the net force by choosing a sufficiently large box around the contact line (see (5)) such that the electric field vanishes along most sections of the closed area Σ. For such a box, only the section along A-B (in (5)) contributes to the integral in eq. (14). As a result, we obtain exactly the same expression as eq. (16). This means in particular that the net force pulling on the contact line is independent of the droplet shape. The result also implies that the edge of any non-deformable, perfectly conductive body would experience exactly the same force [4]. This is in fact not surprising since the net force calculated by integrating the Maxwell stress tensor must be the same as the one obtained by minimizing the energy: the gain in electrostatic energy upon moving the contact line in (Figure 5) by dx is given by the increment in the solid-liquid interfacial area. The contribution of the fringe fields remains constant – independent of the surface profile. (A derivation of the electrowetting equation that makes use of this argument was given in [37]). This shape-independence of the force also implies that the contact angle reduction and the force should be regarded as independent phenomena [48].

2.3. Extensions of the Classical Electrowetting Theory

2.3.1. Fine Structure of the Triple line

In the previous section, we discussed the response of the liquid on a mesoscopic scale. The impact of the fringe fields on the liquid surface in the vicinity of the TCL was ignored. If we look at the surface profile within that range, the liquid surface is expected to be deformed, as first noted by Vallet et al. [36]. In order to calculate the equilibrium surface profile, Buehrle et al. [49] proceeded in analogy with conventional wetting theory in the presence of molecular forces ([30]; see also section 2.1): in mechanical

equilibrium, the pressure Δp across the liquid-vapor interface must be independent of the position on the surface. Therefore any electrostatic pressure $P_{el}(\vec{r}) = \varepsilon_0 E(\vec{r})^2 / 2$ close to the TCL must be balanced by an additional curvature of the surface such that

$$\sigma_{lv}\ \kappa(\vec{r}) - P_{el}(\vec{r}) = \Delta p = const. \qquad (17)$$

Compared to conventional wetting theory, there is one major difference: while the disjoining pressure at a given position $\vec{r}$ depends only on the film thickness at that position [30], the electric field and thus $P_{el}(\vec{r})$ depends on the global shape of the droplet. Thus the droplet shape and the field distribution have to be determined self-consistently. Buehrle et al. [49] addressed this question for the case of droplets of infinite radius. They chose an iterative numerical procedure, which involved a finite element calculation of the field distribution for a trial surface profile followed by a numerical integration of eq. (17) to obtain a refined surface profile. The calculation was two-dimensional, i.e. possible modulations of the profile along the contact line were not included. The procedure was found to converge to an equilibrium profile after a few iteration steps. The following main results were found: (i) the surface profiles are indeed curved, as sketched in (Figure 6). The curvature of the surface profiles and thus the electric field diverge algebraically at the TCL, as in [45] (with a different exponent, however). (ii) The asymptotic slope of the profile at the substrate remains finite and corresponds to θ_Y, independent of the applied voltage. This is only possible because the divergence of the curvature is very weak. In fact, Buehrle et al. [49] confirmed analytically that $P_{el} \propto r^{\nu}$ with an exponent $-1 < \nu < 0$. (iii) The apparent contact angle θ is in agreement with the electrowetting equation (eq. (8)) up to the highest values of η investigated (corresponding to $\theta = 5°$). In view of the discussion in the previous section, this result is not unexpected. It also implies that contact angle saturation does not occur within a two-dimensional electromechanical model – in contrast to some arguments in the literature [45]. Recently, Papathanasiou and Boudouvis repeated the same calculation for droplets of finite size using a slightly different numerical scheme [41]. Except for small deviations from the electrowetting

equation, which may be due to the finite size of their system, they reproduced most of the results presented in ref.[49].

Despite the striking difference between the apparent contact angle and the local one at the contact line, the calculations showed that the surface distortions are significant only within a rather small region of O(d) around the TCL. From an applied point of view, this allows for the comforting conclusion that the simple models, as described in section 2.2 are sufficient as long as the phenomena of interest occur on a length scale larger than d.

2.3.2. Electrolyte Properties

Typical liquids used in electrowetting are aqueous salt solutions. They are conventionally described as perfect conductors with surface charges perfectly screening any external electric field. Microscopically, however, external fields are screened by an inhomogeneous distribution of ions close to the electrolyte surface. For typical ion concentrations, the penetration depth of the electric field is of the order of a few nanometers, given by the Debye length κ^{-1}, with $\kappa = \sqrt{\left(\sum n_i^b q_i^2\right)/\varepsilon_0 \varepsilon_l k_B T}$. (The sum runs over all the ionic species i, with n_i^b and q_i being the bulk concentration and the charge of the i-th species. k_B is the Boltzmann constant and T is the temperature.) The local ion concentration and the electrostatic potential ϕ are coupled via the Poisson-Boltzmann equation [32]

$$\nabla^2 \phi = -\sum_i \frac{q_i n_i^b}{\varepsilon_0 \varepsilon_l} \exp(-q_i \phi / k_B T) \qquad (18)$$

Within this framework, the osmotic pressure

$$\Delta\Pi = \sum n_i^b k_B T (\exp(-q_i \phi / k_B T) - 1) \qquad (19)$$

of the ions has to be taken into account as an extra contribution to the free energy, such that the last term in eq. (10) is replaced by [50]

$$F_{el} = \int \left(\frac{1}{2} \vec{E}\vec{D} + \Delta\Pi \right) dV = \int \left(\frac{\varepsilon_0 \varepsilon_l}{2} (\nabla \phi)^2 + \Delta\Pi \right) dV \qquad (20)$$

In order to calculate F_{el}, a solution of the Poisson-Boltzmann equation is required. For two specific situations the relation between $\Delta\Pi$ and ϕ can be simplified considerably: when $q\phi / k_B T << 1$, the Poisson-Boltzmann equation (as well as the expression for $\Delta\Pi$) can be linearized. In this case, one obtains $\Delta\Pi = \varepsilon_0 \varepsilon_l \kappa^2 \phi^2 / 2$. One should note that $k_B T / e \approx 25mV$ (e: elementary charge) at room temperature. Hence the applicability of the linearized Poisson-Boltzmann equation is limited to situations where the potential drop *within the liquid* is rather small. (While this is usually fulfilled in the center of the droplet, deviations should be expected close to the TCL, where the electric field strength diverges (see preceding section).) The second simple situation corresponds to having monovalent salt solutions with q_1=-q_2 = z e (z: valency) and n_1^{b} = n_2^{b}. In this case, hyperbolic sine and cosine terms appear in eq. (18) and in the expression for $\Delta\Pi$, respectively.

If we consider only the contributions of these terms to the energy per unit area of the solid-liquid interface (i.e. neglecting fringe field contributions), the problem is one-dimensional. Using appropriate boundary conditions (fixed potentials on the electrode and in the bulk liquid), analytic expressions for both ϕ and $F_{\mathrm{el}}/A_{\mathrm{sl}}$ can be obtained. The latter is a correction to the electrostatic contribution in eq. (11), which ultimately leads to a correction to the electrowetting number η in the electrowetting equation (8). More specifically, one obtains for the linearized Poisson-Boltzmann equation [51]

$$\eta_{lin} = \eta \cdot \frac{1}{1 + \varepsilon_d \lambda / \varepsilon_l d} \qquad (21)$$

where $\lambda = \kappa^{-1}$. In the case of monovalent salts, the result is

$$\eta_{mv} = \eta \cdot \left[(1 - \phi_0)^2 + \frac{16 \kappa d}{\nu^2} \frac{\varepsilon_l}{\varepsilon_d} \sinh^2 (\nu \phi_0 / 4) \right] \qquad (22)$$

where $\nu = eU / k_B T$. ϕ_0 is the potential (in units of U) at the solid-liquid interface. It is given by the solution of the equation $1 - \phi_0 - (2\varepsilon_l \kappa d)/(\varepsilon_r \nu) \cdot \sinh(\nu\phi_0 / 2) = 0$ (constant potential boundary conditions [51]). With $\lambda << d$ in typical experiments, it is obvious that the correction in eq. (21) is small. Numerical solutions for ϕ_0 show that the same is true for the correction in eq. (22). As already indicated in section 2.2.1, corrections due to the double layer thus have a rather weak effect on the apparent contact angle.

Kang et al. [52, 53] as well as Chou [54] went one step beyond the above calculation and analyzed specifically the contribution arising from the vicinity of the TCL. They calculated the electrostatic contribution to the line tension τ_e, i.e. to the excess free energy per unit length on the contact line. This excess energy arises from the overlap of the double layers originating from the solid-liquid and from the liquid-vapor interfaces. In ref. [52], analytical results for τ_e were obtained for wedge-shaped surface profiles within the linear approximation of the Poisson-Boltzmann equation. τ_e was found to be of the same order of magnitude as the molecular line tension, i.e. 10^{-12} … 10^{-10} J/m. Numerical solutions for the full non-linear Poisson-Boltzmann equation produced similar results. Like the line tension of molecular origin, the impact of this electrostatic line tension will hence be negligible for droplets with a diameter, of for example, a hundred nanometers or more. This conclusion is supported by numerical calculations of equilibrium surface profiles based on the full Poisson-Boltzmann equation in analogy to the discussion in section 2.3.1 [51].

2.3.3. AC Electric Fields

The theoretical treatment of electrowetting as discussed so far was based on static considerations. In the case of slow variations of the applied voltage, the contact angle and droplet shape can follow adiabatically the momentary equilibrium values. If the AC frequency exceeds the hydrodynamic response time of the droplet (for typical millimeter-sized droplets at frequencies exceeding a few hundred Hertz), the liquid response depends only on the time average of the applied voltage, i.e. the RMS value has to be used in eq. (8). This statement is correct as long as the basic assumptions in the

derivation of the Lippmann equation are not violated: one of them, the assumption that the liquid can be treated as a perfect conductor, however, breaks down upon increasing the frequency. While the dissolved ions can follow the applied field at moderate frequencies and thus screen the electric field from the interior of the liquid, they are not able to do so beyond a certain critical frequency ω_c. Far below ω_c, the liquid behaves as a perfect conductor, far above it behaves as a dielectric. (Electric field-induced actuation of liquids beyond ω_c is still possible. However, the forces in that range are dielectric body forces. For a review on dielectrophoresis, see [10].) For homogeneous bulk liquids, the critical frequency for which ohmic and displacement currents are equal is given by [55]

$$\omega_c = \frac{\sigma_l}{\varepsilon_l \varepsilon_0} \qquad (23)$$

where σ_l and ε_l are the conductivity and the dielectric constant of the liquid, respectively. For an aqueous salt (NaCl) solution with a conductivity of 0.1S/m ($\approx 10^{-4}$ mol/l), we have ω_c=O(10^8 s^{-1}). For demineralized water (σ=4·10^{-6}S/m) ω_c is as low as 4·10^3 s^{-1}. The relevant critical frequency in electrowetting, however, does not only depend on the intrinsic properties of the liquid but also on the geometric and electric properties of the insulating layer. For instance, the characteristic time constant τ_c for charge relaxation in the configuration sketched in (Figure 7) is given by [56]

$$\tau_c = \varepsilon_0 \frac{\varepsilon_d + \varepsilon_l \frac{d}{l}}{\sigma_d + \sigma_l \frac{d}{l}} \qquad (24)$$

Using, for instance d=1μm, l=1mm, ε_d=2, ε_l=81, σ_d=0, and σ_l=0.1S/m (as above), we obtain $2\pi/\tau_c^{-1} \approx 4 \cdot 10^7$ s^{-1} , whereas for demineralized water, we have $2\pi/\tau_c^{-1} \approx 1.6 \cdot 10^3$ s^{-1}.

Figure 8 illustrates this breakdown of electrowetting at high frequency for a millimeter sized droplet of demineralized water. At high frequency, a substantial fraction of the voltage that is applied to the wire drops within the droplet. Therefore, both the voltage at the contact line and thus the energy gain upon moving the latter are reduced.

The continuous nature of the transition from conductive to dielectric behavior as a function of frequency is illustrated in Figure 9 for various salt concentrations.

The details of the contact angle response to the electric field are rather complex and geometry-dependent when the field penetrates substantially into the liquid. The transition from low-frequency electrowetting behavior to high-frequency dielectrophoretic behavior is much better illustrated in experiments that measure the forces exerted by the electric fields. Jones et al. performed a series of experiments in which they studied the rise of liquid in capillaries formed by two parallel electrodes at a distance *D*, each covered with an insulator (Figure 10a) [40, 47]. (Other examples where finite conductivity effects play a role will be discussed in sections 5.3. to 5.5) The authors modeled the liquid as a capacitor in parallel with an ohmic resistor, see (Figure 10a). The electric fields within the different materials can be calculated from elementary electrostatics. Using either the Maxwell stress tensor or the derivative of the total electrostatic energy with respect to the height of the liquid, a frequency-dependent expression for the electric force pulling the liquid upwards is obtained. Balancing this force with gravity, Jones et al. [40] obtained an expression $h = K(\omega)U^2$ with an analytical function $K(\omega)$. The low and high frequency limits are given by

$$h = \begin{cases} \dfrac{\varepsilon_d \varepsilon_0}{4\rho_l g d D} U^2 \quad ; \quad \omega << \omega_c \\ \dfrac{(\varepsilon_l - 1)\varepsilon_0}{2\rho_l g D^2} U^2 \quad ; \quad \omega >> \omega_c \end{cases} \qquad (25)$$

where ρ_l is the density of the liquid and *g* is the gravitational acceleration. The critical frequency $\omega_C = 2\sigma/(D \cdot (2c_l + c_d))$ involves the capacitances per unit area c_l and c_d of the liquid and of the insulating layer, respectively. Figure 10b) shows $K(\omega)$ determined from a series of experimental height of rise vs. voltage curves. Good agreement was achieved with model calculations based on independently measured liquid properties.

In addition to this frequency-dependent reduction of the rise height, Jones et al. [40] also observed a deviation from the predicted parabolic voltage-dependence at high voltage. This observation is in qualitative agreement with earlier experiments [35], in

which electrowetting-induced capillary rise were investigated using DC voltage. According to those authors, the deviation from parabolic behavior in $h(U)$ coincided with the onset of contact angle saturation on a planar substrate made of the same material.

3. Materials Properties

In classical electrowetting theory, the liquid is treated as a perfect conductor. For aqueous salt solutions this corresponds to the limit of either high salt concentration or low frequency, as discussed in the preceding section. The requirements regarding the concentration and nature of charge carriers are not very stringent. A low frequency (f<1kHz), even demineralized water displays substantial electrowetting [40, 57] (see also (Figure 8) and (Figure 10)). Frequently, experiments are performed with salt concentrations on the order of 0.01 to 1 mol/l. Most authors report no significant influence due to the type or concentration of the salt (see for instance [25, 37]). However, Quinn et al. [58] found systematic pH-dependent deviations from eq. (8), which they attributed to specific adsorption of hydroxyl ions to the insulator surfaces. Electrowetting was also observed for mixtures of salt solutions with other species (e.g. glycerol [59-61], ethanol [36, 62]) without deterioration of electrowetting performance. In particular, electrowetting also occurs in the presence of bio molecules such as DNA or proteins [5, 21, 63, 64] and has even been demonstrated for physiological fluids [5]. One complication with biological fluids is, however, that the performance can be affected by unspecific adsorption of bio molecules to the surfaces [63]. Adsorbed bio molecules generally reduce θ_Y and increase contact angle hysteresis. Room temperature ionic liquids [62] were also shown to display electrowetting. Electrowetting is thus a rather robust phenomenon that depends only weakly on the liquid properties.

In contrast, the properties of the insulating layers are much more critical. Substantial activities have been aimed at optimizing the properties of these layers in order to minimize the voltage required for contact angle reduction. At the same time, the materials used should be chemically inert and stable in order to ensure reproducibility and a long lifetime. Two main criteria can be derived immediately from eq. (8): first, the contact angle at zero voltage should be as large as possible, in order to achieve a large tuning range and second, the dielectric layer should be as thin as possible. The first

choice can either be met by using an intrinsically hydrophobic insulator, such as many polymer materials, or by covering hydrophilic insulators with a thin hydrophobic top coating. One possible top coating is self-assembled monolayers (e.g. silanes on glass or SiO_x) [61]. More frequently, however, thin layers of amorphous fluoropolymer (Teflon AF or Cytop) are used. These materials can be deposited by spin coating or by dip coating. Depending on the solution concentration and on the deposition parameters, layers with a thickness ranging from a few tens of nanometers to several micrometers [65] can be produced. Apart from being hydrophobic, Teflon-like layers can be prepared to be very smooth with very small contact angle hysteresis (<10° for water in air). The material is chemically inert and resists both acids and bases. Seyrat and Hayes [65] developed a preparation protocol that leads to very homogeneous Teflon AF layers with high dielectric strength (≈200 V/μm). Furthermore, amorphous fluoropolymer has become very popular, not only as a top coating but also as an insulating layer [19, 20, 58, 60, 65-67].

The critical materials parameter for the insulator is its dielectric strength, or the breakdown field strength E_{BD}. This number limits the minimum thickness of the insulating layer: the voltage required to achieve a desired variation of the contact angle $\Delta\cos\theta$ is given by [65]

$$U(\Delta\cos\theta) = \left(d\sigma_{lv}\Delta\cos\theta/\varepsilon_0\varepsilon_r\right)^{1/2}. \qquad (26)$$

Dielectric breakdown occurs at $U_{BD} = E_c d$. The competition between the two effects is illustrated in (Figure 11). The intersection between the square root function and the straight line determines the minimum insulator thickness required to obtain a certain $\Delta\cos\theta$ for a given dielectric strength – implying a corresponding minimum voltage. The latter can only be reduced by improving the dielectric strength or by using a different material. There are two limitations to this procedure: (i) in view of the diverging electric fields close to the contact line, the breakdown voltage may be exceeded locally, although U/d is still smaller than E_{BD}, and, (ii), the dielectric strength of thin layers may differ from the corresponding bulk values [65].

Popular inorganic insulator materials include SiO_2 [39, 63, 68-71] and SiN [68, 72, 73]. Thin layers with a high dielectric strength can be produced using standard vacuum deposition or growth techniques. In combination with a hydrophobic top coating, they perform well as electrowetting substrates. Compared to Teflon AF (as an insulator), they also offer the advantage of a higher dielectric constant, which contributes to reducing the operating voltage further (see eq. (26)). The dependence on the dielectric constant prompted Moon et al. [68] to study thin layers of a ferroelectric insulator (barium strontium titanate (BST)) with a specifically high dielectric constant of ε_d=180. For a 70nm BST layer covered by 20nm Teflon AF, they achieved a contact angle reduction of 40° with an applied voltage of 15V.

Polymer materials that were used in previous electrowetting studies include parylene-N and parylene-C [22, 35, 37, 40, 42, 47, 74], conventional Teflon films [36, 74, 75], polydimethylsiloxane (PDMS) [76, 77], as well as various other commercial polymer foils of variable surface quality [36, 76, 78, 79]. Parylene films are deposited from a vapor phase of monomers, which polymerize upon adsorption onto the substrate. The surfaces are known to be chemically inert and robust and display a high dielectric strength (200 V/μm; [35]). In electrowetting, Parylene is almost exclusively used in combination with hydrophobic top coatings. One important advantage of the Parylene coatings is that the vapor deposition process allows for uniform conformal coatings on topographically patterned substrates, including the interior of capillaries [22].

Recently, Chiou et al. [80] presented an interesting new approach making use of a photoconductive material, which allowed them to switch the electrowetting behavior optically – a process the authors termed “optoelectrowetting”. The advantage of this approach is that individual addressing of electrodes in a digital microfluidic chip does not require individual electrical connections to all electrodes (20000 in ref. [80]). Electrode activation is achieved by directing a laser beam onto the desired electrode.

4. Contact Angle Saturation

The parabolic relation between the observed contact angle and the applied voltage (eq. (8)) was shown experimentally to hold at low voltage. At high voltage, however, the

contact angle has always been found to saturate. In particular, no voltage-induced transition from partial to complete wetting has ever been observed. (Based on eq. (8), such a transition would be expected to occur at $U_{spread} = \left(2\sigma_{lv} d(1-\cos\theta_Y)/(\varepsilon_0\varepsilon_d)\right)$. Instead, θ adopts a saturation value θ_{sat} varying between 30° and 80°, depending on the system [25, 35-38, 42, 68, 78] (see also (Figure 3)). It has by now become clear that the linear electrowetting models described in section 2 cannot explain the phenomenon of contact angle saturation [41, 49]. However, the latter studies showed that the electric field strength diverges close to the TCL. Although the divergence is cut off at small length scales (κ^{-1}, i.e. a few nanometers), the field strength is expected to reach very high values - several tens or hundreds of volt per micrometer. So far, no consistent picture of contact angle saturation has emerged. Nevertheless, a number of mechanisms have been proposed to explain various observations:

(i) Verheijen and Prins [37] found indications that the insulator surfaces were charged after driving a droplet to contact angle saturation. They suggested that charge carriers are injected into the insulators, as sketched in (Figure 12). These immobilized charge carriers then partially screen the applied electric field. In order to quantify the effect, they assumed that the immobile charges are located at a fixed depth within the insulating layer and that their density σ_T is homogeneous within a certain range ($\approx d$) on both sides of the contact line [81]. With these assumptions, they derived a modified version of eq. (8)

$$\cos\theta = \cos\theta_Y + \frac{\varepsilon_0\varepsilon_d}{2d\sigma_{lv}}(U - U_T)^2, \qquad (27)$$

where U_T is the potential of the trapped charge layer outside the droplet, i.e. $\sigma_T = \varepsilon_0\varepsilon_d U_T / d$. σ_T (and thus U_T) are unknown functions of the applied voltage that depend on the (non-linear) response of the insulator material. The authors determined these functions by fitting eq. (27) to their experimental data. The result was self-consistent, but it was not possible to establish a correlation between this threshold behavior and other known material parameters or microscopic process that could be responsible for the charge trapping. Papathanasiou and Boudouvis [41] tried to establish such a correlation by comparing numerically computed values for the electric field

strength at the contact line (averaged over a certain area) with the dielectric strength of a variety of dielectric materials used in electrowetting experiments. The authors reported good agreement with published experimental saturation contact angles. However, it should be noted that the agreement is sensitive to the size of the box used to average the electric field. The specific choice of 100nm in ref. [41] is not obviously related to any physical length scale of the system (such as κ^{-1}).

(ii) Vallet et al. [36] observed two other phenomena that can coincide with contact angle saturation. They found that the contact line of salt solution droplets luminesces at high voltage. Light was found to be emitted in a series of short pulses with durations of less than 100ns. The wavelength of the emitted light was verified to correspond to known emission characteristics of several ambient gas atmospheres. Simultaneously with the optical observation, the authors measured the current in the system: a series of spikes occurred at the same time as the optical emission pulses, indicating discrete discharge events. Within reasonable error bars, the onset voltage for both processes agreed with the contact angle saturation voltage. Both effects were attributed to the diverging electric field strength close to the contact line.

(iii) In the same publication, Vallet et al. [36] also reported another phenomenon that occurred only for low conductivity liquids (deionized water and water-ethanol mixtures). For these liquids, the contact line was found to become unstable at high voltage leading to the ejection of small satellite droplets from the edge of the main droplet with a characteristic lateral spacing. This observation was later reproduced by Mugele and Herminghaus [61] for mixtures of water and glycerol (see (Figure 13)). Qualitatively, this instability is due to the mutual repulsion of like charges at the contact line. Beyond a certain threshold voltage, surface tension can no longer balance the electrostatic repulsion and the emission of satellites sets in. Vallet et al. performed a linear stability analysis of the contact line. For a sinusoidal perturbation of wavevector q (deduced from the experimental spacing of the satellite droplets) they balanced the electrostatic energy per unit length of the contact line with the additional cost in surface energy. With some simplifying approximations, they found a stability limit that reproduced the experimentally observed onset of the instability. While the model seems to capture the essential physics, it leaves other aspects unresolved, such as the fact that

the instability disappears upon the addition of salt [36] (or at least, the threshold voltage increases substantially [82]).

Finally, there are two other proposed mechanisms that do not refer to the field strength at the contact line: (iv) Peykov et al. [42] suggested that eq. (8) should fail when σ_{sl}^{eff} (cf. eq. (7)) approaches zero. The idea is that the interfacial energy between two phases must always be positive for an interface to remain stable. However, this model has not received broad acceptance because it is not clear whether this criterion is applicable for the *effective* solid-liquid interfacial energy in electrowetting [83].

(v) Contact angle saturation can also occur when either the assumption of a perfectly conductive liquid or a perfectly insulating dielectric or both are violated. In section 2.3.3 we saw already that finite conductivity effects reduce the impact of an applied AC voltage on the contact angle: when the voltage partially drops within the bulk of the droplet, the net force acting on the TCL is reduced. The same effect can occur for DC voltage if the dielectric layer is not perfectly insulating. Shapiro et al. [38] analyzed the field distribution within and around a spherical cap shaped droplet assuming a finite resistivity ratio $A = \rho_d d/(\rho_l R)$ (ρ_d, ρ_l: resistivity of the dielectric and the liquid; R: droplet radius). Their calculations showed that the potential drop within the droplet increases with decreasing contact angle, which causes saturation. Overall, the results seem to compare favorably to some published experimental data. However, the general relevance of the approach – in particular for large resistivity ratios has yet to be demonstrated.

The diversity of explanations indicates that contact angle saturation is still not well understood. Most likely, there may be no unique explanation. It seems clear that diverging electric fields at the contact line can induce several distinct non-linear effects, each of which may independently cause saturation. Which effect dominates depends on the specific conditions of each experiment and identifying these conditions requires more work in the future.

5. Complex Surfaces and Droplet Morphologies

5.1. Morphological Transitions on Structured Surfaces

Classical electrowetting theory was developed for planar substrates with homogeneous electrodes. Applications in microfluidics, however, demand the use of structured substrates (see section 7). In most cases, the substrates are planar and homogeneous but the electrodes are patterned. Sometimes, the surfaces are chemically patterned in addition and in some cases topographical structuring is also used [62, 69, 84]. In most applications one is interested in the behavior of the liquid on a scale that is large compared to the insulator thickness. Hence, effects related to the field distribution close to the contact line can be ignored (as discussed section 2.3.1). The effect of electrowetting is then reduced to a variation of the surface wettability on top of the activated electrode(s). The handiness of eq. (7) now becomes apparent: with this equation, electrowetting on patterned substrates is mapped onto conventional wetting of chemically (and/or topographically) patterned substrates. The free energy F of the system is simply given by [16]

$$F[A] = \sigma_{lv}\left(A_{lv} - \int \cos\theta(\vec{r})\, dA_{sl}\right) \qquad (28)$$

Here, $\cos\theta(\vec{r}) = \cos\theta_Y + \eta(\vec{r})$ with $\eta(\vec{r})$ depends on the voltage applied to the electrode at the position $\vec{r}$. (As in section 2, Eq. (28) has to be supplemented with a constraint of constant volume.) The equilibrium morphology of droplets in electrowetting can thus be calculated by the same methods as the morphology of droplets wetting structured surfaces in the absence of electric fields. The latter subject has attracted considerable attention in recent years both from an experimental and from a theoretical point of view. The presence of either chemical or topographical patterns on surfaces gives rise to complex liquid morphologies. Under favorable conditions, several morphologies may be (meta)stable simultaneously. Abrupt morphological transitions between such competing morphologies can be induced by varying the surface wettability (or some other external control parameter [13, 16, 18, 19, 85]). From an applied perspective, the richness of phenomena gives rise to new opportunities for controlling and manipulating the

behavior of liquids on surfaces. Fundamentally, these phenomena arise from the fact that the prescription of the surface pattern and the liquid volume alone leave substantial freedom for the system to adapt its shape. In particular, the contact angle can assume any value between θ_A and θ_B, when the contact line is pinned along the edge between two domains A and B with the respective contact angles [86].

Except for a few simple geometries, the morphologies of liquid droplets on patterned surfaces have to be computed numerically by minimizing the functional in eq. (28) (under the constraint of constant volume). A popular numerical tool is the public domain software package SURFACE EVOLVER [87]. Application of the SURFACE EVOLVER to electrowetting problems has been demonstrated by several groups [19, 59, 60, 75].

There is one notable exception to the analogy between conventional wetting and electrowetting with patterned substrates: changes of the topology of the liquid are affected by long range electrostatic attraction or repulsion at the contact line. For instance, the coalescence of neighboring droplets can be suppressed by electrostatic repulsion [26]. (Figure 14) illustrates this effect for two adjacent droplets with a specific electrode geometry [59]. For opposing voltages, electrostatic attraction facilitates coalescence (and can even lead to spark generation [60]).

5.2. Patterned Electrodes

The simplest patterned substrate on which droplets display a morphological transition is a hydrophobic surface (e.g. θ =180°) with a stripe of variable wettability (θ_s). For moderate wettability contrasts, there is only one stable morphology, which is a droplet slightly stretched along the stripe. For stronger wettability contrasts (i.e. $\theta_s < \theta_c$, with θ_c being a volume-dependent critical angle), a second morphology appears, namely a section of a cylinder with the contact line pinned along the edges of the stripe. Brinkmann and Lipowsky [18, 85] determined a complete morphological diagram describing the stability of both morphologies as a function of the reduced liquid volume (in units of the cube of the stripe width) and θ_s (see (Figure 15)). Klingner and Mugele [19] verified this prediction experimentally using an electrowetting setup with a stripe electrode. In order to reduce contact angle hysteresis and to achieve a high contact angle at zero voltage as in ref. [18], they used a system of two immiscible liquids (droplets of

salt water in silicone oil). The experiments confirmed the theoretical prediction rather well (see (Figure 15)).

Similar experiments using multilayer substrates with various patterned electrodes separated by dielectric layers were performed by Bienia et al. [75]. For the geometrical conditions of those experiments no morphological transitions occurred. However, the authors proposed an approximate method to incorporate corrections due to field enhancement close to the edges of the electrodes into eq. (28). Continuous morphological changes were also observed for droplets confined between two parallel electrodes at a distance D, each covered with a stripe electrode [57]. (This slit pore geometry is most widely used in microfluidic applications; see section 7.1). For arbitrary misalignment of the stripes in the azimuthal direction, more complex liquid morphologies can be achieved. Again, morphological variations were found to be continuous and could be described based on eq. (28) using the SURFACE EVOLVER [57, 59].

For slit pores with uniform walls slightly inclined with respect to each other such that the gap width D decreased with increasing height, Wang and Jones [47] reported an instability of a rising meniscus beyond a certain threshold voltage U_T (see (Figure 16)). For sufficiently strong inclination, the meniscus height was found to jump abruptly from a certain intermediate height all the way to the top of the electrodes. This bifurcation phenomenon comes about because the energy required to raise the meniscus by Δh decreases with increasing height h, while the electrostatic energy gain remains constant.

5.3. Topographically Patterned Surfaces

The effect of topographical surface patterns on wetting is even more dramatic than that of lateral chemical patterns. Superhydrophobicity and –hydrophilicity are amongst the most spectacular consequences of surface roughness [11]. The influence of roughness on wetting is twofold, as illustrated in (Figure 17). On the one hand, (Figure 17a), roughness increases the actual solid-liquid interfacial area A_{sl} with respect to the apparent, projected one $A_{sl,p}$. As a result, the contact angle on a rough surface will be increased or decreased as compared to the contact angle on a smooth surface of the same material, depending on whether $\theta_Y > 90°$ or $\theta_Y < 90°$, respectively. This effect is

classically described by Wenzel's law, $\cos\theta = r \cdot \cos\theta_Y$, with r=$A_{sl}/A_{sl,p}$. Quantitatively, the validity of this picture turns out to limited to a range of $\theta_C < \theta_Y < 90°$, with θ_C depending on the surface roughness [88]. On the other hand, for $\theta_Y > 90°$, a completely different liquid morphology becomes possible (Figure 17)b). In this morphology A_{sl} is dramatically reduced and much of the apparent solid-liquid interface is in fact a liquid-vapor interface. This reduction in A_{sl} gives rise to a very high mobility with extremely small contact angle hysteresis. In this state the contact angle is given by the Cassie-Baxter equation, $\cos\theta = -1 + f \cdot (1 + \cos\theta_Y)$, where f is the fractional surface area of the pillar tops. The range of stability of both morphologies depends on the aspect ratio, on the spacing between the pillars, and of course on the contact angle [89]. Krupenkin et al. [62] demonstrated the use of electrowetting to switch a liquid droplet from the Cassie Baxter to the Wenzel morphology. They fabricated nanopillars with a diameter of 350nm and a height of 7µm by dry etching a Si wafer. Each pillar had a conductive core of Si covered by a thermally grown insulating SiO layer and a hydrophobic top coating. The transition between the two morphologies was induced at a well-defined threshold voltage. Samples with a variety of different pillar spacings showed that $\cos\theta$ indeed increases linearly with increasing f in the rolling ball state, whereas the opposite tendency was observed in the Wenzel state (as qualitatively expected due to the increase of r with increasing f). In addition, the authors observed another transition from the Wenzel state to a morphology where the droplets spread over the entire surface. Such a state is indeed expected [88]. In contrast to the morphological transition discussed in the previous section, the transition between the Cassie Baxter and the Wenzel state in ref. [62] was not reversible. More recently McHale et al. [84] investigated electrowetting on similar surfaces, with an emphasis on dynamic phenomena.

Baret et al. [69] investigated the wetting behavior of liquids in rectangular trenches with depth and width of 10 – 20µm and 15 – 50µm, respectively. The trenches were etched into a Si wafer and subsequently thermally oxidized and hydrophobized using alkyl silane monolayers. (Figure 18)a) shows a top view of a droplet overlapping with several channels. At zero voltage, there is minimal leakage of the liquid from the droplet into the channels. Beyond a certain threshold voltage, filling of the channels suddenly starts and becomes more and more pronounced the higher the voltage (Figure

18)b). In fact, the trenches are expected to be empty above a certain critical contact angle and completely filled below it if brought in contact with a reservoir such as the droplet in this experiment. The critical angle is determined by the requirement of equal pressures in the channel and in the reservoir. As the contact angle decrease, the curvature of the surface at the end of the liquid fingers (and thus the pressure) decreases. When it becomes equal to the pressure in the droplet filling suddenly sets in (see (Figure 18)b). Interestingly, the length of the liquid fingers remains finite even beyond the critical voltage. Moreover, the length depends on the frequency of the applied voltage. This is due to the finite conductivity effects discussed in section 2.3.3: Due to the small cross section of the trenches and the finite conductivity of the liquid, the ohmic resistance along the channel is substantial. Since the liquid is also coupled capacitively to the substrate, the liquid-filled channel behaves as an electric transmission line. As a result, the voltage at the tip is smaller than the applied voltage and depends on the length of the channel. By taking these effects into account, Baret et al. were able to rescale their frequency dependent data onto a single master curve (see inset of (Figure 18)b).

5.4. Self-Excited Oscillatory Morphological Transitions

An electrode configuration that is particularly relevant to lab-on-a-chip type applications of electrowetting consists of a liquid droplet bridging the gap between two parallel electrodes (Figure 19). In the absence of electric fields, the equilibrium shapes and stability limits of the two competing liquid morphologies (A: capillary bridge; B: two droplets) have been studied in detail [12]. Capillary bridges break when the reduced substrate separation D (in units of $V^{1/3}$) exceeds a certain critical value $D_{c,A}$ which depends on the contact angle. Two separated droplets become unstable upon geometric overlap, i.e. below another – again contact angle-dependent – critical reduced separation $D_{c,B}$. Under electrowetting conditions, these two stability limits are affected differently because the topology of the two morphologies is different [20]. The capillary bridge is simply connected, which means that the liquid is at a fixed potential corresponding to half of the applied voltage and therefore the contact angle decreases with increasing voltage. As a result, $D_{c,A}$ is a monotonously decreasing function of the applied voltage (solid line in (Figure 20)). In contrast, each of the separate droplets assumes a different

potential, namely the one of the electrode the droplet is attached to. As a result, the contact angle remains equal to θ_Y, independent of U. However, the droplets attract each other electrostatically and as a result $D_{c,B}$ is an increasing function of the applied voltage (see dashed line in (Figure 20)). Given the opposing slopes, $D_{c,A}$ and $D_{c,B}$ cross at a certain critical voltage. Beyond this voltage both morphologies are unstable for plate separations between the two instability limits. Under these conditions, the liquid was found to oscillate periodically between the two morphologies. The oscillation rate (1 s^{-1}) was found to be independent of the applied AC frequency (> 1kHz). It is determined by the relaxation of charge deposited on the separate droplets immediately after break up: the contact angle slowly relaxes back to θ_Y as the charge disappears via leakage currents [60]. This oscillatory behavior is reminiscent of the so-called "beating mercury heart" in which a mercury droplet under an acid solution periodically attaches to and detaches from a Fe nail when the latter is immersed into the acid and brought sufficiently close to the mercury surface [90]. The dynamics of the beating mercury heart, however, are far more complex. They are in fact related to the kinetic of electrochemical reactions at the surfaces of the mercury and the nail, respectively.

More recently, Baret et al. [91] found that much faster oscillations can be achieved if the conductivity and the frequency of the applied voltage are matched, such that the charge on the droplet disappears during the pinch-off process when the capillary bridge breaks. The frequency of these oscillations (several tens of Hertz) is determined by the hydrodynamic response time of the droplet to (sudden) changes of the contact angle. These fast oscillations were also found to be useful in promoting mixing in droplets. (Figure 21) shows a series of snapshots recorded during the oscillation of a droplet that was stained with fluorescent dye in its top half in the initial state. The entire droplet (of millimeter size) was mixed within a few seconds, more than 100 times faster than purely diffusive mixing [92].

5.5. Electrostatic Stabilization of Complex Morphologies

The contact line instability discussed in the context of contact angle saturation in section 4 can give rise to rather complex liquid morphologies. In particular, the satellite droplets generated by the instability do not necessarily detach from the main droplet.

Instead mother and satellite droplet sometimes remain connected by a thin liquid bridge (see inset (Figure 13)) [61]. It is obvious that the curvature of the liquid surface (and thus the Laplace pressure) in the satellite droplet is substantially higher than in the mother droplet. Nevertheless, these complex liquid morphologies were found to be stable for poorly conductive liquids and AC voltage of sufficiently high frequency. The reason is related to the finite conductivity of the liquid, as illustrated in (Figure 22). If the ohmic resistance of the liquid channel is larger than the capacitive impedance between the satellite droplet and the substrate electrode, there is a strong electric field around the satellite which causes an additional electrostatic pressure that pulls along the outward direction of the satellite droplet's surface. It turns out that this electrostatic contribution to the total pressure scales with U^2/r_{sat}^2, where r_{sat} is the radius of the satellite droplet [61]. Since the Laplace pressure scales only with $1/r_{sat}$, small droplets can be stabilized with respect to larger ones by this mechanism. This experiment illustrates that the class of liquid microstructures eligible for mechanical stability is no longer restricted to morphologies with constant mean curvature. In the presence of suitable electric fields, more complex morphologies may also be stabilized.

5.6. Competitive Wetting of Two Immiscible Liquids

Another degree of complexity arises when electrowetting experiments are performed in an ambient oil environment rather than in a gas atmosphere. Both liquids, the oil and the aqueous phase compete in wetting the solid surface. Depending on the microscopic interactions (e.g. short range chemical forces, long range van der Waals forces), various scenarios are possible. At finite voltage, electrostatic interactions alter the balance of molecular forces [93]. Since electrowetting substrates are typically hydrophobic, complete wetting of the oil phase at zero voltage is frequently observed. In this case, θ_Y is essentially 180° and the aqueous phase is separated from the substrate by a thick oil layer [94]. As the voltage is increased, electrostatic interactions press the aqueous phase towards the substrate and decrease the thickness d_{oil} of the oil film. For sufficiently thin oil layers, the free energy (per unit area) of the oil film in a van der Waals system is given by [93]

$$F(d_{oil}) \approx \gamma_{so} + \gamma_{ow} + \frac{A}{12\pi\, d_{oil}^2} - \frac{c_d U^2}{2}\left(1 - \frac{\varepsilon_d d_{oil}}{\varepsilon_{oil} d}\right). \qquad (29)$$

where γ_{so} and γ_{ow} are the solid-oil and oil-water interfacial energies, A is the Hamaker constant (>0 for long range wetting) and ε_{oil} is the dielectric constant of the oil. This function has a minimum corresponding to the equilibrium thickness of the oil film at $d_{oil}^* = (\varepsilon_0 \varepsilon_{oil} A/(3\pi\, c_d^2 U^2))^{1/3}$, which can be tuned continuously by varying U. In spite of the obvious practical importance of this oil film – both for reducing contact angle hysteresis as well as for preventing unspecific adsorption of biomolecules onto the substrates [5] – little is known experimentally. Preliminary experiments by Bienia et al. [74] indicate that a characterization is possible using ellipsometry.

6. Dynamic Aspects of Electrowetting

Most of the theory and experiments described so far focused on static properties. For many practical applications, however, the dynamic response of the liquid is of interest. As discussed in section 2.2.3 (see ref. [48]), the reduction of the (equilibrium) contact angle and the net force acting on a droplet in electrowetting should be considered as two independent observables. In dynamic situations, this distinction becomes even more pronounced. On the one hand, the contact angle assumes a time- and speed-dependent value which is determined by local dissipative processes and flow fields in the vicinity of the TCL. On the other hand the entire droplet also responds on a global scale, e.g. by a translation of its center of mass, as for instance in lab-on-a-chip type applications to be discussed in section 7.1. This global response is obviously not only affected by local effects close to the contact line but also by viscous dissipation in the bulk [95]. A consistent hydrodynamic description (ignoring specific effects related to contact line dynamcis) was presented in [4].

Let us first consider center of mass translations. One immediate observation is that Reynolds numbers in electrowetting-induced flows are rather low. With typical velocities on the order of $v \approx 10^{-2}$ … 10^{-1}m/s and droplet sizes of $R \approx 10^{-3}$m or less, one

obtains $\mathrm{Re} = \rho v R / \mu \approx 100$ for water and even smaller for more viscous liquids. Hence, the flow is usually laminar. The forces generated by the electric field have already been discussed in detail in section 2. Within the range of validity of the electrowetting equation (eq. (8)) EW-induced motion is analogous to the motion of droplets on chemically heterogeneous substrates, which was described e.g. by Brochard [96] (see also [30] and references there). The driving force (per unit length *dy* of the contact line) is determined by the energy gain upon displacing the contact line by *Δx*: $\Delta E / dy = \left(\sigma_{sl}^{eff} - \sigma_{sl}\right)\Delta x = -\left(\varepsilon_0 \varepsilon_r U^2 / d\right) \cdot \Delta x = -\sigma_{lv} \eta \, \Delta x$. Hence the force f (per unit length) is given by $f = -\Delta E / \Delta x = \sigma_{lv} \cdot \eta$ (see eq. (16)). This force acts locally perpendicular to the contact line. In order to extract the net force on a droplet, the (vectorial) local force has to be integrated along the contact line using the appropriate local value of $\eta = \eta(\vec{r})$ [97] (see (Figure 23)). As mentioned above, there are several contributions to the net force which oppose the motion. Dissipation contains contributions both from the contact line as well as from the bulk of the droplet. Two extreme cases can be considered [96]: if the dissipation is dominated by contact line friction, the pressure within the droplet equilibrates quickly and the droplet retains its spherical cap shape but with a time-dependent dynamic contact angle θ_d (see (Figure 24)a). If, on the other hand, bulk viscous effects dominate, the contact angle assumes its local equilibrium angle everywhere along the contact line. As a result, the drop shape is non-spherical and a hydrodynamic pressure gradient arises and drives fluid flow within the droplet (see (Figure 24)b). In most practical situations, an intermediate behavior is expected to be observed with both contributions present simultaneously. Quantitative investigations of the center of mass motion are presented in refs. [76, 97, 98]. Two important findings should be noted: first, liquid motion could only be achieved above some threshold voltage. This observation is attributed to contact angle hysteresis: droplet motion can only set in when the contact angle on the leading (trailing) edge of the droplet exceeds (is smaller than) the local advancing (receeding) contact angle. The threshold voltage to initiate droplet motion is found to decrease upon immersing the liquid droplet into an oil environment [76], as expected on the basis of the discussion in section 5.6.

Second, it is found that contact line friction contributes substantially to the dissipation of the submillimeter liquid structures investigated [97, 98].

Contact line friction creates a link between the center of mass motion of the droplet and the dynamic behavior of the contact angle: it is well-known that classical hydrodynamics cannot describe the motion of the TCL. The flow fields required to move the wedge shaped edge of the droplet (see (Figure 2)) give rise to a diverging stress, which in turn requires an infinite force to move the TCL. Several strategies, including the phenomenological concept of slip at the solid-liquid interface, were introduced to resolve the problem (see e.g. [30, 99-101]). In the context of electrowetting, contact line friction was analyzed within the framework of the molecular kinetic model [97, 98, 102, 103]. This model pictures contact line motion as a series of discrete random jumps on a molecular scale involving energy barriers and microscopic adsorption sites [104]. These molecular scale processes give rise to a friction force (per unit length) that is given by the product of a friction coefficient ξ and the velocity v of the contact line. Blake et al. [102] studied the dynamic contact angle of a liquid curtain (glycerol water mixture) wetting a Teflon substrate that was moved at a constant velocity v. The dynamic contact angle increased with increasing substrate speed both in the absence and in the presence of an applied voltage. For any given velocity, the contact angle decreased upon applying a voltage U. For a given U, the variation of $\Delta\cos\theta$ (with respect to zero voltage) turned out to be independent of v, in agreement with the prediction of the molecular kinetic model.

Decamps and DeConinck [103] analyzed the response of the contact angle of a glycerol-water droplet on a Teflon surface upon applying a voltage step. The contact angle decreased from $\theta_Y \approx 110°$ to its voltage-dependent final value within less than 0.2s. The time-dependence was fitted with a formula based on the molecular kinetic model. For a relatively rough Teflon surface (contact angle hysteresis ≈50°), the authors deduced a contact line friction coefficient $\xi \approx 4$ Pa·s. A similar value was recently found for ethylene glycol in capillary rise experiments by Wang and Jones [98].

While the experimental results discussed above were interpreted within the framework of the molecular kinetic model, this does not rule out that other approaches to the problem of contact line motion may be equally well suited to explain the experimental observations.

7. Applications

7.1. Lab-on-a-Chip

Lab-on-a-chip applications of electrowetting were mainly promoted by two laboratories, the one of Richard Fair at Duke University (for a recent review focused on the activities of this laboratory, see [5]) and the one of CJ Kim at UCLA (see [71] and references there) with several other groups joining in more recently [105-107].

The principal idea is to provide a substrate with a series – preferentially an array – of individually addressable electrodes that allow for moving droplets around along arbitrary paths, depending on the freely programmable activation sequence of the electrodes. Small droplets can be extracted from larger reservoir droplets transported to specifically designed locations [71, 108]. The small droplets can be merged and mixed to induce chemical reactions [109-111]. For the practical realization of such a device, several aspects have to taken into account: (i) electrowetting requires electrical contact to the liquid. The usual procedure of immersing wires into the droplets (see (Figure 1)) is not practicable for lab-on-a-chip applications. Therefore, a sandwich design consisting of two parallel substrates with the liquid confined in between has become standard (see(Figure 25)). One of the substrates contains the patterned electrodes required for liquid actuation. The other substrate (the top surface in (Figure 25)) consists of a homogeneous electrode that provides electrical contact to the droplet(s) independent of its (their) position. This electrode, which is frequently made of a transparent ITO layer on a glass substrate, is usually covered with a thin hydrophobic layer that gives rise to large contact angle and weak contact angle hysteresis but does not prevent electrical contact. (ii) In order to allow for reliable droplet actuation, droplet edges must overlap with at least two adjacent electrodes. As a consequence, the smallest liquid volume that can be transported is determined by the size of the electrodes. With substrate separations of 100-500μm and electrode sizes on the order of 1mm, this means typical droplet volumes of 0.1 …1μl. The reliability of droplet actuation is frequently improved by a zig-zag design of the electrode edges [112]. (iii) The vapor pressure of water is rather high at room temperature. Liquid evaporation is therefore a critical issue. The problem is somewhat

reduced by the two plate sandwich design, but thermal treatments as required for some biochemical assays call for additional measures against evaporation. Therefore, lab-on-a-chip devices are frequently operated with oil as surrounding medium [5].

Routine tasks such as moving, merging, mixing, and splitting of droplets have been demonstrated, first independently and later integrated into more complex devices (see [5], [71], and references therein). For typical droplet volumes in the micro liter range, droplet motion typically sets in above a certain threshold voltage of a few tens of volts. Above that threshold, the droplet speed increases rapidly with the applied voltage, reaching values of several cm/s. The detailed numbers depend strongly on the insulator thickness and the quality of the surfaces. Recent work aims at reducing activation voltages to approximately 20V or less, which would simplify practical applications involving battery powered hand held devices for medical applications.

With basic fluid manipulation techniques being established, the next step towards biotechnological applications of electrowetting-based devices is to demonstrate the biocompatibility of the materials and procedures. One challenge for all lab-on-a-chip devices is the tendency of biomolecules to adsorb unspecifically onto hydrophobic surfaces [113]. In the case of electrowetting-based devices this has a specifically detrimental effect: irreversible adsorption of biomolecules reduces the contact angle permanently, thereby compromising the performance of droplet actuation. Yoon and Garrell [63] recently investigated the electrowetting-behavior of droplets of DNA and protein solutions in an ambient air environment. They found that both unspecific adsorption via hydrophobic interaction as well as electrostatic interactions contribute to the adsorption. The latter depends strongly on the charge carried by the specific protein and on the polarity as well as the waveform of the applied voltage. Biomolecular adsorption seems to be suppressed even more efficiently by using an oil phase as the ambient medium instead of air. Srinivasan et al (see [5] and references there) reported not only the successful actuation of various protein solutions but also of physiological fluids such as whole blood and urine. Even after 25000 cycles, droplets could still be actuated with only a minor increase in activation voltage. The reduced adsorption of proteins is attributed to the thin oil film wetting the hydrophobic substrate and preventing direct contact between the droplet and polymer surface [5], as described in section 5.5.

Qualitatively this strategy seems to be successful. However, detailed studies regarding its efficiency and the underlying fundamental mechanisms are lacking.

Other biotechnology-related applications use electrowetting to assist in the handling of tiny amounts of liquid. For instance, DNA and protein arrays are nowadays standard tools in genome research and drug development. Conventionally, arrays are produced using photolithography or more recently, by spotting droplets onto surfaces using e.g. ink jet techniques. In order to reduce the typical spot sizes to 1μm or less, new approaches have been developed, such as dip-pen nanolithography [114]. In this technique, the ink is deposited by establishing direct mechanical contact between the pen and the surface. One challenge of dip-pen lithography is to deposit a sufficiently large amount of liquid onto the pen in a controlled fashion, in order to maximize the number of spots that can be written without refilling the pen. Belaubre et al. [115, 116] presented a microcantilever design for dip-pen lithography, in which electrowetting was used to increase and control the amount of liquid a reservoir on the pen. Using this approach, they were able to write arrays of more than a hundred spots from a single loading with spot sizes from the femtoliter to the picoliter range, containing fluorescent-labeled oligonucleotides and proteins. The same principle on a somewhat coarser scale was used for a glass-tube based micro injector by Hoshino et al. [117]. Yi and Kim [118] presented a principle which they termed “soft printing”. In this approach tiny droplets of controlled volume (~100nl) containing the desired bio material are produced on top of hydrophobic surface. They are deposited onto a hydrophilic carrier by bringing the latter close enough to the hydrophobic surface such that the droplet is transferred by capillary forces. The droplet transfer is thus a rather gentle process, which does not involve splashing or excessive shear forces acting on the biomolecules. The generation and positioning of the pre-metered droplet is performed using electrowetting. Furthermore, electrowetting was used to prepare peptide and protein samples for matrix assisted laser desorption/ionization mass spectrometry [64].

Huh et al.[70] presented an application in which electrowetting was used to manipulate the flow in a channel-based microfluidic system for an air-water two-phase flow (see (Figure 26)). By activating the electrodes the path of the liquid jet within the channel could be controlled on a millisecond time scale. Rapid control of the stream

position may be useful for sorting application. Living cells were shown to survive transport through this system. Cheng and Hsiung presented an EW-driven valve inside a microchannel for continuous flow [119]. The channel walls were partially made of Teflon. Using plasma etching, the Teflon coating was made hydrophilic everywhere inside the channel except for an active area, which thus acted as a hydrophobic barrier. Upon activating electrodes embedded in the active area of the channel walls, the barrier was lowered and water could flow through the channel. Shen et al. [120] produced a chemoreceptive CMOS chip in which they also controlled the filling of closed channels using electrowetting.

7.2. Optical Applications

7.2.1. Microlenses

In mechanical equilibrium, the liquid-vapor interface of sessile droplets has a spherical cap shape. Depending on the refractive index contrast light passing the interface is refracted as in a classical spherical lens made from glass or some other suitable solid material. In contrast to solid lenses, however, liquid lenses are flexible. Their curvature and hence their focal length can be tuned by adjusting their shape. Obviously, this can be achieved by changing the contact angle of sessile droplets via electrowetting. This allows for the design of optical systems with variable focal length that can be addressed purely electrically, as first described by Peseux and Berge [121]. These authors designed a closed cell filled with two immiscible liquids, namely a non-polar oil droplet within an aqueous salt solution. Both liquids were density matched to within 10^{-3} both in order to eliminate the influence of gravity on the interface shape and in order to reduce the susceptibility of the lens to external mechanical shocks. At low voltage, the water contact angle is high, i.e. the oil droplet has a low contact angle and vice versa (see (Figure 27)a). A combination of wettability patterns on the bottom surface and gradients in the thickness of the dielectric layer were used in order to center the droplet on the optical axis of the device. In (Figure 27)b, the refractive power and focal length of the lens are shown as a function of the applied voltage. The lens operated without noticeable hysteresis – presumably thanks to a thin lubricating oil film (see section 5.6) – and could be switched

more than 10^6 times without any sign of degradation. Switching speeds on the order of 10 ms were achieved for a lens with a diameter of 2.5 mm. Maximal speed requires precise adjustment of the liquid viscosity such that the drop motion is critically damped – otherwise the droplet either oscillates several times or relaxes only slowly towards the new equilibrium shape. Krupenkin et al. [73] describe a similar system with patterned electrodes that allows for lateral positioning of the lens. In their case, the activation voltage was as low as 10V. The same authors also presented an interesting study in which they used photopolymerizable conductive liquid droplets to produce microlenses of controlled focal length [122]. The shape and thus the desired focal length were tuned through electrowetting of the monomeric polymer solution. At fixed voltage, the droplets were cured by UV illumination. Subsequently, the voltage could be removed and the (now solidified) droplets kept their shape.

One potential application of interest is in variable focus systems for mobile phones with integrated CCD cameras [123, 124]. Challenges in this application include harsh mechanical shocks as well as a large range of required operating temperatures. Kuiper and Hendriks [123] recently presented yet another design of an electrowetting lens system for this type of application. Theses authors confined the liquid laterally inside a (short) capillary with an internal diameter of 3mm. By applying a voltage of up to 120 V, they could vary the refractive strength from -100 to +50 diopters. The authors also discuss the suppression of chromatic aberrations through the addition of specific solutes to the liquids. Achromatism can thus be achieved easily and at low costs.

7.2.2. Fiber Optics

Electrowetting was assessed in the 1980s as a possible mechanism for switching light in fiber optic applications [125-127]. Mercury droplets were moved inside channels to provide either a reflective surface or to allow for the transmission of light in an optical multiplexer. More recently, the focus shifted to controlling the transmission of optical fibers that were locally stripped of their coating [72, 79]. For stripped fibers, the electromagnetic field of some modes, in particular so-called cladding modes, partially leaks out of the fiber into the surrounding medium. By surrounding the active (stripped) part of the fiber with liquids of suitably chosen refractive index, the transmission through the fiber can be tuned substantially. (Figure 28)a shows a schematic of the setup. The

optical fiber passes a straight section of a racetrack shaped channel with rectangular cross section. The channel is filled with two immiscible liquids of controlled refractive index. One of them is an aqueous salt solution that can be moved via electrowetting such that it overlaps with the active region of the fiber. Both narrow and broad band optical attenuation were demonstrated using different types of optical fibers. (Figure 28)b shows an attenuation of >20dB over a range of 40nm obtained with a fiber with a long period grating that gave rise to specifically strong coupling to cladding modes. One of the interesting properties of this electrowetting-based attenuator is its low power consumption (<1mW) along with the fact that no power is required to hold the droplet in either position after the switching process. Reported response times of the initial design were on the order of 100ms [79].

7.2.3. Display Technology

Feenstra and Hayes [66] presented an electrowetting-based reflective display with potential use in the field of electronic paper. The concept is very simple (see (Figure 29)): an oil droplet containing dissolved dye is confined laterally to a square pixel. At zero voltage, the oil forms a continuous layer wetting the hydrophobic insulator (0.8μm Teflon AF) at the bottom of the pixel. The rest of the pixel between the oil film and the top cover is filled with a transparent aqueous salt solution. Incoming light is strongly absorbed by the dye. Upon applying a voltage, the oil film ruptures and all the oil contracts into one corner of the pixel that can be predefined by a passive chemical wettability pattern. The dye thus covers only a small fraction of the pixel in the activated state. This gives rise to increase in reflectivity (averaged over an entire pixel) from 2.5% at zero voltage to 35% at the absorption wavelength of the dye with an activation voltage of 20V. Any intermediate reflectivity – corresponding to a partially retracted oil film – can be stabilized by stopping at an intermediate voltage thus allowing for arbitrary gray levels. The switching speed of the display depends on the pixel size, on the thickness and viscosity of the oil film as well as on other geometric parameters [67]. (Figure 30) shows that the response time of a 250 x 250 μm^2 pixel is sufficiently fast for video applications. Both the retraction and the spreading of the droplet occur on the same time scale.

By splitting each pixel into three subpixels and arranging two oil layers with different dyes in combination with a color filter on top of each other, Feenstra and Hayes

were also able to generate arbitrary colors [66]. The reflectivity of these color displays was four times strong than that of liquid crystal displays.

7.3. Miscellaneous Applications

Another notable application is the optical absorber presented by Prins et al. [22]. The device was based on electrowetting-induced capillary rise. The authors designed a matrix of 4000 individually addressable capillaries with a diameter of 0.35mm and a length of 20mm. The capillaries were fabricated from commercially available metallized polymer foil that was laser welded to form a honeycomb structure. Electrowetting was used to switch the contact angle of aqueous salt solutions from >90° to <90° giving rise to capillary depression and capillary rise, respectively. Liquid actuation over a distance of 10 mm was achieved within ≈0.2 s. By dissolving suitable absorbers in the liquid, this device can be used as a switchable optical filter. By dissolving heavy salts, Prins et al. demonstrated this principle for the specific case of an x-ray absorber potentially useful for minimizing unnecessary exposure of patients to radiation in medical applications.

Kim et al. [128, 129] created a number of microelectromechanical systems (MEMS) applications based on the continuous electrowetting effect that was also used earlier by Beni, Jackel et al. [125-127]. These systems are based on mercury droplets moving in electrolyte-filled channels (see (Figure 31)). By applying just a few volts along the channel, a potential gradient and thus a charge density and interfacial energy gradient is established along the mercury droplet, which then propels the droplet. A small micro motor was presented, in which the mercury droplet could run continuously around a circular track with a diameter of 2 mm. At a rotation speed of 420 rpm, the power consumption was as low as 10-30 μW for an operating voltage of 2.8 V. Other applications of this principle include switches, latching relays, optical shutters, and micropumps [128, 129].

8. Conclusions and Outlook

The basic principles of electrowetting and electrowetting on dielectric are well understood. If a sessile droplet of a conductive liquid is subject to an external electric field, the distribution of charge carriers on the droplet surface redistribute and the surface morphology adjusts to reach a new equilibrium configuration. Depending on the level of accuracy that is required, different levels of complexity in the description can be chosen (see section 2). On a global scale, the equilibrium surfaces remain surfaces of constant mean curvature because the electric field vanishes along the liquid-vapor interface and therefore capillarity determines the morphology. Under these conditions, electrowetting can be considered simply as a means of controlling the contact angle. Electrowetting on any surface be it homogeneous or structured is then equivalent to conventional wetting on a surface with an identical distribution of local contact angles. This level of description, summarized by the basic electrowetting equation (eq. (8)), proves to be sufficient for almost all practical applications of electrowetting. It has been shown to break down, however, under two related conditions: Within a range corresponding approximately to the thickness of the insulator, electric fringe fields cause distortions of the liquid-vapor interface. Upon approaching the contact line, the electric field strength and the mean curvature of the surface diverge; a result that has yet to be confirmed experimentally. The diverging electric fields are also believed to be responsible for the second limitation of the electrowetting equation, namely contact angle saturation at high voltage, which remains *the* fundamental unresolved problem of electrowetting. Apart from finite conductivity or finite frequency effects, most authors seem to agree that contact angle saturation is related to the onset of some non-linear response of the materials involved to the diverging electric fields. To predict the saturation angle for a given material combination, however, remains a substantial challenge.

The control of the wettability of structured surfaces, in particular topographically structured surfaces, offers rich opportunities for future work. Abrupt variation of the liquid morphology triggered by altering the wettability locally or globally can be rather dramatic, as has been demonstrated by some examples given. The full spectrum of possibilities – in particular with respect to applications – remains to be explored. The

combination of electrowetting with conventional channel-based microfluidic systems offers many opportunities.

From an applied perspective, it is highly desirable to minimize the voltage required to achieve a given contact angle reduction. This is essentially a challenge for material properties. Both current approaches, composite substrates of solid state insulators (e.g. SiO_2) with hydrophobic top coatings as well as homogeneous polymeric insulators, have reached the range of sub-micrometer thickness. Activation voltages of few tens of volts have been demonstrated in several laboratories. Future improvements will probably enable many electrowetting devices with driving voltages in the range of 10-20V.

Several applications of electrowetting have already reached or are about to reach the state of commercially available products. Electrowetting-controlled variable focus lenses are commercially available. Cameras for mobile phones or handheld PCS with EW-controlled lenses were presented at major trade shows in 2005, opening the door to a huge market. If high quality liquid lenses of larger diameter (e.g. several cm) can be produced, an even broader range of variable focus optics where mechanical compactness is an issue becomes accessible. Display technology and fiber optics offer opportunities for similarly broad markets. Biomedical applications for point-of-care testing of physiological fluids are also within reach. Test devices controlled by handheld PCs are under development in several companies. Commercial products seem to be achievable within few years time from now. Additional fields of applications may exploit the overwhelming strength of capillary forces at small scales for mechanical actuation.

9. Acknowledgements

We would like to thank Stephan Herminghaus and Tom Jones for numerous discussions and for their comments on the manuscript. We are also grateful to Dirk van den Ende and to Ileana Carpen for corrections of the manuscript. Furthermore we thank Jürgen Bührle, Anke Klingner, Renate Nikopoulos, and Dagmar Steinhauser for their experimental work on electrowetting in recent years in my laboratory. Financial support is acknowledged from both the German Science Foundation within the priority program

Wetting and Structure Formation at Interfaces and from the Institute of Mechanics, Processes and Control – Twente (IMPACT).

References:

1. A. Manz and H. Becker, eds. *Microsystem Technology in Chemistry and Life Science*. Topics in Current Chemistry. Vol. 194. 1998, Springer: Berlin.

2. S.C. Jakeway, A.J. de Mello, and E.L. Russell, *Miniaturized total analysis systems for biological analysis.* Fresenius J. Anal. Chem. **366**, 525 (2000).

3. J.W. Hong and S.R. Quake, *Integrated Nanoliter Systems.* Nature Biotechnology **21**, 1179 (2003).

4. J. Zeng and T. Korsmeyer, *Principles of droplet electrohydrodynamics for lab-on-a-chip.* Lab Chip **4**, 265 (2004).

5. V. Srinivasan, V.K. Pamula, and R.B. Fair, *An integrated digital microfluidic lab-on-a-chip for clinical diagnostics on human physiological fluids.* Lab Chip **4**, 310 (2004).

6. V. Cristini and Y.-C. Tan, *Theory and numerical simulation of droplet dynamics in complex flows - a review.* Lab Chip **4**, 257 (2004).

7. Y.C. Tan, J.S. Fisher, A.I. Lee, V. Cristini, and A.P. Lee, *Design of microfluidic channel geometries for the control of droplet volume, chemical concentration, and sorting.* Lab Chip **4**, 292 (2004).

8. A. Wixforth, C. Strobl, C. Gauer, A. Toegl, J. Scriba, and Z. von Guttenberg, *Acoustic manipulation of small droplets.* Anal. Bioanal. Chem. **379**, 982 (2004).

9. O.D. Velev, B.G. Prevo, and K.H. Bhatt, *On-chip manipulation of free droplets.* Nature **426**, 515 (2003).

10. P.R.C. Gascoyne, J.V. Vykoukal, J.A. Schwartz, T.J. Anderson, D.M. Vykoukal, K.W. Current, C. McConaghy, F.F. Becker, and C. Andrews, *Dielectrophoresis-based programmable fluidic processors.* Lab Chip **4**, 299 (2004).

11. P.G. deGennes, F. Brochard-Wyart, and D. Quéré, *Capillarity and Wetting Phenomena*. 2004, New York: Springer.

12. D.W. Langbein, *Capillary surfaces: shape-stability-dynamics, in particular under weightlessness*. 2002, Berlin; New York: Springer. xviii.

13. H. Gau, S. Herminghaus, P. Lenz, and R. Lipowsky, *Liquid Morphologies on Structured Surfaces: From Microchannels to Microchips.* Science **283**, 46 (1999).

14. B.S. Gallardo, V.K. Gupta, F.D. Eagerton, L.I. Jong, V.S. Craig, R.R. Shah, and N.L. Abbott, *Electrochemical Principles for Active Control of Liquids on Submillimeter Scales.* Science **283**, 57 (1999).

15. A.A. Darhuber and S. Troian, *Principles of Microfluidic Actuation by Modulation of Surface Stresses.* Ann. Rev. Fluid Mech. **37**, 425 (2005).

16. R. Lipowsky, *Morphological wetting transitions at chemically structured surfaces.* Curr. Opinion Coll. Interf. Sci. **6**, 40 (2001).

17. T. Pfohl, F. Mugele, R. Seemann, and S. Herminghaus, *Trends in microfluidics with complex fluids.* ChemPhysChem **4**, 1291 (2003).

18. M. Brinkmann and R. Lipowsky, *Wetting morphologies on substrates with striped surface domains.* J. Appl. Phys. **92**, 4296 (2002).

19. A. Klingner and F. Mugele, *Electrowetting-induced morphological transitions of fluid microstructures.* J. Appl. Phys. **95**, 2918 (2004).

20. A. Klingner, S. Herminghaus, and F. Mugele, *Self-excited oscillatory dynamics of capillary bridges in electric fields.* Appl. Phys. Lett. **82**, 4187 (2003).

21. V. Srinivasan, V.K. Pamula, and R.B. Fair, *Droplet-based microfluidic lab-on-a-chip for glucose detection.* Anal. Chim. Acta **507**, 145 (2004).

22. M.W.J. Prins, W.J.J. Welters, and J.W. Weekamp, *Fluid Control in Multichannel Structures by Electrocapillary Pressure.* Science **291**, 277 (2001).

23. The number of publications on electrowetting has been increasing from less than five p.a. before 2000 to 8 in 2000, 9 (2001), 10 (2002), 25 (2003), and 34 (2004)

24. G. Lippmann, *Relations entre les phénomènes électriques et capillaires.* Ann. Chim. Phys. **5**, 494 (1875).

25. B. Berge, *Electrocapillarite et mouillage de films isolants par l'eau.* C.R.Acad. Sci., Ser. II: Mec., Phys., Chim., Sci. Terre Univers. **317**, 157 (1993).

26. C. Quilliet and B. Berge, *Electrowetting: A recent outbreak.* Curr. Opinion Coll. Interf. Sci. **6**, 1 (2001).

27. Note that the ambient phase can be another liquid, immiscible with the droplet, instead of vapor.

28. Note that these conditions are only necessary not sufficient. In addition, the second variation of F must be positive. In the presence of complex surfaces, some morphologies may indeed be unstable although both necessary conditions are fulfilled (ref. [13]).

29. The vertical force component is balanced by normal stresses in the stiff solid substrate.

30. P.G. deGennes, *Wetting: statics and dynamics.* Rev. Mod. Phys. **57**, 827 (1985).

31. J.O. Indekeu, *Line tension near the wetting transition: results from an interface displacement model.* Physica A **183**, 439 (1992).

32. A.W. Adamson, *Physical Chemistry of Surfaces*. 5 ed. 1990, New York: John Wiley & Sons, Inc.

33. This description ignores any deviations that may occur close to the TCL.

34. J.A.M. Sondag-Huethorst and L.G.J. Fokkink, *Potential-Dependent Wetting of Electroactive Ferrocene-Terminated Alkanethiolate Monolayers on Gold.* Langmuir **10**, 4380 (1994).

35. W.J.J. Welters and L.G. Fokkink, *Fast Electrically Switchable Capillary Effects.* Langmuir **14**, 1535 (1998).

36. M. Vallet, M. Vallade, and B. Berge, *Limiting phenomena for the spreading of water on polymer films by electrowetting.* Europ. Phys. J. B **11**, 583 (1999).

37. H.J.J. Verheijen and M.W.J. Prins, *Reversible Electrowetting and Trapping of Charge: Model and Experiments.* Langmuir **15**, 6616 (1999).

38. B. Shapiro, H. Moon, R.L. Garrell, and C.J. Kim, *Equilibrium behavior of sessile drops under surface tension, applied external fields, and material variations.* J. Appl. Phys. **93**, 5794 (2003).

39. T.B. Jones, J.D. Fowler, Y.S. Chang, and C.J. Kim, *Frequency-based relationship of electrowetting and dielectrophoretic liquid microactuation.* Langmuir **19**, 7646 (2003).

40. T.B. Jones, K.L. Wang, and D.J. Yao, *Frequency-dependent electromechanics of aqueous liquids: Electrowetting and dielectrophoresis.* Langmuir **20**, 2813 (2004).

41. A.G. Papathanasiou and A.G. Boudouvis, *A manifestation of the connection between dielectric breakdown strength and contact angle saturation in electrowetting.* Appl. Phys. Lett. **86**, 164102 (2005).

42. V. Peykov, A. Quinn, and J. Ralston, *Electrowetting: A Model for Contact-Angle Saturation.* Coll. Polym. Sci. **278**, 789 (2000).

43. L.D. Landau and E.M. Lifschitz, *Elektrodynamik der Kontinua*. Lehrbuch der Theoretischen Physik. Vol. VIII. 1985, Berlin: Akademie Verlag.

44. T.B. Jones, *On the Relationship of Dielectrophoresis and Electrowetting.* Langmuir **18**, 4437 (2002).

45. K.H. Kang, *How Electrostatic Fields Change Contact Angle in Electrowetting.* Langmuir **18**, 10318 (2002).

46. We will see in section 2.3.1 [49], that this assumption is not correct. However, the main conclusion with respect to the contact angle remains valid.

47. K.L. Wang and T.B. Jones, *Frequency-dependent bifurcation in electromechanical microfluidic structures.* J. Micromech. Microengineering **14**, 761 (2004).

48. T.B. Jones, *An electromechanical interpretation of electrowetting.* preprint (2005).

49. J. Buehrle, S. Herminghaus, and F. Mugele, *Interface Profiles Near Three-Phase Contact Lines in Electric Fields.* Phys. Rev. Lett. **91**, 086101 (2003).

50. R. Brdicka, *Grundlagen der Physikalischen Chemie*. 1969, Berlin: VEB Deutscher Verlag der Wissenschaften.

51. J. Buehrle, *Freie Flüssigkeitsoberflächen in elektrischen Feldern am Beispiel der Elektrobenetzung*, in *Fakultät für Naturwissenschaften*. 2004, Universität Ulm: Ulm.

52. K.H. Kang, I.S. Kang, and C.M. Lee, *Electrostatic Contribution to Line Tension in a Wedge-Shaped Contact Region.* Langmuir **19**, 9334 (2003).

53. K.H. Kang and I.S. Kang, *Validity of the Derjaguin Approximation on Electrostatic Effect in the Frumkin - Derjaguin Approach.* Langmuir **19**, 9962 (2003).

54. T. Chou, *Geometry-Dependent Electrostatics near Contact Lines.* Phys. Rev. Lett

87, 106101 (2001).

55. H.H. Woodson and J.R. Melcher, *Electromechanical Dynamics*. Vol. 2. 1968, New York: John Wiley & Sons.

56. This equation can be derived using the boundary conditions for the electric and displacement fields at the solid liquid interface in combination with the continuity equation [55]. An alternative derivation based on equivalent circuit diagrams was described by Jones et al. [e.g. 39] for the specific case $\delta_d = 0$.

57. F. Mugele, A. Klingner, J. Buehrle, D. Steinhauser, and S. Herminghaus, *Electrowetting: A Convenient Way to Switchable Wettability Patterns.*

58. A. Quinn, R. Sedev, and J. Ralston, *Influence of the electrical double layer in electrowetting.* J. Phys. Chem. B **107**, 1163 (2003).

59. A. Klingner, *Änderung der Flüssigkeitsmorphologie durch elektrische Felder zur Anwendung in der Mikrofluidik*. 2004, Ulm: Ulm.

60. A. Klingner, J. Buehrle, and F. Mugele, *Capillary bridges in electric fields.* Langmuir **20**, 6770 (2004).

61. F. Mugele and S. Herminghaus, *Electrostatic Stabilization of Fluid Microstructures.* Appl. Phys. Lett. **81**, 2303 (2002).

62. T.N. Krupenkin, J.A. Taylor, T.M. Schneider, and S. Yang, *From rolling ball to complete wetting: The dynamic tuning of liquids on nanostructured surfaces.* Langmuir **20**, 3824 (2004).

63. J.Y. Yoon and R.L. Garrell, *Preventing biomolecular adsorption in electrowetting-based biofluidic chips.* Anal. Chem. **75**, 5097 (2003).

64. A.R. Wheeler, H. Moon, C.J. Kim, J.A. Loo, and R.L. Garrell, *Electrowetting-based microfluidics for analysis of peptides and proteins by matrix-assisted laser desorption/ionization mass spectrometry.* Anal. Chem. **76**, 4833 (2004).

65. E. Seyrat and R.A. Hayes, *Amorphous Fluoropolymers as Insulators for Reversible Low-Voltage Electrowetting.* J. Appl. Phys. **90**, 1383 (2001).

66. R.A. Hayes and B.J. Feenstra, *Video-speed electronic paper based on electrowetting.* Nature **425**, 383 (2003).

67. T. Roques-Carmes, R.A. Hayes, B.J. Feenstra, and L.J.M. Schlangen, *Liquid*

behavior inside a reflective display pixel based on electrowetting. J. Appl. Phys. **95**, 4389 (2004).

68. H. Moon, S.K. Cho, R.L. Garrell, and C.J. Kim, *Low voltage electrowetting-on-dielectric.* J. Appl. Phys. **92**, 4080 (2002).

69. J.C. Baret, R. Seemann, and S. Herminghaus, preprint (2005).

70. D. Huh, A.H. Tkaczyk, J.H. Bahng, Y. Chang, H.H. Wei, J.B. Grotberg, C.J. Kim, K. Kurabayashi, and S. Takayama, *Reversible switching of high-speed air-liquid two-phase flows using electrowetting-assisted flow-pattern change.* J. Am. Chem. Soc. **125**, 14678 (2003).

71. S.K. Cho, H.J. Moon, and C.J. Kim, *Creating, transporting, cutting, and merging liquid droplets by electrowetting-based actuation for digital microfluidic circuits.* J. Microelectromech. Systems **12**, 70 (2003).

72. B.R. Acharya, T. Krupenkin, S. Ramachandran, Z. Wang, C.C. Huang, and J.A. Rogers, *Tunable optical fiber devices based on broadband long-period gratings and pumped microfluidics.* Appl. Phys. Lett. **83**, 4912 (2003).

73. T. Krupenkin, S. Yang, and M. P., *Tunable liquid microlens.* Appl. Phys. Lett. **82**, 316 (2003).

74. M. Bienia, F. Mugele, C. Quilliet, and P. Ballet, *Droplets profiles and wetting transitions in electric fields.* Physica A**339**, 72 (2004).

75. M. Bienia, C. Quilliet, and M. Vallade, *Modification of drop shape controlled by electrowetting.* Langmuir **19**, 9328 (2003).

76. J.S. Kuo, P. Spicar-Mihalic, I. Rodriguez, and D.T. Chiu, *Electrowetting-induced droplet movement in an immiscible medium.* Langmuir **19**, 250 (2003).

77. W. Satoh, M. Loughran, and H. Suzuki, *Microfluidic transport based on direct electrowetting.* J. Appl. Phys. **96**, 835 (2004).

78. B. Janocha, H. Bauser, C. Oehr, H. Brunner, and W. Gopel, *Competitive electrowetting of polymer surfaces by water and decane.* Langmuir **16**, 3349 (2000).

79. P. Mach, T. Krupenkin, S. Yang, and J.A. Rogers, *Dynamic tuning of optical waveguides with electrowetting pumps and recirculating fluid channels.* Appl. Phys. Lett. **81**, 202 (2002).

80. P.Y. Chiou, H. Moon, H. Toshiyoshi, C.J. Kim, and M.C. Wu, *Light actuation of liquid by optoelectrowetting.* Sensors and Actuators A **104**, 222 (2003).

81. These assumptions seem somewhat artificial for homogenous dielectric layers. However, it should be recalled (see section 3) that many electrowetting experiments – including the one of Verheijen and Prins [37] – are performed on composite substrates made of a thicker main insulating layer and a thin hydrophobic top coating.

82. F. Mugele, *unpublished data.*

83. Recall that the electrostatic energy gain, which is responsible for the negative term in eq. 11 takes place in the battery.

84. G. McHale, M.I. Newton, and D. Herbstson, *Electrowetting on super-hydrophobic surfaces*, in *4th International Discussion Meeting on Electrowetting*. 2004: Blaubeuren (Germany).

85. M. Brinkmann, *Benetzung lateral strukturierter Oberflächen*, in *Max-Planck-Institut für Kolloid- und Grenzflächenforschung*. 2002, Universität Potsdam: Golm. p. 131.

86. P. Lenz and R. Lipowsky, *Stability of Droplets and Channels on Homogeneous and Structures Surfaces.* Eur. Phys. J. E **1**, 249 (2000).

87. K. Brakke, *The surface evolver.* Exp. Math. **1**, 141 (1992).

88. A. Lafuma and D. Quéré, *Superhydrophobic States.* Nature Materials **2**, 457 (2003).

89. J. Bico, C. Marzolin, and D. Quéré, *Pearl Drops.* Europhys. Lett. **47**, 220 (1999); J. Bico, C. Tordeux, and D. Quéré, *Rough Wetting.* Europhys. Lett. **55**, 214 (2001).

90. J. Keizer, P.A. Rock, and S.W. Lin, J. Am. Chem. Soc. **101**, 5637 (1979).

91. J.C. Baret, D. Steinhauser, R. Seemann, S. Herminghaus, and F. Mugele, *Dynamics of self-excited droplet oscillations in electrowetting*, in *4th International Discussion Meeting on Electrowetting*. 2004: Blaubeuren (Germany).

92. D. Steinhauser, *Elektrowetting in Fluid-Fluid-Systemen*, Diplomarbeit, Fakultät für Naturwissenschaften, Universität Ulm 2004: Ulm (Germany).

93. C. Quilliet and B. Berge, *Investigation of effective interface potentials by electrowetting.* Europhys. Lett. **60**, 99 (2002).

94. Under these conditions, the droplets are obviously extremely mobile because any surface heterogeneity that might cause pinning and contact angle hysteresis is smeared out by the oil film.

95. For large droplets of low viscosity liquids, intertial effects may also play a role.

96. F. Brochard-Wyart, *Motions of Droplets on Solid Surfaces Induced by Chemical or Thermal Gradients.* Langmuir **5**, 432 (1989).

97. H. Ren, R.B. Fair, M.G. Pollack, and E.J. Shaughnessy, *Dynamics of electro-wetting droplet transport.* Sensors and Actuators B **87**, 201 (2002).

98. K.L. Wang and T.B. Jones, *Electrowetting dynamics of microfluidic actuation.* preprint (2005).

99. P.G. deGennes, *On Fluid/Wall Slippage.* Langmuir **18**, 3413 (2002).

100. L.M. Pismen, *Mesoscopic hydrodynamics of contact line motion.* Coll. Surf. A **206**, 11 (2002).

101. A. Oron, S.H. Davis, and S.G. Bankoff, *Long-scale evolution of thin liquid films.* Rev. Mod. Phys. **69**, 931 (1997).

102. T.D. Blake, A. Clarke, and E.H. Stattersfield, *An investigation of electrostatic assist in dynamic wetting.* Langmuir **16**, 2928 (2000).

103. C. Decamps and J.D. Coninck, *Dynamics of spontaneous spreading under electrowetting conditions.* Langmuir **16**, 10150 (2000).

104. T.D. Blake and J.M. Haynes, J. Coll. Interf. Sci. **30**, 421 (1969).

105. Y. Fouillet and J.L. Achard, *Digital microfluidic and biotechnology.* Comptes Rendus Physique **5**, 577 (2004).

106. S. Arscott, F. Caron, and J.-C. Fourrier, *Droplet transport by EWOD of patterned wetting surfaces for biochemical applications*, in *4th International Discussion Meeting on Electrowetting*. 2004: Blaubeuren (Germany).

107. J. Sterling, *Nucleic acid amplification using electrowetting droplet control*, in *4th*

International Discussion Meeting on Electrowetting. 2004: Blaubeuren (Germany).

108. M.G. Pollack, A.D. Shenderov, and R.B. Fair, *Electrowetting-based actuation of droplets for integrated microfluidics.* Lab Chip **2**, 96 (2002).

109. P. Paik, V.K. Pamula, and R.B. Fair, *Rapid droplet mixers for digital microfluidic systems.* Lab Chip **3**, 253 (2003).

110. P. Paik, V.K. Pamula, M.G. Pollack, and R.B. Fair, *Electrowetting-based droplet mixers for microfluidic systems.* Lab Chip **3**, 28 (2003).

111. J. Fowler, H. Moon, and C.J. Kim. *Enhancement of mixing by droplet based microfluidics*. in *IEEE International Conference of MEMS*. 2002. Las Vegas: IEEE.

112. M.G. Pollack, R.B. Fair, and A.D. Shenderov, *Electrowetting-based Actuation of Liquid Droplets for Microfluidic Applications.* Appl. Phys. Lett. **77**, 1725 (2000).

113. D.G. Castner and B.D. Ratner, *Biomedical surface science: Foundations to frontiers.* Surf. Sci. **500**, 28 (2002).

114. D.S. Ginger, H. Zhang, and C.A. Mirkin, *The evolution of dip-pen nanolithography.* Angew. Chem. Intern. Ed. **43**, 30 (2004).

115. P. Belaubre, M. Guirardel, G. Garcia, J.B. Pourciel, V. Leberre, A. Dagkessamanskaia, E. Trevisiol, J.M. Francois, and C. Bergaud, *Fabrication of biological microarrays using microcantilevers.* Appl. Phys. Lett. **82**, 3122 (2003).

116. P. Belaubre, M. Guirardel, V. Leberre, J.B. Pourciel, and C. Bergaud, *Cantilever-based microsystem for contact and non-contact deposition of picoliter biological samples.* Sensors and Actuators A **110**, 130 (2004).

117. K. Hoshino, S. Triteyaprasert, K. Matsumoto, and I. Shimoyama, *Electrowetting-based pico-liter liquid actuation in a glass-tube microinjector.* Sensors and Actuators A **114**, 473 (2004).

118. U.C. Yi and C.J. Kim, *Soft printing of droplets pre-metered by electrowetting.* Sensors and Actuators A **114**, 347 (2004).

119. J.Y. Cheng and L.C. Hsiung, *Electrowetting (EW)-based valve combined with hydrophilic Teflon microfluidic guidance in controlling continuous fluid flow.* Biomed. Microdev. **6**, 341 (2004).

120. N.Y. Shen, Z.T. Liu, B.C. Jacquot, B.A. Minch, and E.C. Kan, *Integration of chemical sensing and electrowetting actuation on chemoreceptive neuron MOS (CvMOS) transistors.* Sensors and Actuators B **102**, 35 (2004).

121. B. Berge and J. Peseux, *Variable focal lens controlled by an external voltage: An application of electrowetting.* Europ. Phys. J. E **3**, 159 (2000).

122. S. Yang, T.N. Krupenkin, P. Mach, and E.A. Chandross, *Tunable and latchable liquid microlens with photopolymerizable components.* Adv. Materials **15**, 940 (2003).

123. S. Kuiper and B.H.W. Hendriks, *Variable-focus liquid lens for miniature cameras.* Appl. Phys. Lett. **85**, 1128 (2004).

124. B. Berge, *Varioptic Website*. 2004.

125. G. Beni, S. Hackwood, and J.L. Jackel, *Continuous electrowetting effect.* Appl. Phys. Lett. **40**, 912 (1982).

126. G. Beni and M.A. Tenan, *Dynamics of electrowetting displays.* J. Appl. Phys. **52**, 6011 (1981).

127. J.L. Jackel, S. Hackwood, J.J. Veselka, and G. Beni, *Electrowetting switch for multimode optical fibers.* Appl. Optics **22**, 1765 (1983).

128. J. Lee and C.J. Kim, *Surface-tension-driven microactuation based on continuous electrowetting.* J. Microelectromech. Systems **9**, 171 (2000).

129. K.S. Yun, I.J. Cho, J.U. Bu, C.J. Kim, and E. Yoon, *A surface-tension driven micropump for low-voltage and low-power operations.* J. Microelectromech Systems **11**, 454 (2002).

Figures

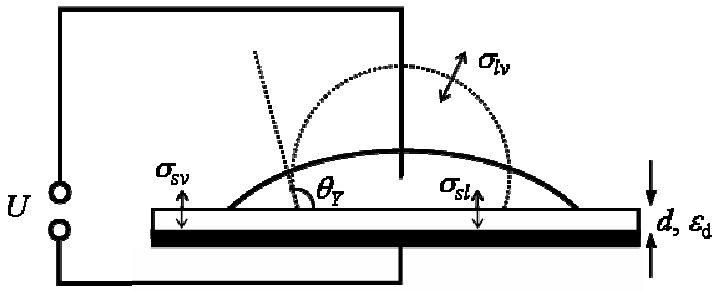

Figure 1. Generic electrowetting setup. Partially wetting liquid droplet at zero voltage (dashed) and at high voltage (solid). See text for details.

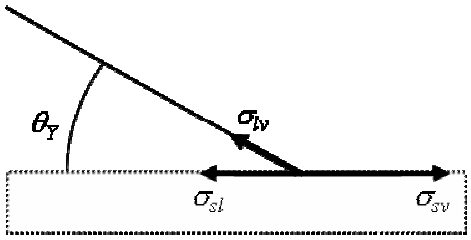

Figure 2. Force balance at contact line (for θ_Y approx. 30°).

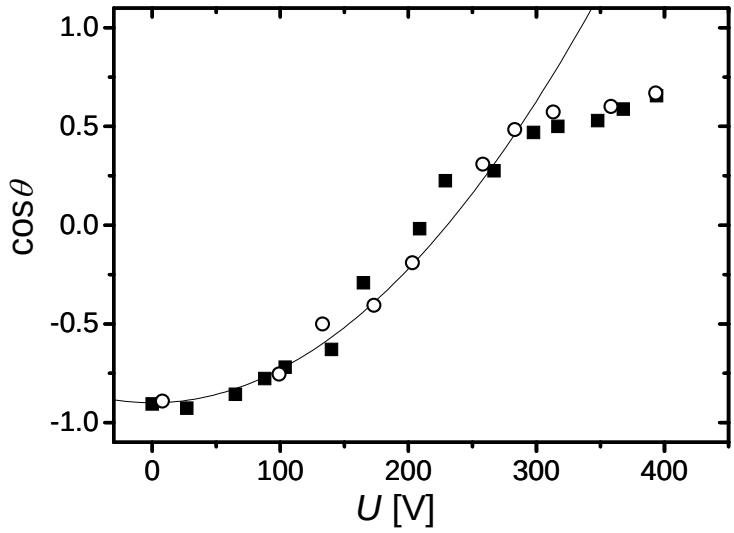

Figure 3. Contact angle vs. applied (RMS) voltage for a glycerol-salt (NaCl) water droplet (conductivity: 3 mS/cm; AC frequency: 10 kHz) with silicone oil as ambient medium. Insulator: Teflon AF 1601 (d ≈ 5µm). Note the θ_Y is almost 180° for this system. Filled (open) symbols: increasing (decreasing) voltage. Solid line: parabolic fit according to eq. 8. (reproduced from Ref. 59)

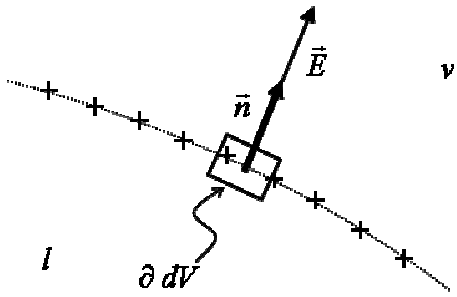

Figure 4. Force acting on a volume element dV at the liquid-vapor interface with surface charges ('+'). Solid box: Area for surface integral.

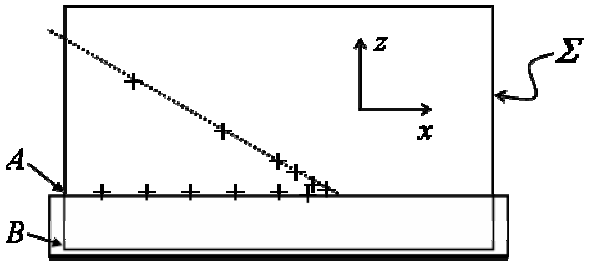

Figure 5. Integration box for the calculation of the net force acting on the contact line.

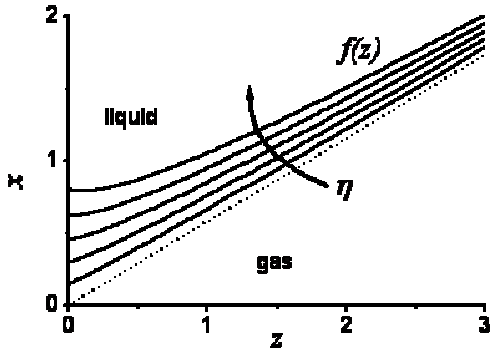

Figure 6. Equilibrium surface profiles. (θ=60°; η= 0.2, 0.4, ..., 1.0; ε_d= 1) Reprinted with permission from ref. [49]: Buehrle J., Herminghaus S. and Mugele F., Phys. Rev. Lett. 91, 086101, 2003. Copyright 2003 by the American Physical Society .

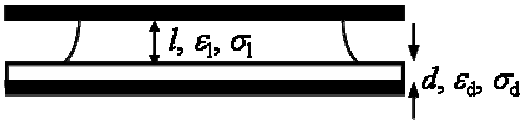

Figure 7. Capillary bridge between bare and insulator-covered electrode (see text for details).

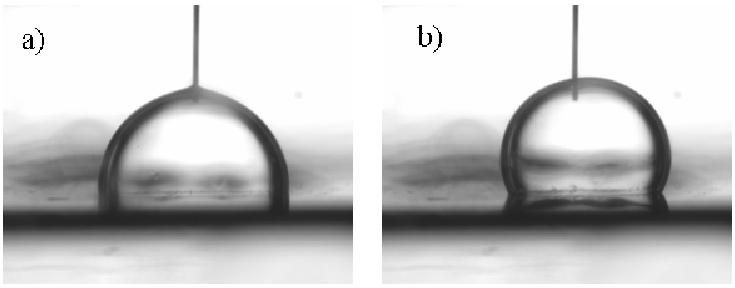

Figure 8. Frequency dependence of contact angle (insulator: 1µm thermally grown Si oxide, hydrophobized with a monolayer of Octadecyltetrachloro-siloxane). Droplet: salt (NaCl) water; conductivity: 0.2 mS/cm; diameter: approx. 2mm. ambient medium: silicone oil; U_{RMS}=50V.a) f=1 kHz. b) f=20 kHz. (reproduced from Ref. 92)

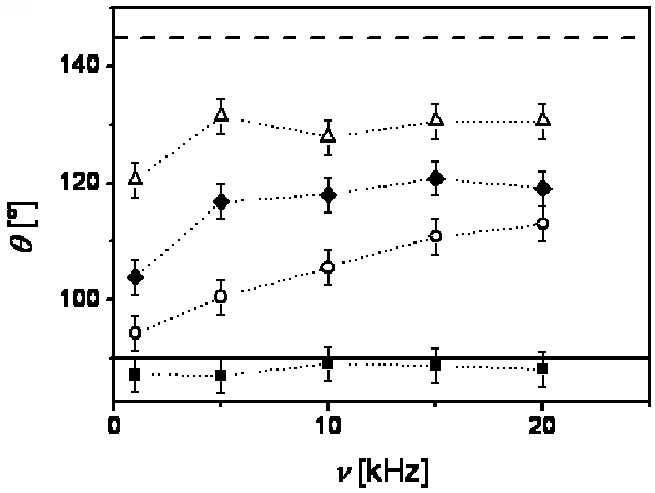

Figure 9. Contact angle θ versus frequency (see Figure 8 for experimental details). Conductivity: 1850μS/cm (squares), 197μS/cm (circles), 91μS/cm (diamonds), and 42μS/cm (triangles). θ_Y and θ are shown as dashed and solid lines, respectively. Reprinted from ref. [57].

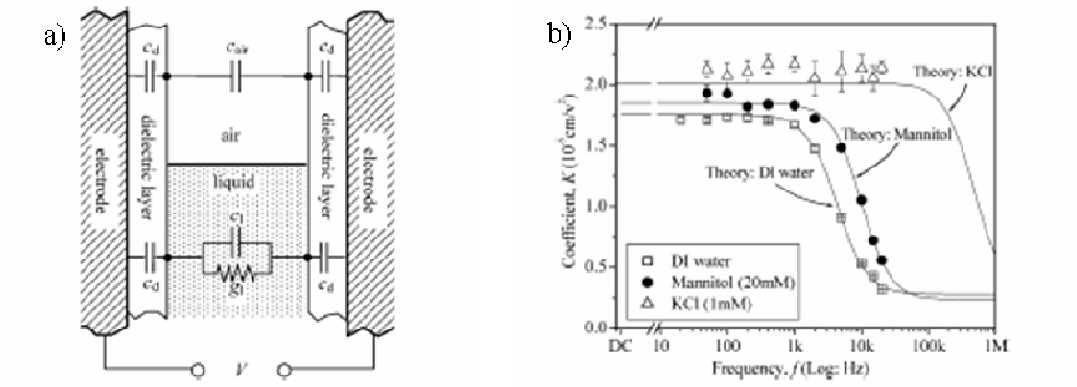

Figure 10. Pellat experiment: Electrowetting-induced capillary rise. a) Schematic setup and electric equivalent circuit. b) Frequency dependence of K(w) for DI water, mannitol, and KCl. Reprinted with permission from ref. [40].

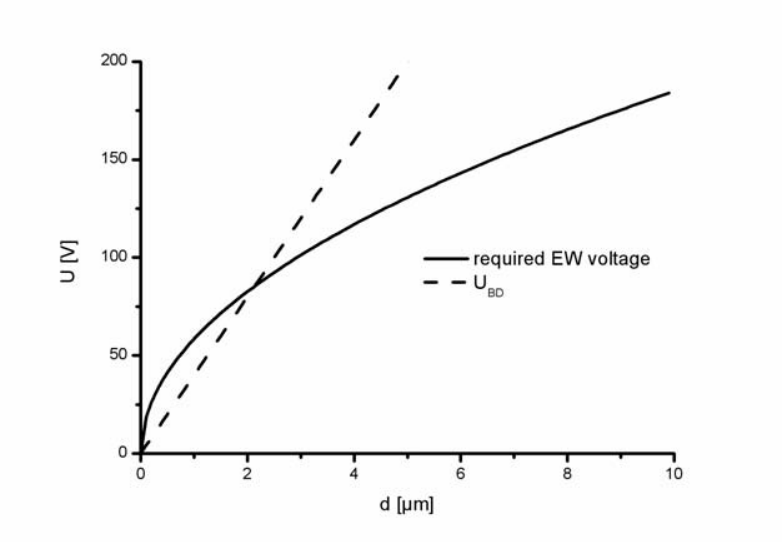

Figure 11. Electrowetting and dielectric breakdown voltage vs. insulator thickness. Solid line: voltage required for a contact angle decrease from 120° (0V) to 70° (for ε_d=2; σ_{lv}=0.072 J/m2). Dashed line: Critical voltage for dielectric breakdown (for EBD=40 V/µm)

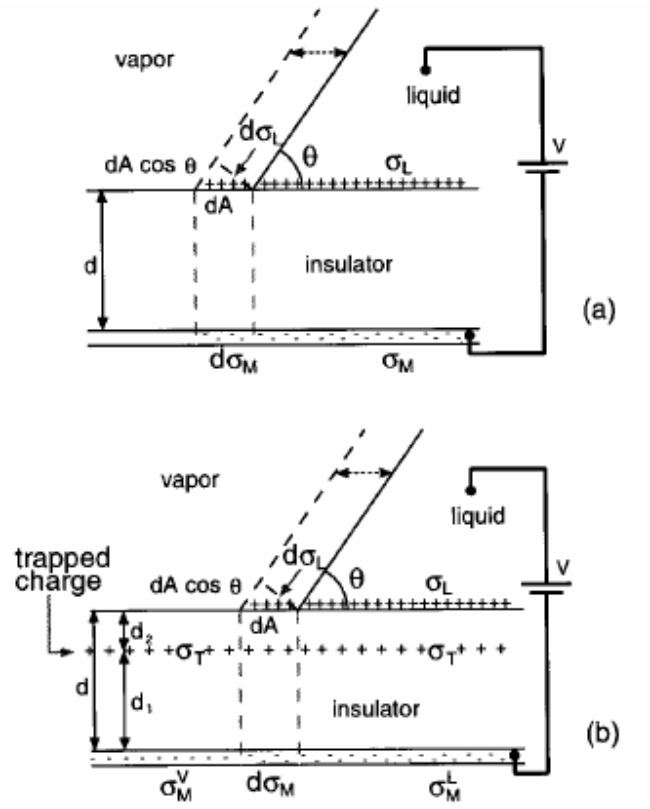

Figure 12. (a) Schematic picture of the virtual displacement of the contact line in the presence of a potential across the insulator. An infinitesimal increase in base area dA at fixed voltage V changes the free energy of the droplet, as a result of a change in interface area and the placement of additional charge $d\sigma_L$ and image charge $d\sigma_M$. (b) The virtual displacement of the contact line in the presence of a sheet of trapped charge. Now, the infinitesimal increase dA alters the free energy not only via the charge distribution between the electrode and the liquid but also via the charge distribution below the vapor phase. Reprinted with permission from [37].

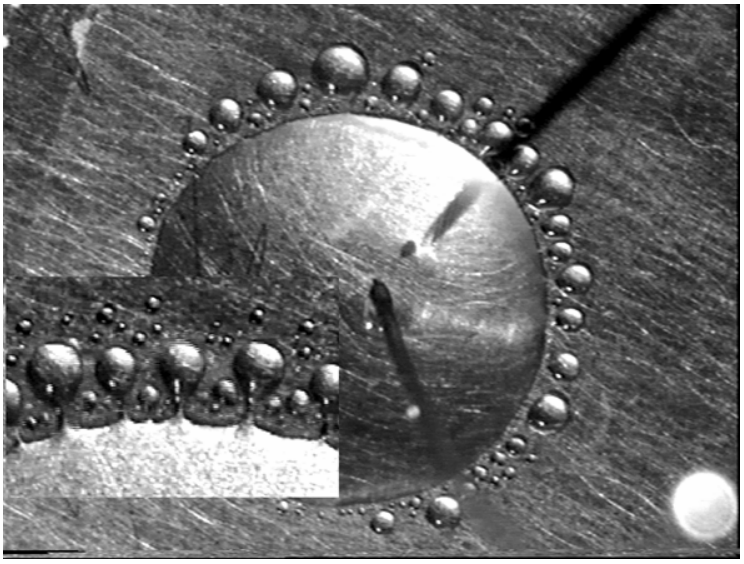

Figure 13. Contact line instability and emitted satellite droplets at high voltage. (deionized water on silanized glass; droplet diameter ≈ 3mm). Note the liquid necks between the satellites and the large droplet (inset).

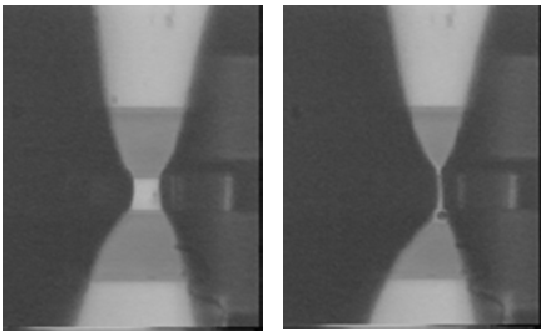

Figure 14. Electrostatic repulsion between adjacent droplets. A voltage applied to the central stripe electrode (width 20 μm) produces a protrusion at moderate voltage (91V; left image). At high voltage (210V; right image) the protrusions approach each other and flatten. Droplet coalescence is suppressed by electrostatic repulsion. Reproduced from ref. [59].

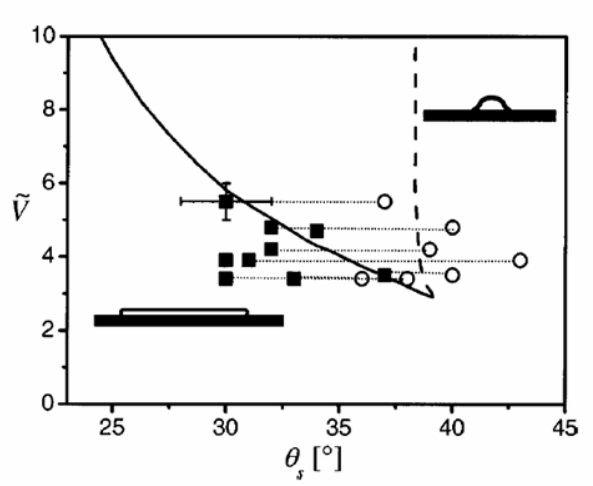

Figure 15. Morphological phase diagram (θ_s-V -plane). The solid and the dashed lines, which were taken from Ref. [85], represent numerically obtained instability lines for the bulge and channel morphologies, respectively. For small angles only the channel cylindrical morphology is stable, for high angles onlythe stretched droplet morphology is stable (cf. sketched side view images of both morphologies). In the region between the solid and dashed lines both morphologies are (meta)stable. Solid squares and open circles represent the experimentally determined values for the stretched droplet instability and cylinder instability, respectively. Thin dotted lines connect data points that were recorded in a single experimental run. Reprinted from ref. [57].

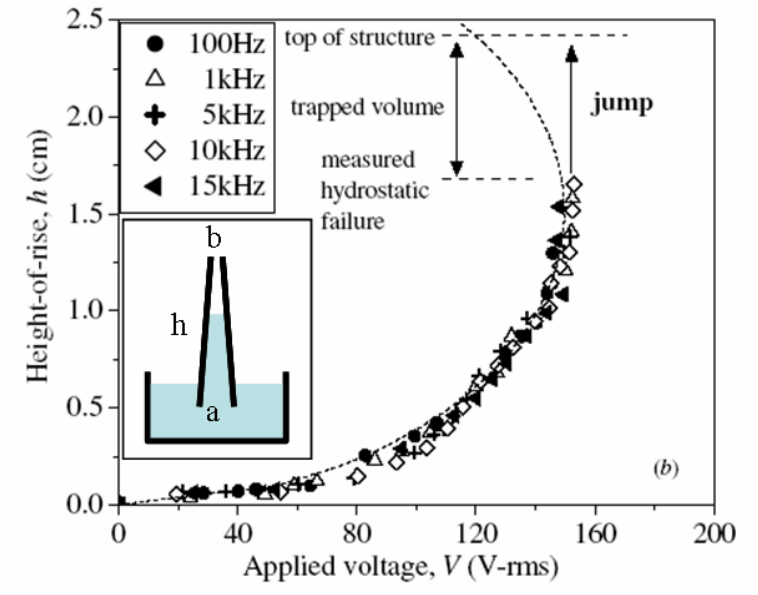

Figure 16. Height of rise vs. voltage . Symbols: experimental data for various frequencies for a 1 mM KCl solution (conductivity 1.4 × 10−2 S m−1) with a = 0.12 mm, b = 0.49 mm, H = 24 mm. Dashed line: model. Inset: geometry. (adapted from ref. [47])

.

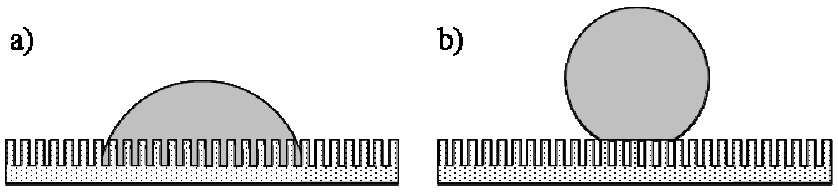

Figure 17. Droplets wetting rough surfaces. a) Wenzel state with enhanced solid-liquid interfacial area. b) Cassie-Baxter state with entrapped air underneath the droplet.

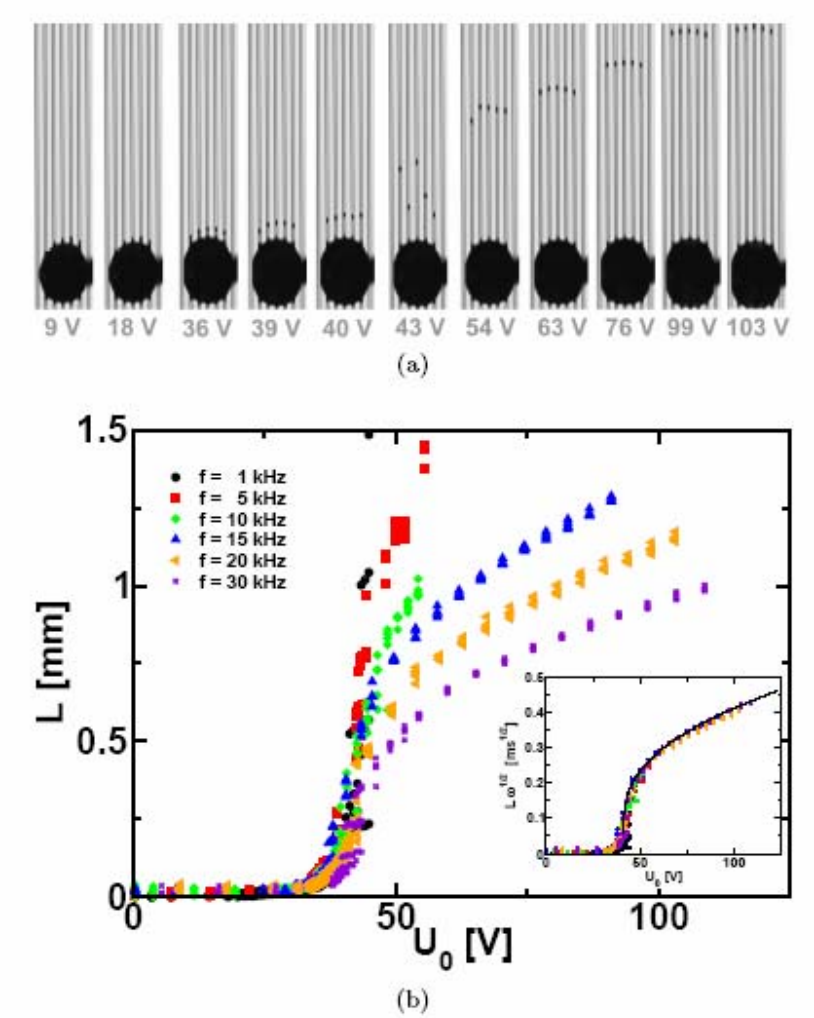

Figure 18. (a) Top-view of the channels for different voltages. The frequency of the voltage is 20 kHz and the drop wets 5 channels. On the right of the drop one see the contacting electrode. (b) Measurements of the length as a function of the applied voltage for different frequencies. The threshold voltage is obtained at 43 V. Inset: rescaled data. (courtesy of R. Seemann and J.-C. Baret)

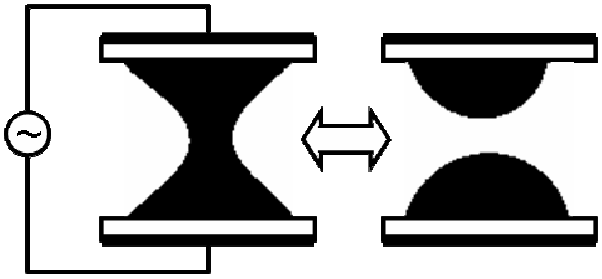

Figure 19. A liquid droplet between two electrowetting substrates can either form a capillary bridge (morphology A; left) or two separate droplets (morphology B; right).

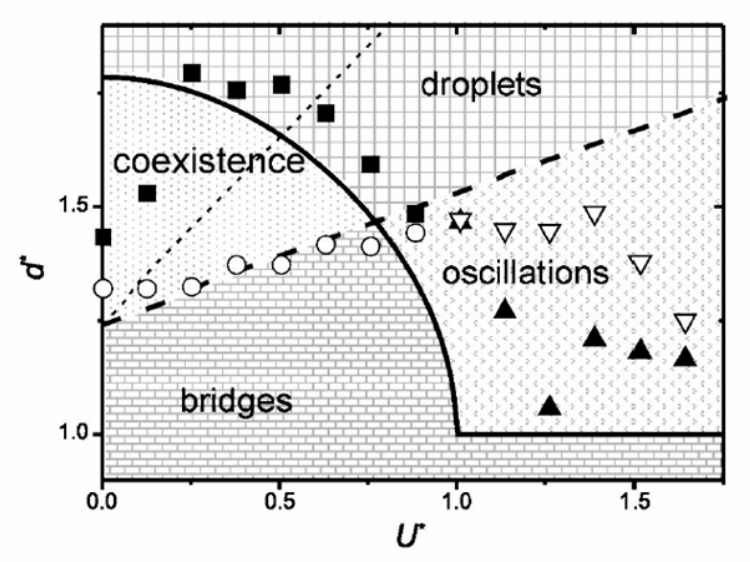

Figure 20. Phase diagram. Normalized plate separation vs normalized voltage. Symbols: Experimental results. Lines: Model results. Bridge stability limit (solid); droplet phase stability limit for V=30 nL (dashed) and for V=30 pL (dotted). Reprinted with permission from ref. [20].

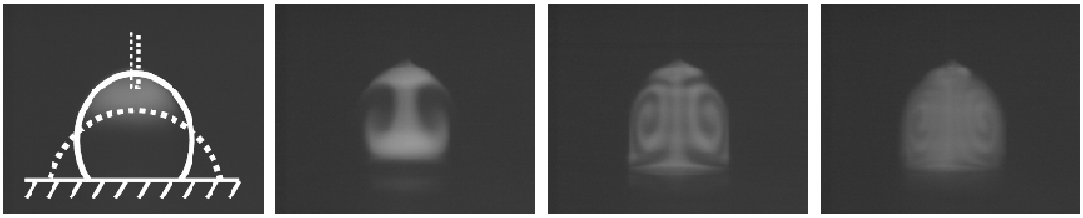

Figure 21. Oscillation-induced mixing. Water droplet, initially dye-stained in the top part, oscillating at 81 Hz between the two morphologies indicated in the left picture. Droplet diameter: 1mm. Time between consecutive images: 1s.

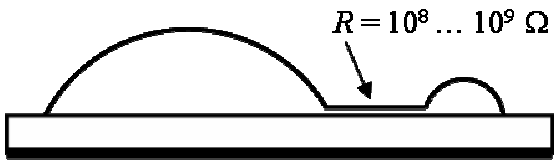

Figure 22. Schematic of a small satellite droplet connected to the reservoir drop via a thin channel. The ohmic resistance of the channel can exceed the capacitive impedance between the satellite and the bottom electrode (thick black line).

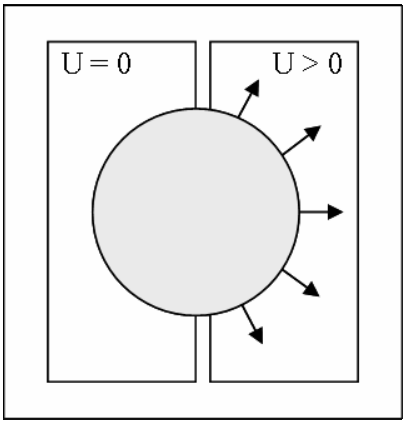

Figure 23. Top view of a droplet partially overlapping with an activated (right) and a deactivated (left) electrode. Arrows indicate the force acting on the contact line.

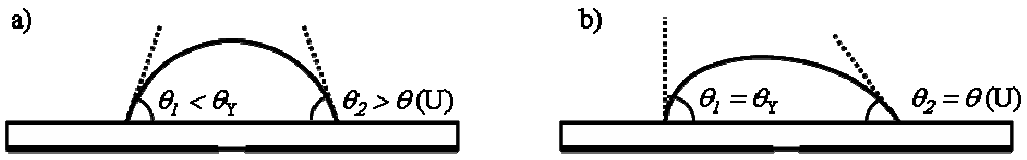

Figure 24. Side view of imbalanced droplets partially overlapping with a deactivated (left) and with an activated (right) electrode. a) droplet dominated by contact line friction. b) droplet dominated by bulk viscous dissipation.

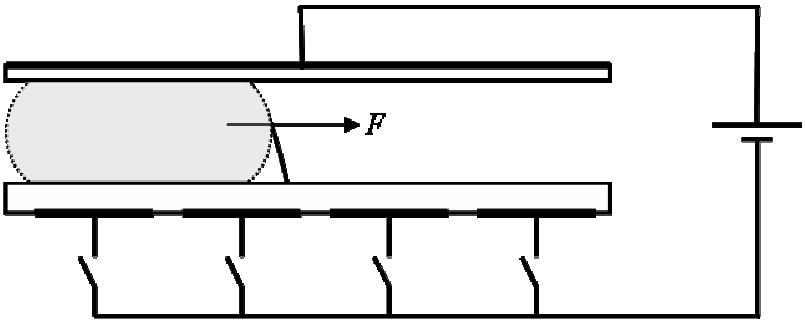

Figure 25. Schematic of a typical lab-on-a-chip system. The thin white layer on the top surface is usually a hydrophobic top coating that is does not insulate the droplet electrically. By activating the second electrode, the bottom right contact angle is reduced and the droplet is distorted accordingly.

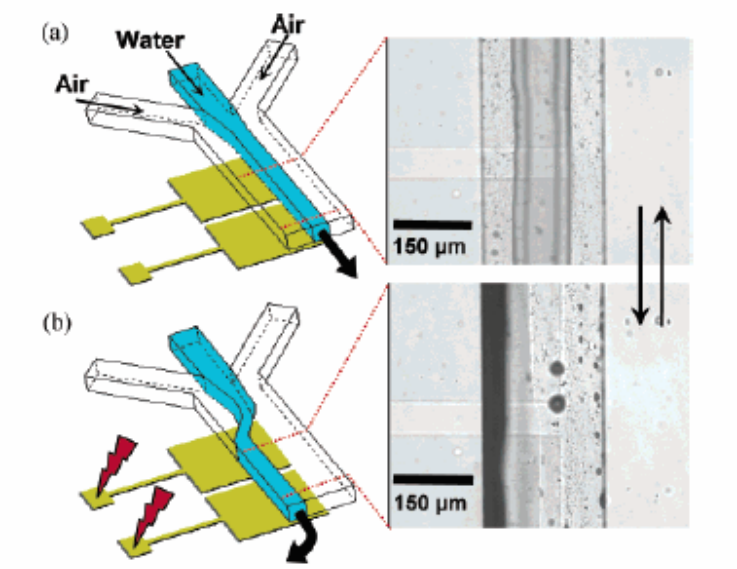

Figure 26. Electrically induced switching of surface energy caused (a) a focused high-speed water stream in the middle to (b) swerve to its right (relative to the direction of fluid flow), guiding the flow along the sidewall. Water was injected at 20 mL/h, and air flows were driven by 400 mmHg vacuum at the outlet. Channel height is 100 µm. (reproduced with permission from ref. [70])

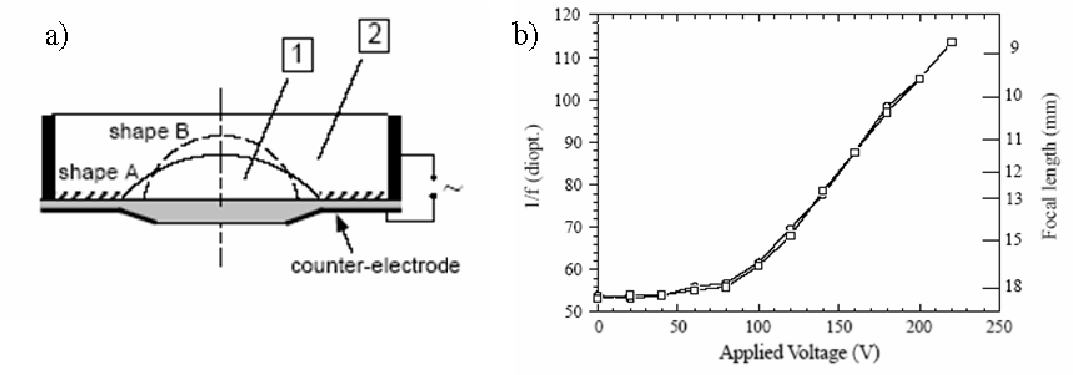

Figure 27. Electrowetting lens. a) Schematic representation of the system, not to scale. The cell is filled with water (2) . A drop (1) of an insulating and non-polar liquid is deposited on the bottomw all, which is made of an insulating and transparent material, in gray. The central disc on the bottom surface is hydrophobic, in order to trap the drop. The outer zone, hatched in the figure, is hydrophilic. The optical axis is shown as a shortlong–dashed line. b) Inverse focal length of a particular lens of 6 mm diameter, filled with α-chloronaphtalene as the insulating liquid, and a Na_2SO_4 solution in water, as a function of voltage. The two curves which correspond to increasing (◦) and decreasing (□) voltage, are superimposed. (reproduced with permission from ref. [121])

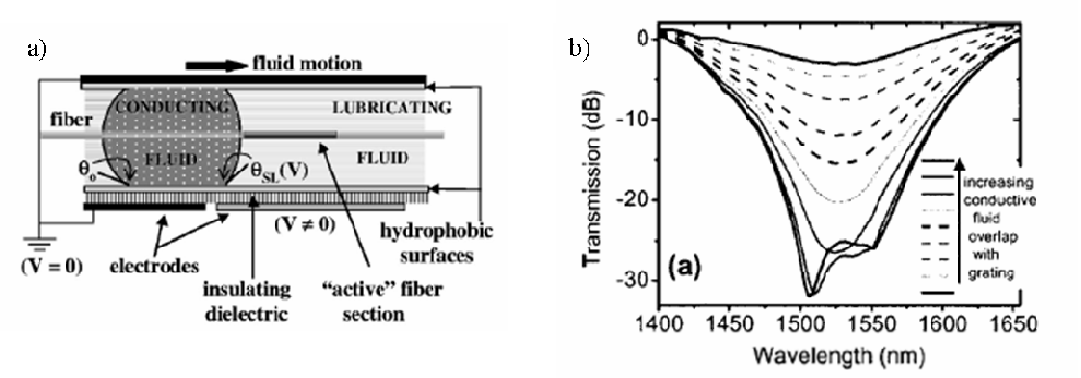

Figure 28. a) Schematic cross section of assembly utilized to tune optical fiber transmission via electrowetting actuation of a conductive fluid. (reproduced with permission from ref. [79]) b) Evolution of the transmission spectrum as the conductive plug (water with ionic salt) advances over the fiber optimized in silicon oil. (reproduced with permission from ref. [72])

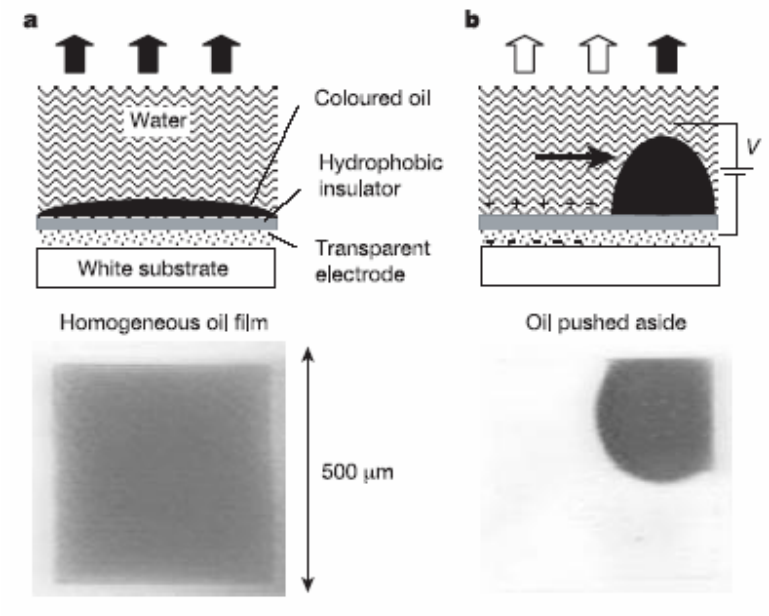

Figure 29. Electrowetting display principle. a) No voltage applied, therefore a coloured homogeneous oil film is present. b) d.c. voltage applied, causing the oil film to contract. Top row, diagrams; bottom row, photographs. The photographs show typical oil motion obtained with an homogeneous pixel electrode. (reproduced from ref. [66] .)

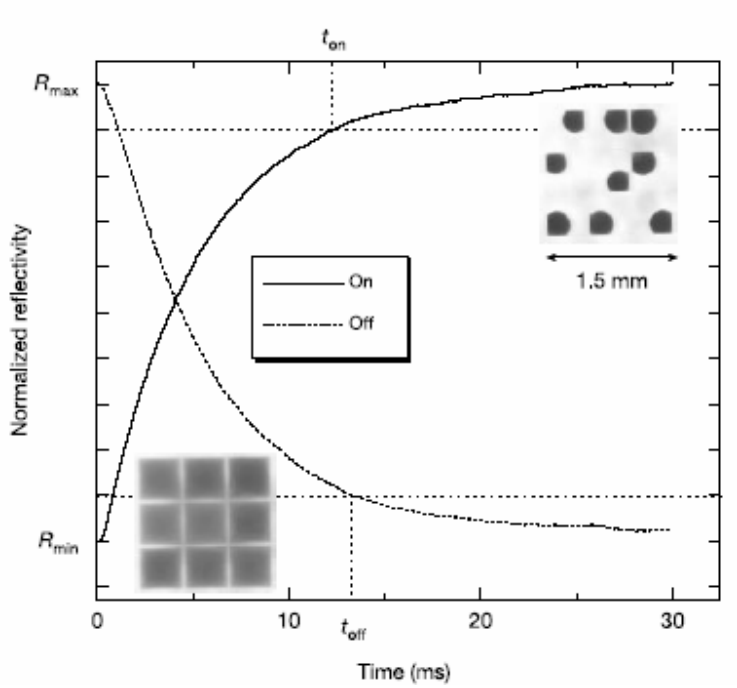

Figure 30. Electrowetting pixel kinetics. Temporal behaviour of a 250 x 250mm2 pixel, demonstrating the video-speed response. The oil film thickness is 15mm and the insulator thickness is 0.8mm. The on and off response times are 12 and 13 ms respectively. The reflectivity is shown in normalized units, which does not affect the time axis. t on and t off are defined as the time it takes to complete 90% of the optical modulation. Insets, photographs showing the corresponding optical state for a 3 x 3 array of 500 x 500mm^2 pixels. (reproduced from ref. [66]).

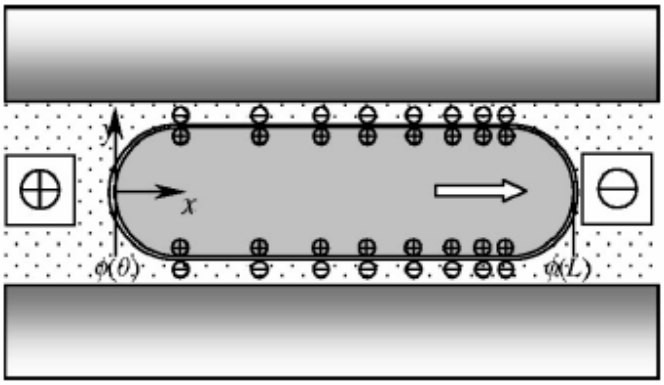

Figure 31. Mercury droplet in an electrolyte-filled channel. (reproduced with permission from Ref. [128].

Appendix A

Relationships between electrical and capillary phenomena

G. Lippmann, *Annales de Chimie et de Physique*, 5^e série, t.V. (1875)

Introduction to Lippmann's original paper

The basic paper on electrowetting was published in 1875 by the French physicist and later Nobel prize winner Gabriel Lippmann. The original work appeared in French and is therefore not accessible to the majority of potentially interested readers today. Given the recent progress and increasing interest in elesctrowetting, we felt that it would be appropriate to provide an English translation such that this paper receives the attention that it deserves.

We aimed at reproducing the original style with respect to both the way of presenting scientific research as well as language. This implies for instance that figures are presented without captions. At a few occasions, we found that the original argument is somewhat difficult to follow, if not misleading, for a 21^{st} century reader. In these cases, we decided to keep the translation as close as possible to the French original but added footnotes (NOTE) to relate to modern reasoning. In the same spirit, we also kept the old-fashioned units and linked them to today's SI units in footnotes.

We hope that this translation will help people interested in electrowetting to trace back its roots. We found it amazing to see how Lippmann covered

the entire range starting from fundamental considerations all the way to practical applications for electrical measurements (electrometer), for electromechanical actuation (electrocapillarity-driven motor) and for life sciences (considerations about measurements of nervous currents in muscles): this is an essential feature that characterizes electrowetting and electrocapillarity research until today; already 130 years ago the title of Lippmann's paper could have been: *"Electrocapillarity, from basics to applications"*!

Jean-Christophe Baret & Frieder Mugele.

Historical record

The shape of a liquid surface in equilibrium fulfils the well-known equation given by Laplace. It is known that Laplace's analysis rests on the assumption of certain molecular forces acting in the vicinity of the surface; experiments have always confirmed the results of this analysis. One can divide the experimental studies of capillarity in two parts: 1) experimental verification of Laplace's equation, notably of one of its consequences, Jurin's law; 2) numerical determination of the unique coefficient contained in Laplace's equation named capillary constant or interfacial tension. While the first part gave some satisfactory results, it is not the case for the second. For a surface of a given nature, for the mercury-water interface for instance, experiments give values which vary without any apparent reason, which decrease in time. These variations have first been noticed by Mr. Quincke[1]. This physicist found that the interfacial tension of the liquid surfaces he studied (air-water, mercury-air, water-mercury, alcool-mercury, etc) is continuously decreasing from the first moment of the experiment. These variations have been regarded as accidental perturbations linked to the deposition of impurities brought by the air or by the liquid; yet the author has neither succeeded in showing clearly these impurities nor preventing their action. One will see later that these so-called impurities have an electrical origin and that one can make them disappear on demand.

The study of electromotive forces of contact has up to now provided a complete chapter distinct from the study of capillary phenomena with variable results. The electromotive force or electrical difference at the contact between metals and pure or acidic water varies with surface preparation (scraping, polishing, etc.) and with time; for example: the water-mercury surface gave to Hankel the numbers 0.06 and 0.30, a unit reference corresponding to the zinc-copper electrical difference [2].

One may have thought to link these two physical properties of contact surfaces together, the electromotive force and the interfacial tension, and to search for a constant relation between them, had one not gotten used to look

[1] Georg Hermann Quincke, *Annales de Poggendorff*, t.CXXXIX, p. 1;1870

[2] Wiedemann, *Galvanismus*, t. I, p. 36; 1872

the latter as a specific constant (and not as a variable) and to explain its variations by the presence of invisible impurities; thus the idea that such a link should *a priori* exist does not seem to have arisen to anybody.
The experiments presented below have as starting point some fortuitous observations made by cleaning mercury, analogous to Paalzow's experiments on the attack of mercury by chromic acid [3]. They are linked to motion of mercury electrodes. One will find in Chapter A.7 the history of these phenomena; one will see that they have been first seen as effects of the current where interfacial tension did not play a role and later, as capillary perturbations which were not thought to be related to the simultaneous changes undergone by the electrical difference. The explanation has been found sufficient and the study of the phenomenon has been abandoned.
The first results of my experiments having been very briefly published in 1873[4], Mr. Quincke[5] busied himself with refuting them, but in my opinion without having well understood their meaning. The definitions, the conclusions and the object of the experiments have been missed by this skilful research worker; he mixed up two distincts laws (Chapters A.1 and A.2), in order to create a third one which he takes unnecessary trouble to refute. The author concludes: 1) that the variations of interfacial tension he observed are caused by impurities coming from inside and impossible to avoid; 2) that these variations are not subject to any law; 3) that for these reasons, one should not be able to apply capillary phenomena to the measurement of electrical phenomena, refering to the electrometer described in the Chapter A.6. Without paying more attention to Mr Quicke's Memoire I think that these conclusions can find their place in this historical record because they show the state of the art at the beginning of the present work.

[3] *Annales de Poggendorff*, t.CIV, p. 419; 1858

[4] *Comptes rendus des scéances de l'académie des sciences*, 9 juin 1873, et *Annales de Poggendorff*, t.CXLIX, p.561; 1873

[5] *Annales de Poggendorff*, t.CLIII, p.161-205; 1874

A.1 First Law

A.1.1 Definitions

The name *capillary constant* or *interfacial tension* has been given to the coefficient A of the Laplace's equation (A.1):

$$p = A\left(\frac{1}{R} + \frac{1}{R'}\right) \tag{A.1}$$

p is the normal pressure in any point of the surface; R and R' are the principal radii of curvature in this point. A liquid being in equilibrium its shape is determined when the numerical value of A is given in addition to the boundary conditions. Mutually, A is determined from the shape of the liquid; it is a number given by the experiment.

Electrical equilibrium being established, the electrical potential inside the mercury is known to have a unique value V; likewise the electrical potential inside the body of water (or acidic water) has a uniform value V_0. On both sides of the surface of contact, the potential difference is thus $x = V_0 - V$. I will call this difference *electrical difference* at the water-mercury surface.

This being defined, experiments show that if the apparatus is set such that x takes a *fixed* value x_0, A takes a value A_0 perfectly defined, *i. e.* the perturbations observed with the ordinary settings do not occur. If x is set to another value x_1, A takes another value A_1, value perfectly determined and without perturbations. To each value of x corresponds then one and only one value of A.

A.1.2 First method

A vertical glass capillary GG' communicates at its bottom with a mercury reservoir A (see Fig. A.1). This mercury penetrates into the capillary tube where it undergoes a depression.

The upper part of the tube contains a mixture of water and sulfuric acid (10 % in volume) [6]; the acidic water baths the meniscus M that ends the

[6] cold and diluted sulfuric acid does not attack mercury. It is more conducting and wets glass better than distilled water: the junction angle of mercury with glass is equal to 0

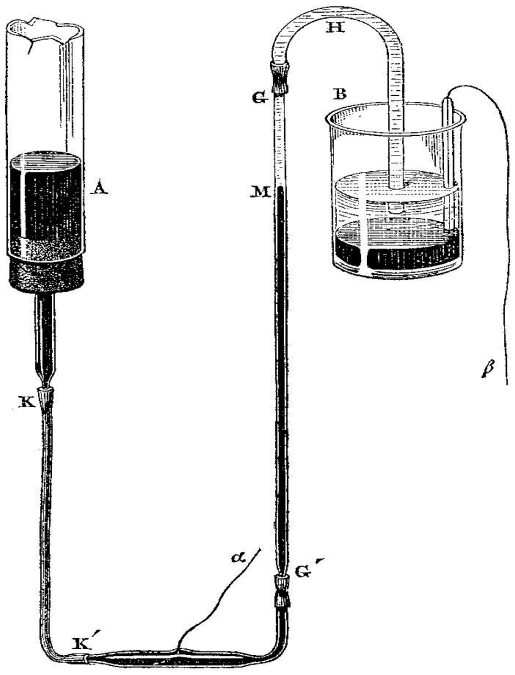

Figure A.1:

mercury column and wets the glass inner wall along this column; this water also fills a glass siphon following the tube GG' and ending up inside a glass beaker B filled with the same acid solution. A layer of mercury lies at the bottom of the beaker B. The mercury in A and that in B can communicate with the outside via the platinum wires α and β.

A cathetometer is set up in front of the tube GG'. The wires α and β being brought into metallic communication with one other the telescope of the cathetometer is raised until its reticulum seems tangent to the equilibrium position M_0 taken by the meniscus M. The apparatus is now installed.

When the communication established between α and β is suppressed, such that α remains insulated, the apparatus does not differ from those usually used to measure the capillary constant. Consequently, when α remains insu-

in diluted acid. The same holds for distilled water but only for a short time; the water sheet between glass and mercury is torn apart shortly after being formed and retracts into droplets; the junction angle takes then a different value. With the acid this change occurs only after several hours: one therefore does not have to worry about it.

lated the perturbations that have always been described in the measurement of this constant are also observed; when the mercury column has been moved for a while, the meniscus does not come back to its original equilibrium position M_0. The value of the capillary constant has changed following the displacement. One will see below according to which laws this change occurs. On the contrary, as the metallic communication between α and β is restored the meniscus M comes back *exactly* at the position M_0.

As long as α and β are in metallic communication, there is no trace of perturbations.

In order to easily produce the oscillations of the mercury column, the air pressure at the top of the reservoir can be varied; for this purpose, a plug with a rubber tube in which one can blow in or suck up is fixed at the top of the reservoir. Each time the atmospheric pressure is re-established the position M_0 of the meniscus is exactly recovered, but only in the presence of the metallic communication between α and β.

The effect of this communication is to keep the electrical difference constant at the surface of the mercury column M.

Let C be the unknown value of the electrical potential inside the acidic water; D the (unknown) electrical difference at the surface of contact between the mercury and platinum; x_0 the electrical difference at the surface of contact between the acidic water and the mercury in B; x the analogous quantity in M. The value of the potential on the wire α is

$$C - x - D$$

On the wire β the value of the potential is

$$C - x_0 - D$$

The difference of the potential values on the wires α and β is thus $x - x_0$. When these two wires are brought in metallic communication one has $x - x_0 = 0$. The effect of this communication is thus to maintain x constant and equal to x_0.

I have assumed above that the value of x_0 was constant. For this condition to be fulfilled, two precautions have to be taken in setting up the apparatus. The first one is to put the mercury in the beaker B several hours

before starting the experiments and not to touch it anymore; one will indeed see below that the electrical difference at the mercury surface increases as a consequence of the change it undergoes in its shape as it is poured. This difference subsequently decreases with time until it takes a perfectly fixed value which depends only on the composition of the liquid in which the mercury is immersed. I will call this final state reached by the mercury surface the *constant state*. The mercury surface has to reach the constant state in B before starting the experiments. The second precaution is to give to the electrode of the mercury in B a much larger surface than the mercury surface in M. In one of the apparatus used, with a tube GG' of 0.32 mm radius, a beaker B approximately 35 mm radius, the area ratio was thus 10^4.
Thus, for $x = x_0$, there is a constant equilibrium position M_0; A has thus a perfectly determined constant value A_0.
The same apparatus has been used to demonstrate that if the electrical difference takes a new value x_1, the capillary constant takes a new value A_1 which remains constant as long as x_1 does.
In order to maintain the electrical difference in M equal to x_1, I have placed

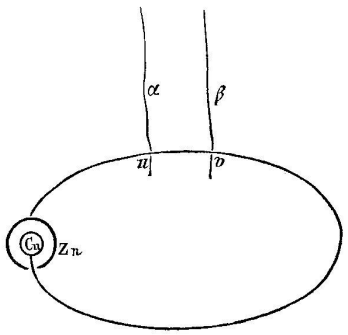

Figure A.2:

next to the apparatus a metallic circuit in which an electrical current produced by a Daniell cell (see Fig. A.2) is flowing. The wires α and β were connected with two points u and v of this circuit, u being taken between the zinc pole and the point v. A derived current flows briefly through the apparatus going from B to M through the acidic water. Due to this current

the electrical difference in M increases until electrical equilibrium is restored; the electrical difference in B did not change in the meanwhile because the quantity of electricity required to charge the surface M (to polarize hydrogene) can polarize the surface B which is for exemple 10^4 times larger only partially. Let e_1 be the excess of the potential v_1 at the point v on the potential u_1 at u. Following Ohm's and Kirchoff's laws, it is clear that electrical equilibrium will be reached when $v = C - x_0 - D$ and $u = C - x - D$; *i.e.* when

$$e_1 = x_1 - x_0$$

The meniscus takes a new equilibrium position M_1 which is invariable as the previous one: A has thus a corresponding value A_1.
Changing the points u and v the value of e varies on demand; for each value of e one corresponding equilibrium position is determined, leading to one and only one value of A. Since $x = e + x_0$, x_0 being constant, there is one and only one value of A for each value of x.
One can measure the diameter of the capillary tube, the value of the depression corresponding to each value of x and deduce from this the value of A.
The method described below does not give the values of A but the ratio of variation of A. This is an extremely sensitive method for variation measurements.

A.1.3 Second method: Use of a microscope

An ordinary glass tube A (7 mm diameter and about 1 m high) open at both ends is maintained vertically by a firm support. The lower part has been tapered with a lamp in order to present a capillary part with an extremely small inner diameter (approximately 5 μm). This tube is filled with a column of mercury A sufficiently high for the mercury to penetrate into the tapered part of the tube under its own pressure and be maintained there by the capillary pressure of the meniscus that ends it. This tapered part is immersed in acidic water filling a tube. A volume of mercury B has been poured at the bottom of the tube. Two platinum wires, one of them being carefully

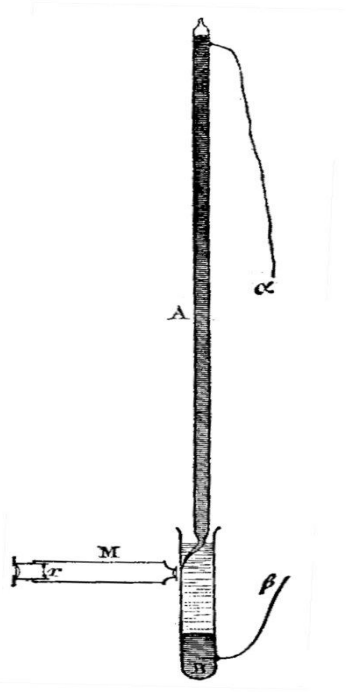

Figure A.3:

insulated are used to connect the mercury volumes A and B with the inside[7]. The air volume kept in the tapered part of the tube is removed by compressing the air volume at the top in order to push a bit of mercury out of the tube; α and β have to remain in metallic connection during this operation. As soon as the compression stops, the mercury takes the equilibrium position it must have into the tapered part. A 220 times magnification microscope (the numbers I cite refer to the first apparatus of this kind I have carried experiments with) equiped with a reticulum points at this equilibrium position such that the horizontal mark of the reticulum is tangent to the meniscus. The apparatus is now in working mode. A capillary depression of 75 cm of mercury is observed.

This apparatus has the same properties as the apparatus of the Fig. A.1 with more accuracy and sensitivity. First, if α is kept insulated from β the perturbations described above are recovered. As soon as α is brought back in

[7]NOTE: more likely "outside"

metallic communication with β the meniscus M goes back *immediately* and *exactly* to touch the horizontal mark of the reticulum.
When different electromotive forces are included between α and β using the method described previously (see page 96) a corresponding equilibrium position is observed for each of these, as perfectly determined as the first one. Same result when the magnification of the microscope is increased to 500 diameters.
One obtains thus a more accurate verification of the fact stated above; the law is obtained without any accidental perturbation.

First Law – *The capillary constant at the mercury / diluted sulfuric acid interface is a function of the electrical difference at the surface.*

This law has been verified with different proportions of sulfuric acid in water. It has been extended to more or less diluted chloric and phosphoric acid . Pure water is a poor electrical conductor and poorly wets the glass; despite this, the verification works also for water but at the condition that the water wets the glass. The height of the mercury column (the capillary depression) has in some cases reached up to 1.30 m of mercury. A variation of e of a few 10^{-2} Daniell[8] shifts the equilibrium position out of the microscope field of view; a variation of a few 10^{-4} Daniell produces a very significant displacement.
The existence of the law being demonstrated its form is determined by the measurements. The apparatus of the Fig. A.2 has been used for this purpose; it does not give the value of the capillary constant since the tube is too thin to be calibrated but its variations with a good sensitivity.
The wires α and β being in metallic communication, the microscope is oriented in a position such that the horizontal mark of the reticulum is tangent to the meniscus. The microscope is not moved during the measurements. Using the method of page 96 a value e_1 is given to e.
The mercury column takes immediately a new equilibrium position usually out of the field of view. The microscope is left in place and the meniscus is moved back to its original position, given by the horizontal mark of the retic-

[8]NOTE: The electromotive force of a Daniell cell is equal to 1.08 V

ulum, by exerting at the top of the mercury column a pressure Δp_1 by the mean of a brassing air pump. The pressure Δp_1, measured with a mercury manometer is written down as a function of the electromotive force e_1. Since this pressure is used to compensate the increase of the capillary constant in order to maintain constant the position (and as a consequence the curvature of the meniscus) I will name it *compensating pressure*. The theoretical meaning of this quantity is easily understood: one has for $e = 0$,

$$p_0 = A_0 \left(\frac{1}{R} + \frac{1}{R'} \right),$$

p_0 being the pressure of the mercury column in the glass tube A; for $e = e_1$ one has

$$p_0 + \Delta p_1 = (A_0 + \Delta A_1) \left(\frac{1}{R} + \frac{1}{R'} \right),$$

thus

$$\frac{\Delta p_1}{p_0} = \frac{\Delta A_1}{A_0};$$

i.e. the ratio $\Delta p_1 / p_0$ is equal to the ratio of the variation of the capillary constant.

In order to determine e with an accuracy given by the sensitivity of the apparatus, the variations of the battery resistance have to be negligeable. It is sufficient for that to give to the metallic resistance a value much larger than the one of the battery; thus the resistance of the battery being equal to 3 meters, a resistance of 12200 meters has been included in the circuit; between the points u and v where the wires α and β are connected, as many resistances as desired measurements points have been successively set up; for example, inserting 7000 meters between u and v one obtains for the electromotive force

$$e = \frac{7000}{12200 + 7000 + 3} = 0.364;$$

the corresponding compensating pressure was 235 mm of mercury.

The compensating pressures are, as we can see, far from being small; they reached almost 0.5 atm. All the determinations are self-consistent.

A.1.4 Numerical results - shape of the function

How does the capillary constant vary with the electrical difference ? Let us plot the different values of e (electromotive force of polarization) in abscissa, the values of Δp in ordinates; we obtain a curve with the shape displayed in Fig. A.4. The capillary constant increases approximately linearly with

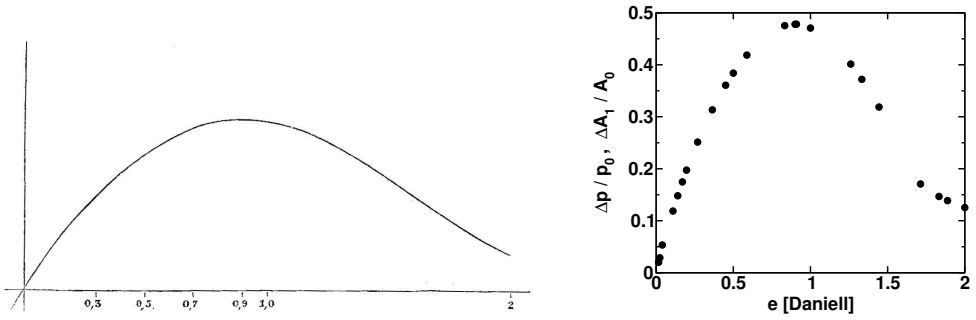

Figure A.4: Left: original figure; Right: figure obtained using data of the Table A.1. $p_0 = 750$ mm.

the electromotive force up to a maximum at $e = 0.9$ Daniell which is the 147/100 of the original value (358.7/750 = 0.47). It decreases then when e is increasing up to 2 Daniell.
I will cite here a part of the figures I obtained for sulfuric acid (1/6 in volume) for $p_0 = 750$ mm. The values of e larger than 1 Daniell have been obtained by

e	Δp [mm]	e	Δp [mm]	e	Δp [mm]
0.016	15	0.364	235	1.261	301
0.024	21.5	0.450	270.5	1.333	279
0.040	40	0.500	288	1.444	239
0.109	89	0.588	314	1.713	128
0.140	111	0.833	356.5	1.833	110
0.170	131	0.900	358.5	1.888	104
0.197	148	0.909	358.5	2.000	94
0.269	188.5	1.000	353		

Table A.1:

inserting a Daniell cell on the way of the wire α, zinc being in communication with mercury A and copper with the point u. The electromotive force of this Daniell cell is thus added to the difference of potential existing between v and u (Fig. A.5). One sees that when e increases from zero to 2 Daniell, A

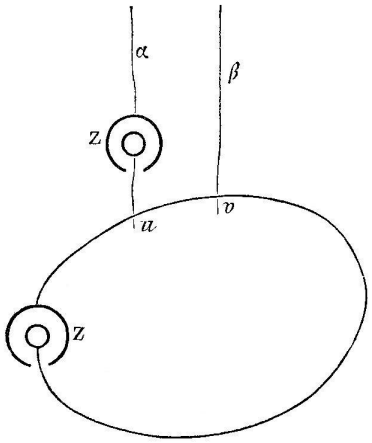

Figure A.5:

increases up to a maximum at $e = 0.9$. For each value of e one and only one value of A is found; in other words, A is a function of e. Since one has:

$$x = e + x_0,$$

x_0 being a constant one can write

$$A = f(x)$$

Note. – For each value of x there is only one value of A; but for each value of A there are two values of x.

A.2 Second Law

A.2.1 Statement

Experiments have demonstrated a new property of the mercury - water surface of contact.

When this surface is mechanically deformed, in order to increase its area, the value of the electrical difference at the surface increases. On the contrary, when the area decreases, the electrical difference decreases.
One has seen (First Law) that A is a function of x; thus when the area increases A increases too, A decreases when the area decreases.
If x has a value larger than the one giving the maximum of A, x decreases when the area increases. The inverse occurs when the area increases. One can bind these four cases in a single statement:

Second Law – *When a liquid surface is mechanically deformed, the electrical difference of this surface varies in such a way that the interfacial tension developped following the First Law opposes to the continuation of the motion.*

This statement reminds Lenz's law; and indeed experiments and theory have shown independentely that the First and Second Laws drive two series of reversible and inverse phenomena.

A.2.2 Verification

In order to deform the water - mercury surface, different means can be used: inclining the beaker containing the mercury, depressing the mercury surface; or using a pipette the tip of which is immersed in the mercury adding or removing some mercury, etc. But spreading water on a previously dry mercury surface using a brush is out of question here since this would consist in creating a new interface in addition to the old one and not stretching the existing surface.
In order to observe the change in the electrical difference a second electrode has to be introduced in the acidic water; the easiest way is to take a mercury electrode. One can set the experiment has follow: two glass beakers containing both mercury covered by acidic water are set side by side; they are set in electrical communication together using a coton wick or some filter paper. Both mercury volumes can communicate with the outside via two platinum

wires which do not touch the acidic water.
These wires are plugged to the ends of a galvanometer. Once this is done, one of the two beakers is inclined. Immediately, the needle of the galvanometer deviates, indicating a current going from the inclined glass to the straight one.
If instead of a galvanometer an electrometer is used this instrument indicates that the mercury of the inclined glass is negatively charged compared to the mercury of the straight glass.
This charge disappears with time.
If the beaker is immediately set upright again after the inclination, the charge disappears straight away. Besides, the electrical voltage varies very irregularly with the glass inclination.
Instead of inclining one of the two glasses, the mercury surface contained in it can be increased by depressing the surface. A glass, wood or paper rod is for example immersed in it. The use of a sensitive galvanometer is not required. If one uses an electrometer, either Thomson's quadrant electrometer or better the *capillary electrometer* described below is sufficient.
One of the two beaker of the previous experiment can be replaced by a beaker with a hole at its bottom through which mercury can flow in or out. A funnel or a glass tube or capillary can be used.
In the latter case the apparatus is not different from the one of the Fig. A.1. If the wires α and β of this apparatus are contacted to the poles of an electrometer, one observes that the electrometer deviates at each motion of the mercury column; α is negatively or positively charged whether the mercury rises or falls in the tube GG'.
With the different dispositions described here, an increase of the surface instead of a decrease can be produced. The electrical phenomena are then reversed.
As for the variations of the capillary constant linked to the variations of the electrical constant they have already been noticed above (see chapter A.1).

A.2.3 Funnel experiment - Production of an indefinite electrocapillary current. The First Law is a consequence of the Second Law, the principle of conservation of the energy being assumed.

A peculiar experiment based on the same principle is described in the following. A tapered funnel contains mercury A flowing out of its tip. This tip is immersed in acidic water poured in the beaker B. At the bottom of this glass beaker a layer of mercury B collects the mercury flowing out of the funnel. Using two wires α and β the two volumes of mercury communicate with the ends of a galvanometer. This one indicates a current flowing from top to bottom through the liquid which last as long as the flow, *i.e.* indefinitely; because one can indefinitely take some mercury in B and pour it in A.

One has here an apparatus which gives an indefinite current, a quantity of

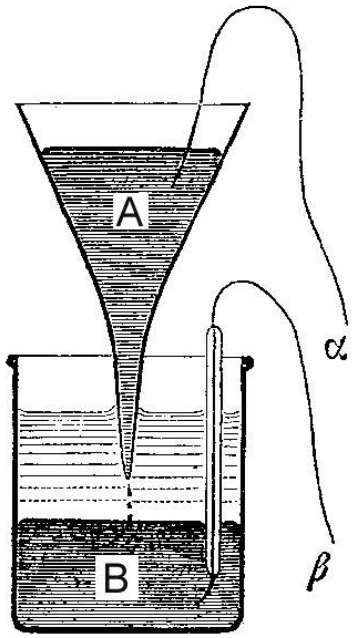

Figure A.6:

electrical work as large as desired and which is at the end of an experiment thought as long as wanted in the same state as in the beginning. Indeed elec-

trical work is supplied at the expense of the mechanical work accomplished by moving the mercury from B to A. Let us study in more details the mecanism through which electricity is produced and mechanical work absorbed.
The production of a current is the consequence of the Second Law. When a drop is formed and grows at the tip of the funnel, the electrical difference at its surface increases; the mercury in A becomes thus negative compared to the mercury in B.
At the moment where a detached drop merges into the mercury in B, there is in B an action which is added to the first one: when the drop disappears the surface decreases which decreases the electrical difference in B. One can check directly that the electrical difference between the wires α and β varies during the formation of each drop; but one can not use for that a Thomson electrometer whose indications give only an average and would be to slow; the capillary electrometer described above has to be used [9]. The absorption of mechanical work which takes place when the electrical work happens is a consequence of the First Law. Indeed, the work spent is made out of two parts: the first part depends on the speed and is used to overcome the friction during motion; we do not have to take it into account here; the second part is used to overcome the capillary pressure; the total work is the sum of the two terms. Let S be the total surface area of the drops formed per minut for example, A the mean value of the capillary constant at their surface; from Gauss's equation, the work spent to form the drops is equal to $A \times S$. When the drops merge with the mercury B, the capillary pressure gives back, through a motion a work equal to $A' \times S'$, A' being the mean value of the capillary constant in B. One has $S = S'$ since the drops formed at the top are the one which disappear at the bottom. The work which has disappeared is thus $(A - A') \times S$. There is an electrical work produced by the current only if $x - x' \lesseqgtr 0$, x and x' being the mean values of the electrical difference at the tip of the funnel and in B. In this case, in order to have expenditure of mechanical work, it is necessary and sufficient that $(A - A') \times S \lesseqgtr 0$ or

[9] The funnel experiment has been repeated recentely (Quincke, *Annales de Poggendorff*, t.CLIII, p.161; 1874) and extended to a large number of liquids: alcool, salty water, pure and air-free distilled water, etc. The current goes in the same direction with all the liquids used by Mr. Quincke.

that $A \lessgtr A'$ when $x \lessgtr x'$. This is the First Law. Thus it is sufficient to admit that the electrical work has not been produced out of nothing in order to deduce the First Law from the Second.

A.2.4 First and Second Law govern two inverse series of phenomena

One will notice besides that the First Law and the Second Law govern two reversed series of phenomena. Considering a globule of mercury surrounded by acidic water; increasing the electrical difference at its surface the capillary constant is increased leading to a contraction of the globule, a decrease of its surface (Gauss).
Inversely, when the surface is increased, the electrical difference increases; this is the Second Law. Thus the electrocapillary phenomena studied in this work are reversible (See ChapterA.4).
When a liquid surface is deformed the electrical difference varies in such a way that the interfacial tension developed under the terms of the First Law opposes to the continuation of the motion.
The funnel apparatus described above underlines this relation existing between the electrical phenomenon and the capillary phenomenon. Assuming that the wires α and β are insulated from each other, *i.e.* an open electrical circuit, when the funnel is filled carefully with only a small amount of mercury, it does not flow through the tip of the funnel. It is sustained by capillary effect. One can besides check that α is negative compared to β. When the circuit is closed the electrical current flows through the circuit and immediately the mercury flows through the tip of the funnel and this, as long as the current flows. If the circuit is opened, the mercury flow stops: the mercury flow takes place only if the apparatus produces a current; in the absence of current, the mercury stops flowing; the work expenditure stops with the current.

A.3 Mathematical theory

A.3.1 Notations

Let A be the interfacial tension, x the electrical difference at the surface of contact water - mercury, S the area of its surface. A is a function of x; *i.e.* for each value of x, A has one and only one value: this is the First Law demonstrated above.
One can graphically represent the state of the surface of contact for each time as follow. On two rectangular axes of coordinates, S is the absissa and A the ordinate: one obtain thus a point P (Fig. A.7). When the state of the surface

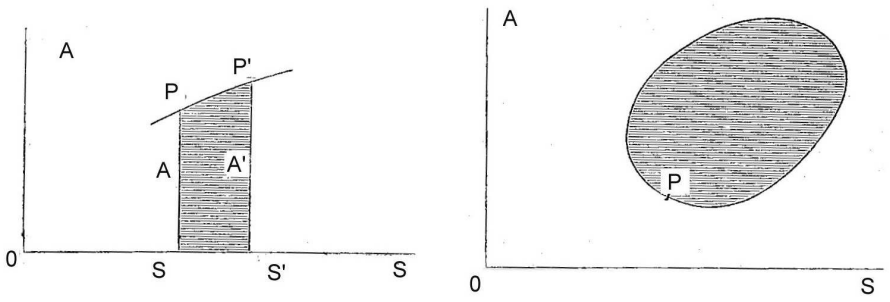

Figure A.7:

changes, P moves along a certain curve. A being a function independent of S, it follows that the representative curve can have any form and it particular that it can be closed.
The external work $\mathrm{d}T$ supplied during a deformation infinitely small of the surface has for expression

$$\mathrm{d}T = -A \times \mathrm{d}S$$

This work is thus graphically represented by the area generated by the displacement of the ordinate A. In the case where the representative curve is a closed curve the external work supplied during the deformation is equal to the area included inside the representative curve. $\mathrm{d}q$ being the quantity of electricity flowing through the surface from water to mercury, one can write:

$$\mathrm{d}q = X\mathrm{d}S + Y S\mathrm{d}x$$

X represents the quantity of electricity flowing through the surface when the surface S varies of 1 mm^2, x being kept constant. X can be named the *electrical capacity of the surface unit at fixed electrical difference.* The analytical expression of the second law is $X \leqslant 0$. Y is the quantity of electricity that has to flow through the surface unit in order to increase x of one unit, S being constant; this is what has been named the *electrical capacity of a metal electrode*; one has to add: *at fixed surface.* Y is a function of x independent of S.
This being defined, I will look which conditions the functions X and Y have to fulfil in order to follow the conservation of energy during any deformation of the interface. One can obtain this condition by two different ways.

A.3.2 Conservation of energy

I consider first the case where the representative curve is closed. The external work supplied by the surface is represented by the integral $-\int A\mathrm{d}S$. The electrical work spent in the same time or the decrease of the electrical energy expresses as $\int x\mathrm{d}q$. In order to understand this, let us assume a volume of acidic water large enough to have a constant electrical potential V_0 during one cycle; let us assume that the potential of the mercury is varied, connecting successively the mercury with different insulated mercury volume, with infinite electrical capacities and respectively at electrical potential V, V', ...
When the quantity of electricity $\mathrm{d}q$ flows through the surface from water to mercury, the charge of the water volume (whose potential is V_0) decreases of a quantity $\mathrm{d}q$; the electrical energy of the free-surface of water decreases of $V_0 \times \mathrm{d}q$. Indeed the total charge spread on the free-surface of water (the surface of contact between water and air) being q and the potential V_0, the corresponding electrical energy is equal to $V_0 \times q/2$; V_0 being proportional to q it follows that $\mathrm{d}(V_0 \times q/2) = V_0 \times \mathrm{d}q$; in contrary, the electrical energy of mercury increases of $V\mathrm{d}q$; the decrease of the electrical energy is thus $V_0 \times \mathrm{d}q - V \times \mathrm{d}q = x\mathrm{d}q$ since $x = V_0 - V$ by definition. The electrical energy decreases thus in total of $\int x\mathrm{d}q$. After having followed a closed cycle, the state of the surface is the same as in the origin, the external work supplied is

thus necessarily equal to the decrease of the electrical energy; one has then for any closed cycle

$$\int x\mathrm{d}q = -\int A\mathrm{d}S, \text{ or } \int (x\mathrm{d}q + A\mathrm{d}S) = 0$$

In other words, $x\mathrm{d}q + A\mathrm{d}S$ has to be an exact differential; replacing $\mathrm{d}q$ by its value,

$$xX\mathrm{d}S + xYS\mathrm{d}x + A\mathrm{d}S$$

has to be an exacte differential; this condition is fulfiled if

$$\frac{\mathrm{d}(A + xX)}{\mathrm{d}x} = xY \tag{A.2}$$

This is the equation of condition we were looking for[10]. It can also be found as follows.

Other proof. Let ϕ be the total inner energy of the surface unit water - mercury. ϕ is an unknown function of x. $\phi \times S$ is the total inner energy of the surface S. When x varies of $\mathrm{d}x$ and S of $\mathrm{d}S$, $\phi \times S$ increases by $\mathrm{d}(\phi \times S)$; in the same time the electrical energy decreases by $x\mathrm{d}q$ and the potential energy of the external forces decreases by $-\mathrm{d}T = A\mathrm{d}S$. One has to have:

$$\mathrm{d}(\phi S) = A\mathrm{d}S + x\mathrm{d}q$$

by development and replacement of $\mathrm{d}q$ by its value

$$\phi\mathrm{d}S + S\frac{\mathrm{d}\phi}{\mathrm{d}x}\mathrm{d}x = A\mathrm{d}S + xX\mathrm{d}S + xYS\mathrm{d}x;$$

This equation has to be fulfiled for any values of $\mathrm{d}x$ and $\mathrm{d}S$; the coefficient of these differentials have to be zero separately leading to:

$$\phi = A + xX \tag{A.3}$$

and

$$\frac{\mathrm{d}\phi}{\mathrm{d}x} = xY$$

which gives Eq. A.2 by elimination of ϕ,

$$\frac{\mathrm{d}(A + xX)}{\mathrm{d}x} = xY$$

[10]The consequence is that X is a function of x independent on S

Concerning the value of ϕ which has just been found one can make two remarks:

1. The value of ϕ can be found more directly. When a surface equal to unity decreases to zero, while in the same time, using a current the electrical difference is kept constant, there is the production of a mechanical work equal to A and of an electrical work equal to xX. The sum of these two works $A + xX$ is equal to the inner energy ϕ of the surface since the surface vanishes when producing them.

2. One knows that in his theory of capillarity Gauss assigned a constant potential energy to the molecular forces acting on each surface unit. This is exactly what is found taking $X = 0$ in Eq.A.3 *i.e.* without paying attention to the Second Law.

A.3.3 Conservation of electrical quantities

In order to fuly determine X and Y a second relationship between these two functions has to be writen . This relation is given by the condition that $\int \mathrm{d}q$ is zero for any closed cycle. I say that this condition is necessary.
$\int \mathrm{d}q$ represents the quantity of positive electricity lost by the acidic water; let us assume $\int \mathrm{d}q > 0$. This quantity of electricity can be restored to the volume of acidic water by connecting it with an electrical source via a platinum wire. When one repeats the same operation n times after the surface S has made n closed cycles, the platinum wire would have brought a quantity of electricity equal to $n \times \int \mathrm{d}q$. The wire being used as an entering electrode for the electrical flux a quantity $n \times \int \mathrm{d}q$ of oxygen has been produced or condensed at the wire. This quantity is obviously zero since the corresponding hydrogen cannot be condensed at a point of the surface since all this surface (not only the free-surface but also the water - mercury surface) came back after n cycles to the initial state. The hydrogen has not been given off neither. It can only be in excess since the water composition is unchanged. Thus $\int \mathrm{d}q$ can not be positive. The same argument based on hydrogen instead of oxygen would show that $\int \mathrm{d}q$ cannot be negative.

Thus $\int \mathrm{d}q = 0$ for any closed cycle; $\mathrm{d}q$ has to be an exact differential or

$$\frac{\mathrm{d}X}{\mathrm{d}x} = Y \tag{A.4}$$

A.3.4 Consequences: Expression of the two electrical capacities of a surface

Eq. A.4 and Eq. A.2 determines X and Y:

$$X = -\frac{\mathrm{d}A}{\mathrm{d}x} \tag{A.5}$$

and

$$Y = -\frac{\mathrm{d}^2A}{\mathrm{d}x^2} \tag{A.6}$$

These equations can be translated in everyday words:

1. *The electrical capacity of the surface unit at constant electromotive force is equal to the opposite ot the first derivative of the interfacial tension.*

2. *The electrical capacity of the surface unit at constant surface is equal to the opposite of the second derivative of the interfacial tension.*
   One will notice that the signs are in agreement with the experiments. The function A has been determined experimentally (see Chapter A.1), but it is not known analytically; so are X and Y.

A.3.5 Reciprocity of the two laws found in the experiments

From Eq. A.5 one can deduce easily that the first experimental law is a necessary consequence of the second and the other way round; indeed, if X is different from zero (Second Law), $\mathrm{d}A/\mathrm{d}x$ is different from zero where A is a function of x which is the First Law. Inversely, if $\mathrm{d}A/\mathrm{d}x$ is different from zero (First Law), X is different from zero which is the Second Law. The first of these consequences has already been demonstrated using different arguments (see Chapter A.2.3)[11].

[11] 1) The analogy of $\int \mathrm{d}q = 0$ with Carnot's equation has to be noticed.
2) The proof of the equation is independent on the one of the Eq. A.2

A.4 Electrocapillary motor

A.4.1 Creating a closed cycle. Description and functioning of the machine

A mercury surface running on a closed cycle is a device able to transform an indefinite quantity of electricity into mechanical work, or inversely, without undergoing any changes, some electrical work is supplied or absorbed depending on the direction of the motion of the point P on the cycle (clockwise or anticlockwise). The apparatus can be built up in different ways. The following shape has been designed. Two glasses GG (Fig. A.8), containing some mercury are set in a glass bath KK filled with acidic water (1/6 of acid in water). A bundle B of open vertical glass tubes (diameter about 2 mm, Fig. A.9) is immersed in the mercury of each glass. Each bundle is tightened by a platinum wire and holds along its axis a glass stick used as the rod of a piston to transmitt to the outside the backward and forward motion the bundle receives through capillary forces. Each of the bundles B is filled with liquid, mercury at the bottom, acidic water at the top such that both liquids are in contact not only outside but also inside the bundles. The height and diameter of each bundle are roughly 6 centimeters and they are immersed in 4 cm of mercury. The mercury in the tubes and in the space between the tubes undergoes a capillary depression; inversely the bundle receives from the mercury an upward vertical thrust equal to the weight of the depressed liquid. This thrust would push the bundle higher if the interdependent vertical central rod would not be held by the metal part U. This part itself is held by the beam HH (at the end of which it is binded) to which the capillary thrust is transmitted. This beam HH is mobile around an horizontal axis A. The apparatus having been built up symmetrically, the vertical thrust undergone by the bundles BB and transmitted to the arcs UU are in equilibrium at then end of HH, like the weights of the plates of a balance are in equilibrium at the end of the beam. This equilibrium is destroyed perodically by the effect of the electrical current.

The metallic conductors ee hold platinum wires immersed in the mercury of the glass GG without touching the acidic water; the top of the platinum

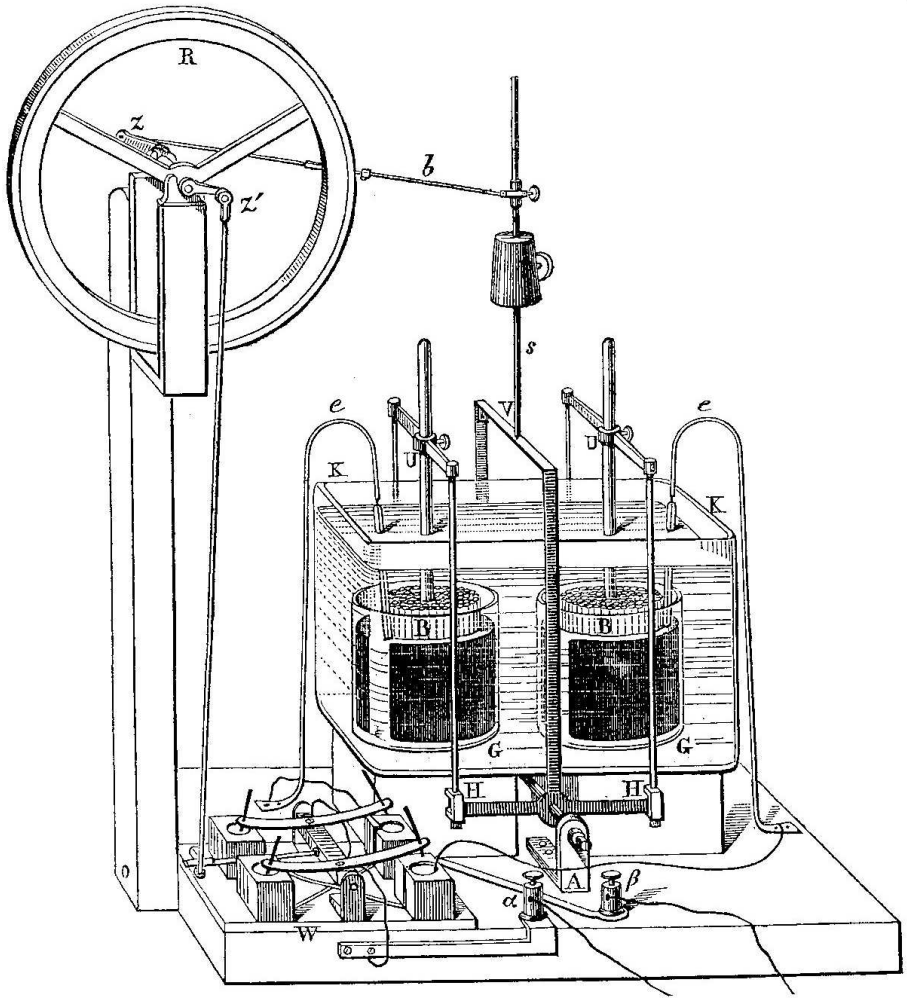

Figure A.8:

wires is surrounded by glass tubes to insulate them from the acidic water. The conductors ee can be connected to the poles of a Daniell cell. Let us assume for clarity that the mercury on the right is in communication with the zinc pole of the cell; the capillary constant is increased on this side and decreased on the other side; the right bundle is submitted to a larger thrust than previously; it is elevated while the opposite occurs on the other side. The beam H rocks around the horizontal axis A. Through the rigides pieces V, s, the rod b and the crank z this oscillatory motion is transmitted to

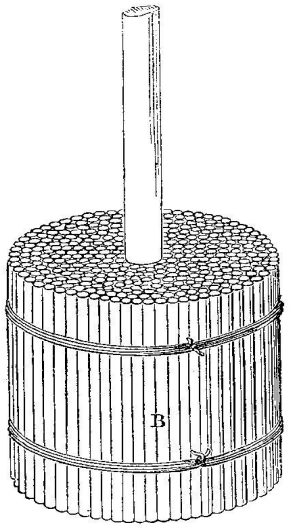

Figure A.9:

the wheel R which starts to turn. The current from the battery, instead of coming directly to the conductors ee goes through a switch W. The motion of the wheel R is transmitted to the switch in order to reverse the current when the rock motion of HH is complete. This rock motion occurs then in the other direction and the wheel R continues its rotation.
Once the rotation has started it continues indefinitely, *i.e.* as long as the battery is working. The speed reaches 100 to 120 rpm. The apparatus works indefinitely without any damage. It is only required to use a Daniell and not a Bunsen cell since the latter would decompose the water and oxidize the mercury.
In order to get the maximal speed a Daniell cell with a small resistance has to be used and the solid friction of the moving parts have to be reduced. It is also wise to tune the crank z' such that the current is reversed before the bundles BB have reached their maximal position.

A.4.2 Properties of the apparatus. The power of a capillary motor does not depend on its volume. Its maximal efficiency is the same as the one of an electromagnetic motor.

The model which has just been described gives every seconds a work of only a fraction of kg×m. It has thus only a limited practical interest as a motor, at least with the dimensions indicated above. On the theoretical point of view it is the first example of a class of peculiar apparatus:

1. This is a motor actuated by capillary forces and which through these forces converts an indefinite quantity of electrical work into mechanical work.

2. The power of such a device can be for a given volume as large as desired. The work delivered depends indeed on the variation of the contact surface S and not on the variation of the volume since the work has for expression $\int A\mathrm{d}S$[12]. And this surface of contact water - mercury can be assumed as large as desired for a given volume of liquid, only limited by the practical restrictions.

The electrical motors have the same efficiency as the electromagnetic motors [Verdet[13]]. They can deliver a work load equivalent to the whole quantity of heat that the battery would have produced for the same zinc expense if the electrical circuit would have been closed by a simple metallic wire.
I first assume a simple case:
A mercury surface increases from A to B while its electrical difference is kept constant and equal to x_0. Then the surface increases from B to C while the electrical connections are opened. Then the surface decreases from C to D while the electrical difference is kept constant and equal to x_1. Finally the

[12] S is the contact surface acidic water - mercury, including the contact surface glass - mercury provided that glass is wetted by water. When the apparatus is left a longtime without working, glass is not wetted by water anymore; in this case it is thus necessary to rise the bundles out of the mercury befor closing the electrical circuit: glass is then wetted once again and stays so as long as the apparatus works.

[13] *Exposé de la théorie mécanique de la chaleur*, Note W.

surface decreases from D to A while the electrical connections are once again opened.

One obtain then a closed cycle analogous to Carnot's cycle and made out of two lines at constant electrical difference AB and CD and two lines *without current* BC and DA. From the First Law the lines AB and CD are parallel to the abscissa. The lines BC and DA can be drawn only by points.

From the previous chapter, they are determined by the differential equation

$$-\mathrm{d}q = \mathrm{d}\left(S \times \frac{\mathrm{d}A}{\mathrm{d}x}\right) = 0$$

One would obtain their equation on a final form by eliminating x between this equation and the one giving A as a function of x, but the shape of these lines is not important here.

Let us only assume that the deformation of the mercury surface is infinitely slow, in such a way that the intensity i of the electrical current is infinitely small. The expense of zinc per seconds being proportional to i, the quantity of heat produced proportional to i^2, the latter is infinitely small compared to the first one. The efficiency of the machine is thus infinitely close to the unit. The maximal efficiency is thus reached.

This maximum is reached for an infinite number of cycles other than the one considered here since the sufficient condition (as we have seen) is that i and the speed of the machine are infinitely small, or in other words that the conditions of electrical equilibrium are reached at each time. For the particular case of the motor described above we will see without any problem that the maximum efficiency is reached when the following condition is fulfiled: it is sufficient that the current is interrupted during a fraction of the motion such that the difference of the electrical potential on the conductors ee changed its sign without changing its value during the interruption.

One should notice that the property of the mercury surface regarding the Second Law is playing in the capillary motor the same role as the corresponding property of the expansion in thermal machines. When the mercury surface is allowed to contract it executes a mechanical work; in the same time its electrical difference decreases, as well as its capillary constant which depends on it, unless a current keeps these quantities constant. There is then absorption of electrical work. This is how a saturated vapor is allowed

to relax, its temperature decreases as well as the elastic force which depends on it, unless by heat conduction these quantities are kept constant: there is then heat absorption.

A.4.3 The motor is reversible. Experiments.

The electrocapillary motor demonstrates directly the reversibility of the actions which take place in it. Instead of producing a work, it can be used to produce an electrical current.
In order to make the experiment, the battery D is removed and a galvanometer is set-up instead. With the hand or with any motor a rotation is imposed to the wheel R. The needle of the galvanometer deviates as long as the rotation takes place, *i.e.* as long as desired.
When the rotation is reversed the needle deviates once again in the opposite direction. The apparatus is thus an electromotor producing an electrical current from the muscular work which keeps it rotating.

A.5 Measurement of the capillary constant of mercury in a conducting liquid

A.5.1 Necessity to measure the capillary constant keeping the electrical difference constant

We have seen previously that the capillary constant varies with the electrical difference. The capillary constant can only be determined at the surface between mercury and acidic water for a given value of the electrical difference as the vapor tension is determined only by fixing the temperature.
The apparatus of the Fig. A.1 allows to keep the electrical difference constant and to measure in the same time the capillary constant. For the determination of the capillary constant performed under these only rational conditions I will give the following figures. They have been obtained with the apparatus of the Fig. A.1 for 5 positions of the reservoir A. This reservoir, linked to the capillary tube GG' via a rubber tube, could be moved vertically while

the vertical tube was fixed. In the same time the level of acidic water was increased in B such that it was approximately at the altitude of the meniscus M in order to reduce the correction due to the water pressure above the meniscus. The wires α and β were connected.
In the Table A.2, the column I contains the height of the horizontal surface of the mercure A read on the cathetometer; the column II the heigth of the meniscus M; the column III the heigth of the acidic water in B, IV the reduced correction in mercury due to the water pressure and the column V the corrected depression. Specific weight of acidic water: 1.105.

I	II	III	IV	V
260.8	246.4	250.3	-0.34	14.10
264.6	250.6	250.3	+0.02	14.02
263.7	249.6	250.2	-0.05	14.05
273.8	260.0	258.4	+0.11	13.91
272.2	258.2	258.4	-0.01	13.99
			Average...	14.01

Table A.2:

The cathetometer used was only giving the tenth of a millimeter. One sees that the numbers of the column V do not differ from their average more than 1/10 mm. The tube GG' had a radius of 0.32 mm which leads to a capillary constant of 30.4 mgr[14,15].

A.5.2 Explanation of the perturbations observed in previous methods

The method used here differs from the ordinary method only by the introduction of the electrical connections which keep constant the electrical difference

[14]The same result has been obtained using a tube with a different diameter which is a confirmation of Jurin's law.

[15]NOTE : The calculation based on the data of the Table A.2 gives 0.30 N/m. For comparison the surface tensions mercury-air and mercury-water are respectively 0.460 and 0.370 N/m

at the meniscus surface. These communications remove the perturbations observed in the old set-up and attributed to the action of impurities brought by the air. The explanation for these perturbations is now clear; each variation of the surface produces a variation of the electrical difference and of the capillary constant (Second Law). These variations are the source of the perturbations. Let us assume for instance that at the bottom of the beaker containing the water a large drop of mercury is introduced using a pipette in order to measure its height and to deduce from that the value of the capillary constant, method used by Mr. Quincke. While the drop is formed its surface increases; as a consequence, its capillary constant increases in the same time as its electrical difference increases[16]; This mechanical modification of the electrical and elastic properties of the surface disappears with the time, first fast and then slower and slower; and indeed, it has always been observed that the capillary constant of mercury was decreasing first fast and then slowly in time. Same phenomenon when the mercury is introduced in a tube where the capillary depression is observed.
Using the electrode B and the wires α and β the change in the electrical difference is directly monitored. When the wires α and β are connected to the poles of an electrometer α is charged negatively compared to β when the mercury rises in the tube. When α and β are connected through the wire of a galvanometer, the perturbation and the charge of α disappear in the same time as the needle of the galvanometer deviates, indication of an electrical current flowing from the liquid A to the liquid B.

A.5.3 Note on the case of non conducting liquids and air

If instead of a conducting liquid like water an insulating liquid like oil is used the previous experiment can not be performed anymore since the circuit can not be closed.
It is noticeable that in the case of an insulating liquid the perturbations are the same as in water when the circuit is open; it is natural to ask if the laws established for acidic water are still true for an insulating liquid; so far there

[16]The first quantity can vary up to 47 % of its value, the second up to 0.9 Daniell.

is no method known to check these laws. I keep this point in reserve for a future work.
I will restrict myself to one fact: the capillary constant of mercury in air is far from being a constant quantity.

A.6 Capillary electrometer

A.6.1 Description of the apparatus

Experiments have shown that the laws stated in the Chapter A.1 can be applied to the measurement of electromotive forces.
The capillary electrometer based on this principle seems to be the most accurate and the most invariable of the electrometers; it is besides really easy-to-use. It does not differ in any essential point from the one represented in the Fig. A.1 of the Chapter A.1.
An ordinary glass tube A (Fig. A.10) – 1 meter high, 7 mm in diameter – is hold vertically. The lower part has been tapered under a lamp in two steps such that the inner diameter of the thinner part is decreased to a few microns. This *capillary tip* is immersed in diluted sulfuric acid (1/6 in volume of water) contained in a glass tube fixed at the bottom of the first tube. At the bottom of this tube a volume of mercury has been poured. In the tube A, a mercury column is poured, sufficiently high so that the mercury penetrates by its own pressure in the capillary tip (750 mm for example). The mercury volumes A and B are connected to 2 insulated electrical poles via the the wires α and β soldered to these poles. The wire β does not touch the acid of the tube B.
The capillary tip is set against the wall of the tube B to be in the focus of the microscope M, fixed horizontally with a 250 magnification. In order to simplify the focusing this microscope is mounted on a tripod with fixation screws. The tips of the three screws rest on a platform which is part of the support of the apparatus. The tip of one of the screw turns in a small conical hole; the tip of the second is mobile is a rectangular groove; the tip of the third rests on an horizontal plan; a strong spring pushes the tripod to the platform. This device is used to focus and reduce the vibrations. The mi-

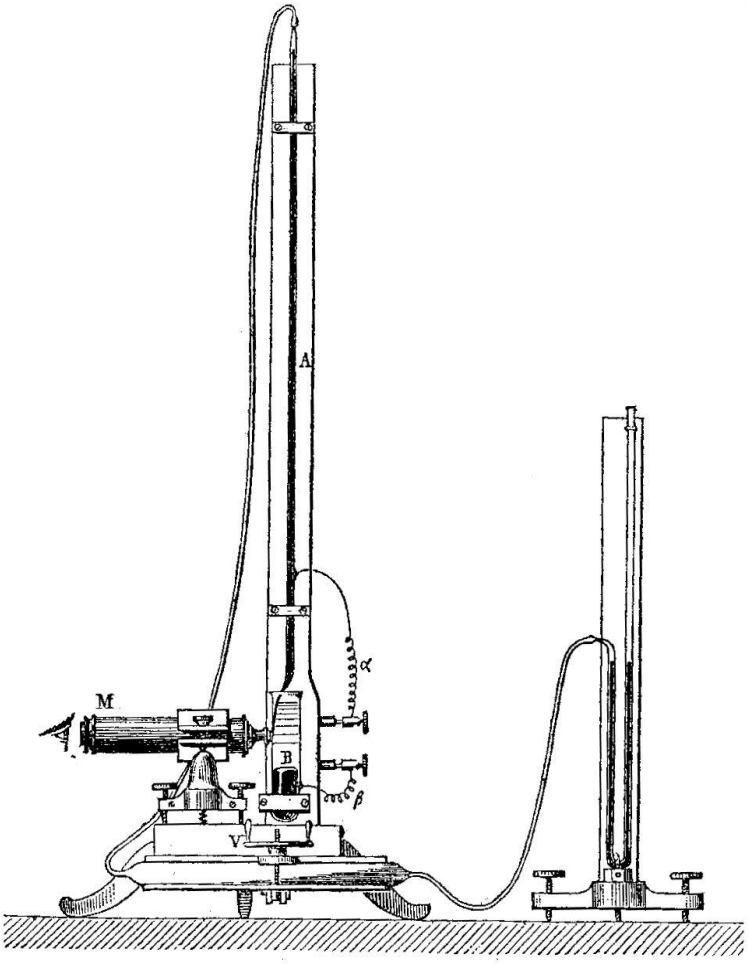

Figure A.10:

croscope is equiped with a reticulum or even better with an eye-micrometer drawn on the glass. To get a sharp image the axis of the microscope has to be perpendicular to the wall of the tube B.

To compress the air at the top of the mercury A, the apparatus is equiped with a screw-press actuated by the wheel V; under this press is mounted an elongated rubber bag with a thick wall filled with air. This bag communicates with the tube A at one side and with an open-air manometer at the other side.

Once the apparatus has been filled, the air bubble captured in the capillary

tip is expulsed by pressing the air at the top of A in order to let a bit of mercury flow out; during this operation α and β are connected together. Once this in done, the atmospheric pressure is established at the top of A. The meniscus M which ends the mercury column in the capillary tip stops then to a fixed equilibrium position which could be named the zero of the apparatus. The microscope is then moved to put the zero of the micrometer tangent to the meniscus; the microscope will then always keep this position. The apparatus is now installed. It is wise to notice that the zero is not constant right after the filling but after a while. It goes down slowly during two or three days.

A.6.2 Instructions. Graduations

The capillary electrometer has all the properties of an accurate electrometer. It can be used to measure electromotive forces.
In order to measure the electromotive force of a battery cell for example, the negative pole is connected to α, the positive pole to β; the wheel is rotated until the meniscus reaches the zero and the value of the pressure is read on the manometer.
The measurement is now done; the pressure has to be converted into electromotive force. For this purpose, either use a table made in advance or a curve obtained in the map electromotive force - compensating pressure (for the creation of such a table see Table A.1, page 101). Such a table electromotive force as a function of compensating pressure produces an experimental graduation of the electrometer. As we have seen previously all the capillary electrometers are comparable for a given acid concentration.
Let us assume that we have an apparatus where the mercury column A is 900 mm instead of 750; the graduation is obtained by multiplying the compensating pressures of the Table A.1 by the ratio 900/750. Even if this calculation is simple it is as simple and more direct to do the graduation oneself, provided that one has a well-designed box of resistances.
I would also like to point out that a graduation between zero and 0.5 Daniell is sufficient; one can always lower the quantity to be measured to a value smaller than 0.5 Daniell. Indeed the electromotive force that has to be mea-

sured is always equal to an integer number of Daniell plus or minus a fraction smaller than 0.5. Adding one or several Daniell to the cell studied one obtains a measured difference less than half of a Daniell. There is an advantage in working that way: the device is more sensitive in this area and the curve is easy to plot since it does not differ much from a straight line.

A.6.3 Determination of a few electromotive forces. Numerical examples

Here are a few examples of experimental results.

Measurement of the electromotive force of a Leclanché cell. The carbon pole of a Leclanché is connected to the copper pole of a Daniell, the zinc pole of the Daniel is connected to β, the zinc of the Leclanché to α. The mercury goes out of the field of view. The wheel W is turned until the mercury level is at zero. The manometer indicates 270.5 mm of mercury which corresponds to $e = 0.450$ from the Table A.1. Thus

$$1 \text{ Leclanché} = 1.450 \text{ Daniell}^{17}$$

Measurement of the electromotive force of a Daniell cell loaded with acid. A Daniell cell loaded with acid is opposed to an cell charged with zinc sulfate, *i.e.* the copper poles are connected together, the zinc of the normal cell is connected to α, the other zinc is connected to β. The mercury is set to zero using the wheel for a pressure of 52 mm of mercury. The electromotive force is thus 0.061. The cell loaded with acid has an electromotive force equal to 93.9 % of the electromotive force of the normal cell.

Measurement of the electromotive force of a cell amalgam zinc - zinc sulfate - ordinary zinc The amalgam zinc communicates with α, the ordinary zinc with β. The mercury is set to zero using the wheel V

[17]NOTE: The EMF of a Leclanché cell is equal to 1.45 V. The ratio of the EMF is in reasonable agreement with the present data.

indicating a pressure of 8 mm. The electromotive force is 0.0081 Daniell.
The capillary electrometer has been used for a large number of measurements; It has been used in particular to repeat the electromotive force measurements of batteries previously done by Mr. Bunsen and the series of experiments done by Mr. du Bois-Reymond on the muscular and nervous currents.

A.6.4 Properties of the electrometer. Invariability. Accuracy

The invariability of the indications of the capillary electrometer has always been perfect. When the apparatus is charged the mercury level goes out of the origin; when it is discharged by connecting α and β with a metal wire the mercury comes back immediately and perfectly at zero. This perfect invariability is achieved for any pressure and electromotive forces used.
The sensitivity of the apparatus varies with its dimensions; it depends on the height of the column A and on the shape more or less cylindrical of the capillary tip. Indeed the compensating pressure corresponding to a electromotive force is from the theory of the apparatus proportional to this height. For 750 mm of mercury the compensating pressure for 0.500 Daniell is 288 mm of mercury; for one meter this pressure would be 360 mm of mercury.
The shape of the capillary tip determines the sensitivity on another point of view. The minimal variation of the electromotive force which produces a noticeable displacement depends on this shape. For a perfectly cylindrical tip the meniscus equilibrium would be unstable for any value of the capillary constant; for a tip with an equilater hyperbola-shaped meridian section with a small parameter (the value can easily be calculated) the equilibrium would be indifferent for a given value of the capillary constant and unstable for values in its vicinity. In a conical tip the equilibrium is stable and in this case the sensitivity is large.
In practical cases the latter condition, the most suitable for the device is obtained directly. It requires a conical tip but close to a cylinder. And a very thin tip is obtained by a very quick stretch and fulfils the previous condition. Thus all the capillary electrometer I experimented with had a sensitivity of the order of 10^{-4} Daniell.

Here is a numerical example linked to a particular apparatus.
The micrometer has 30 divisions; in between α and β is included 1/60 Daniell, the mercury moves on 28 divisions. A displacement of 1 division would then correspond to $1/(28\times60) = 5.95 \times 10^{-4}$ Daniell. The divisions were sufficiently separated to estimate a fraction of this interval, for example 1/6. This fraction would then correspond to 9.9×10^{-5} Daniell.

A.6.5 Speed of the indications. Applications of this property

The indications given by the apparatus are really fast, *i.e.* the displacements of the mercury are most of the time too fast to be followed by eye. The apparatus can be charged and discharged several times per seconds; the motion of the mercury follows the variation of the charge; one can create oscillations fast enough to make then impossible to be counted.
This property of the electrometer is important when a short-time electrical phenomenon (or changing with time) has to be studied. These phenomena were not observable with the devices used up to now (galvanometer, Thomson electrometer). I will give some examples.
The phenomenon of rapid negative variation of nervous current on a tetanized muscle is known; on the contrary, a short irritation of the nerve does not produce any effect on the galvanometer. With the electrometer the negative variation linked to the irritation is observed.
The electrometer being connected to two platinum wires used for water decomposition one can follow in a continuous way the gradual loss of the charge; one can also follow the slow formation of the residual of the charge,*i.e.* the charge which is slowly reformed after the two wires have been discharged via a metal wire.

A.6.6 The measurements are independent on the resistance. Experiments on the electricity of friction

The measurements obtained with the capillary electrometer are independent on the electrical resistance of the apparatus whose electromotive force is

being measured; one can assume this resistance as variable and large as desired: neither the measurement of the electromotive force nor the sensitivity are affected; it is known that the sensitivity of the methods based on a galvanometer is inversely linked to the resistance.
Indeed the capillary electrometer does not measure the intensity of a current but the difference of potential existing between its poles, the electrical *equilibrium* being reached. This is why it has to be named *electrometer*.
The apparatus has besides all the properties of an ordinary extremely sensitive electrometer. In the experiments described above, it has been used to measure the free voltage at the boundaries of a battery or any electrical apparatus; but it is clear that it also reacts to the influence of a electrised body at a distance.
Thus β being connected to earth, α being insulated, α is approached to an electrised rubbed resin rod for example, the mercury column rises; when the rod is removed, the mercury goes back to zero, and so on; it is possible to operate at a distance and move the rod as fast as possible; the mercury column follows all its displacements.

A.6.7 Other properties of the apparatus

Some peculiar experiments can also be performed on the capillary electrometer itself which are consequences and verifications of the Second Law (Chapter A.2).
When α and β are connected the mercury in the tip is extremely mobile. By pressing with the finger the rubber bag source of the compensating pressure it oscillates easily. But if α is insulated from β this mobility suddently disappears: the liquid seems to have become viscous.

Second experiment. α and β being in metal connection, the wheel V is turned until the mercury flows quickly from the tip. If the connection between α and β is turned off the flow suddently stops; it continues when the connection is set back.
In both experiments one can check directly using an auxilliary electrometer that the interuption of the motion is due to the electrization that the motion

produces following the Second Law.

A.7 Theory of the whirls discovered by Gerboin

The experimental laws stated above have been demonstrated at equilibrium; they link the conditions of mechanical equilibrium to the conditions of electrical equilibrium. Only the static and quasi-static case[18] have been considered above.
These laws also explain some motion phenomena discovered a long time ago that we would like to discuss in the following.

A.7.1 Historical background

Henry from Manchester has observed in 1800[19] that the mercury he was using as an electrode changed its shape while tarnishing. In 1801, Gerboin[20] discovered a new phenomenon. When the current of the battery flows through pure or acidic water in contact with mercury, this water is strongly shaken by whirls that are displayed prominently by an inert powder in suspension in water (sawdust or spanish wax); these whirls are at a fixed position as long as the wires through which the electrical current flows are fixed. In 1809, Erman[21] studied these whirls; he has drawn their sometimes very complex shape. Thus the two platinum electrodes being close to the mercury and the current being strong, one observes at the mercury surface some currents diverging from the electrodes and colliding along a closed line separating them, creating there a liquid rod; this line forms sometimes on the mercury the top of a sharp ridge. Erman was the first to observe also that a mercury drop placed between the two electrodes on a rough bottom is moving to the negative electrode. The oxidation of the mercury due to the current complicates a lot this phenomenon.

[18] where the surface deforms infinitely slowly
[19] *Gilberts Annalen*, t.VI, p.270
[20] *Annales de Chimie et de Physique*, t.XLI, p.196, 1801
[21] *Gilberts Annalen*, t.XXXII, p.261, 1809

J.-F.-W. Herschel[22] in 1824 took over the study of Gerboin's whirls. He replaced mercury by a melted Sn-Pb-Bi alloy under sugared water. Gore[23] used later melted Bi, Pb, Cd, and Sn under potassium cyanure; all these liquid metals behave like the mercury, while a solid metal (platinum) does not give anything. Herschel noticed two crucial points: 1) all the points of the surface have a tangential velocity, while the shape stays constant. This velocity produces eddies, whirls (Gerboin's whirls) by lateral communication and friction. When there is friction of the surface on the rough bottom of the glass, the mercury globule is progressing by an effect of reaction. 2) The solids produced by oxidation behave like perfectly inert impurities; they can form a shell which prevents the lateral communication, but they can neither produce nor prevent the motion of the surface.

Draper[24] in 1845 observed that the depression of the mercury column in a capillary tube filled with water decreases with the flow of an electrical current from water to mercury; this physicist admitted as an explanation that water acquires the property to wet the mercury during the flow of the current. This was a mistake; the water wets the mercury, even before the currents flows; besides the depression does not come back to its original position when the current stops. Draper considered as likely the "identity of capillary and electrical forces".

Paalzow[25] assigned the motion of the electrodes to the fact that the water wets more or less the mercury surface depending on the oxidation or deoxidation action of the electrial current. To enforce his explanation, Paalzow showed new experiments: the chromium acid (oxidizing compound) produces the effect of a current which would enter through the mercury; Sodium hyposulfite would produce the opposite effect. A chromium acid cristal thrown in water close to a mercury globule dissolves producing whirls similar to Gerboin's experiment. Paalzow's experiments can be used as an example for a series of experiments where the use of a current is replaced by the intro-

[22] *Annales de Chimie et de Physique*, t.XXVII, p280 and *Philosophical Transactions*, p.162, 1824.

[23] *Phil. Mag. [4], t.XIX, p.149, 1860*

[24] *Philosophical Magazine* [3], t. XXVI, p.185, 1845 and *Annales de Poggendorff*, t.LXVII, p. 284.

[25] *Annales de Poggendorff*, t.CIV, p.419, 1858

duction of susbtances in mercury or water: for example the introduction of potassium or other metals in mercury. One will find in the authors already cited, in those added in note[26] and in the work of Mr. Wiedemann (*Galvanismus*, t.I, p.542; 1872) the description of these experiments.
Mr. Quincke[27] looked at the motion of the mercury electrodes as a capillary phenomenon due to the deposition of a more or less thick layer of free hydrogen gas released by the current.

A.7.2 Extension of Laplace's analysis to the case of a moving surface

The correct explanation of the phenomenon of tangential velocities of a liquid surface of unknown shape requires the extension of the demonstration of the Laplace equation in the case of a motion.

PROBLEM – *Finding the expression of the forces acting on an element of a liquid surface.*

The most general situation is the one of a motion and non-uniform tension on the surface. I imagine lines of equal tension infinitely close drawn on the surface and I consider an infinitely small rectangular element of the surface, cut by four normal plans, oriented in such a way that two opposite sides σ of the rectangle are part of two lines of equal tension, the sides σ' being perpendicular to the first one (Fig. A.11). Let R and R' be the radii of curvature of the sides σ and σ'; α and α' their contingency angles, one has

$$\sigma = R\alpha,\ \sigma' = R\alpha'.$$

The normal component of the forces acting on the surface element $\sigma\sigma'$ is the

[26]Runge, *Annales de Poggendorff*, t.VIII, p.107, 1826, t.XV, p.95, t.XVI, p. 304, t. XVII, p.472. – Sérullas, *Annales de Chimie et de Physique*, t.XXXIV, p.192, 1827. – Davy, *Philosophical Transactions*, t.XV, p.135, and *Annales de Chimie et de Physique*, t.XXXIII, p.315, 1826. – Gore, *Philosophical Magazine* [4], t.XIX, p.149, 1860, t.XXII, p555, t.XXIV, p.401 and 403. – Stokes, *Philosophical Magazine*, t.XXIV, p.404

[27]Annales de Poggendorf, t.CXXXIX, p.70, 1870, and t.CLIII, p.261, 1874.

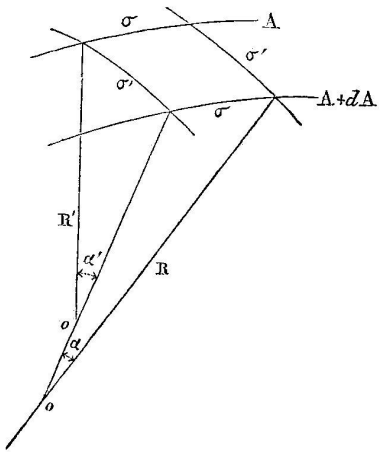

Figure A.11:

sum of several terms. The first one is the normal component of the actions exerted on the surface of the element by the volumes it separates. This component is $p\sigma\sigma' = pR\alpha R'\alpha'$. The rest of the surface exerts on the element $\sigma\sigma'$ actions which can be replaced by tangential forces (I assume the surface perfectly flexible). The actions along σ have a resultant equal to $A\sigma = AR\alpha$, normal to σ and tangent to the surface. The projection of this resultant on the normal to the surface is $AR\alpha\alpha'/2$; similarly the side parallel to σ gives the term $(A + \mathrm{d}A)R\alpha\alpha'/2$. The tension varying in a *continous* way along the surface $\mathrm{d}A$ is negligeable compared to A. The forces acting on the sides $\sigma'\sigma'$ have as a projection two terms each of them equal to $A'R'\alpha'\alpha/2$, A' being the mean value of the tension along $\sigma'\sigma'$ and infinitely close to A. The component N on the normal is equal to the sum of these four projections. Thus factorizing $RR'\alpha\alpha'$ and paying attention to the signs one obtains:

$$N = RR'\alpha\alpha' \left[p - A \times \left(\frac{1}{R} + \frac{1}{R'} \right) \right].$$

The actions exerted by the rest of the surface on the element $\sigma\sigma'$ have as tagential components along σ and σ', $\sigma\mathrm{d}A$ and 0. $T\sigma\sigma'$ and $T'\sigma\sigma'$ being the component of all the other forces (friction, etc.) counted along the same directions, the total components along these directions are

$$\begin{aligned} T_1 &= T\sigma\sigma' - \sigma \mathrm{d}A \\ T_2 &= T'\sigma\sigma'. \end{aligned}$$

N, T_1 and T_2 are the expressions we were looking for.
From this we have the following consequences:

1. The conditions of equilibrium of a liquid surface on which no external tangential forces acts are $\mathrm{d}A = 0$ and $N = 0$. The second condition is Laplace's equation. The first one indicates that the tension A is the same in every point of the surface; it is equivalent to two conditions. These three equations have to be fulfiled in any point of the surface; they are besides sufficient since it is obvious that the actions we consider have a zero momentum balance along any axis.

2. Laplace's equation $N = 0$ represents the fact that the acceleration normal to the element studied is zero. It is fulfiled in the case where the speed of an element of surface is directed along the tangent to this element.

3. The tangential acceleration of the element is the one which would be due to the simultaneous actions of an external force and a tangential force along σ', *i.e.* perpendicular to the lines of equal tensions and equal to the derivative $\mathrm{d}A/\sigma$.

A.7.3 Application in the study of the whirls

Gerboin's whirls are precisely the realization of the case where Laplace's equation only is fulfiled while the other equilibrium conditions are not.
When a drop of mercury is in contact with the acidic water in which a current flows, a part of the current flows in the mercury through certain points of the surface and flows out through others and produces in these different points different electromotive forces of polarization. Assuming a stationary state, if one considers lines of equal electrical differences that could be drawn on the surface, these lines would be in the same time lines of equal capillary

tension (First Law, Chapter A.1); thus each point of the surface will then have a tangential velocity perpendicular to these lines of constant tension. The direction and position of the liquid current can be predicted. In a point a of the surface, close to the positive wire, the electrical difference is maximal; in a point b it is minimum; it varies continuously between these two points. If this value of the electrical difference in a is smaller or equal to the value m which gives a maximal capillary constant, all the points of the surface moves along trajectories from b to a; it is one of the cases described above.
If the value of the electrical difference in a is larger than m, the capillary constant is maximal along a line which separates a from b. In this case, the phenomenon described is the ridge presented above. All the points of the surface describe trajectories going from a on one hand, from b on the other hand and meeting orthogonally to the line m. The line m is the meeting line of two surface currents with opposing velocities. This line forms the sharp ridge of a liquid rod produced by the meeting. If one operates with water containing 1/6 volumes of sulfuric acid, the line m is the one for which the electromotive force of polarization is equal to 0.9 Daniell (See page 101).

Summary

Two distincts laws have been demonstrated by the experiments. The First Law (Chapter A.1) links the capillary constant to the electrical difference. The Second Law (Chapter A.2) links the variation of the electrical difference to the variations of the area of the surface.
These two laws, established separately from the experiments are linked together by a crucial theoretical argument.
It has been shown (Chapter A.2) rigourously and without hypothesis that in the funnel experiment which is based on the Second Law some electrical work would be produced if the First Law was not assumed.
In the mathematical theory of the Chapter A.3 this relationship has been re-established in an analytical form; this analysis is based on two principles: 1) conservation of the energy; 2) conservation of electrical quantities. No other hypothesis besides has been used neither in this analysis nor in the rest of the present work. This is to avoid to introduce any of them that I have

not given a physical theory, an explanation of the properties that have been observed[28].
The electrocapillary motor described in the Chapter A.4 shows directly that: 1) an indefinite quantity of electrical work can be converted into mechanical work by means of capillarity; 2) the phenomena described above are *reversible*.
When these phenomena are compared to those of thermodynamics, one sees that the First Law echoes back to the law of thermal dilatation and the Second Law to the one of cooling during expansion.
The First Law received two applications: 1) Measurement of the capillary constant; this measurement was up to now illusory (Chapter A.5); 2) Measurement of the electromotive forces. The electrometer described in the Chapter A.6 is the most accurate of all the electrometers known up to know.
The Chapter A.7 gives the explanations of Gerboin's whirls. The principle used to explain them is of potential interest for future applications.

NOTES

A. – The junction angle

The junction angle between glass and mercury under pure or acidic water is equal to zero at the condition that the water wets the glass. This condition is fulfiled with water only for a short time; with acidic water for several hours or even days. When the motor described above is left a long time without working it is wise to raise the bundles above the mercury to wet them again with the acidic water. The same condition holds for the electrometer after any deviation in the instrument.

[28]The hypothesis which assigns the variation of the electrical difference at the electrodes to the chemical action of the current (which leads to the terms *polarization by hydrogen, by oxygen*) has neither been called nor discussed in the present work; I will try to show that the chemical action and the electrical phenomenon can be produced *separately*

B. – Precaution when checking the First Law

In the Chapter A.1 and A.6 it has been assumed all the time that the wire α is connected to the negative pole of the electromotive force included between α and β. If this electromotive force is very small the connections can be reversed; it will then be observed that the curve of the page 101 continues below the x-axis; but in the case of an electromotive force of 1 Daniell for example, it is forbidden to connect the copper pole to α if one does not want to put the apparatus out of order for a while. Indeed, the electromotive force developed in this case by the current at the surface M (polarization by oxygen) reaches a maximum smaller than 1 Daniell; the current continues then to flow when this maximum has been reached and this until the electromotive force developed at the surface re-establishes the electrical equilibrium: in the same time the mercury in A is oxidized. And when the electromotive force x_0 stops being constant the value of x cannot be determined anymore (Chapter A.1); the zero of the apparatus has been changed.

C. – Measurement of the coefficient X

Measurements performed to determine the numerical value of X (Chapter A.3) have shown that X is independent on s; this value has been determined with only a low accuracy and by default. The reason is that the values of x are getting closer to a constant value x_0 with time and this faster when they are much different than x_0; this kind of loss of charge has been exactly compensated during the verification of the First Law. The study seems to be too complicated to be explained here.